

GL-TR-90-0104

AD-A223 279

Regional Phase Propagation in Three Dimensionally Heterogeneous Media

Brian L.N. Kennett

Australian National University
Research School of Earth Sciences
GPO Box 4
Canberra ACT 2601
AUSTRALIA

11 April 1990

Scientific Report No. 1

APPROVED FOR PUBLIC RELEASE; DISTRIBUTION UNLIMITED

GEOPHYSICS LABORATORY
AIR FORCE SYSTEMS COMMAND
UNITED STATES AIR FORCE
HANSCOM AIR FORCE BASE, MASSACHUSETTS 01731-5000


90 06 25 16 6

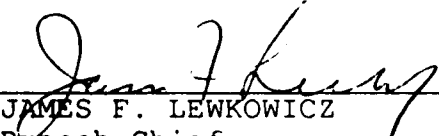
SPONSORED BY
Defense Advanced Research Projects Agency
Nuclear Monitoring Research Office
ARPA ORDER NO 5299

MONITORED BY
Geophysics Laboratory
AFOSR-89-0330

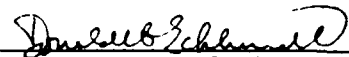
The views and conclusions contained in this document are those of the authors and should not be interpreted as representing the official policies, either expressed or implied, of the Defense Advanced Research Projects Agency or the U.S. Government.

This technical report has been reviewed and is approved for publication.


JAMES F. LEWKOWICZ
Contract Manager
Solid Earth Geophysics Branch
Earth Sciences Division


JAMES F. LEWKOWICZ
Branch Chief
Solid Earth Geophysics Branch
Earth Sciences Division

FOR THE COMMANDER


DONALD H. ECKHARDT, Director
Earth Sciences Division

This report has been reviewed by the ESD Public Affairs Office (PA) and is releasable to the National Technical Information Service (NTIS).

Qualified requestors may obtain additional copies from the Defense Technical Information Center. All others should apply to the National Technical Information Service.

If your address has changed, or if you wish to be removed from the mailing list, or if the addressee is no longer employed by your organization, please notify GL/IMA, Hanscom AFB, MA 01731-5000. This will assist us in maintaining a current mailing list.

Do not return copies of this report unless contractual obligations or notices on a specific document requires that it be returned.

REPORT DOCUMENTATION PAGE

1a REPORT SECURITY CLASSIFICATION UNCLASSIFIED			1b RESTRICTIVE MARKINGS	
2a SECURITY CLASSIFICATION AUTHORITY			3 DISTRIBUTION AVAILABILITY OF REPORT Approved for Public Release Distribution Unlimited	
2b DECLASSIFICATION/DOWNGRADING SCHEDULE				
4 PERFORMING ORGANIZATION REPORT NUMBER(S)			5 MONITORING ORGANIZATION REPORT NUMBER(S) GL-TR-90-0104	
6a NAME OF PERFORMING ORGANIZATION Research School of Earth Sciences		6b OFFICE SYMBOL (If applicable)	7a NAME OF MONITORING ORGANIZATION Geophysics Laboratory	
6c ADDRESS (City, State, and ZIP Code) Australian National University GPO Box 4, CANBERRA ACT 2601, AUSTRALIA			7b ADDRESS (City, State, and ZIP Code) Hanscom AFB Massachusetts 01731-5000	
8a NAME OF FUNDING/SPONSORING ORGANIZATION Air Force Geophysics Laboratory		8b OFFICE SYMBOL (If applicable)	9 PROCUREMENT INSTRUMENT IDENTIFICATION NUMBER Grant AFOSR-89-0330	
8c ADDRESS (City, State, and ZIP Code) Hanscom AFB Massachusetts 01731-5000			10 SOURCE OF FUNDING NUMBERS	
			PROGRAM ELEMENT NO 61101E	PROJECT NO 9A10
11 TITLE (Include Security Classification) Regional Phase Propagation in Three Dimensionally Heterogeneous Media (Unclassified)				
12 PERSONAL AUTHOR(S) KENNETT Brian L.N.				
13a TYPE OF REPORT Scientific #1	13b TIME COVERED FROM 89/4/1 TO 90/3/31	14 DATE OF REPORT (Year, Month, Day) 1990 April 11	15 PAGE COUNT 104	
16 SUPPLEMENTARY NOTATION				
17 COSATI CODES			18 SUBJECT TERMS (Continue on reverse if necessary and identify by block number) Wave Propagation, Regional Phases Lg waves Heterogeneity, Coupled Modes Ray Tracing	
FIELD	GROUP	SUB-GROUP		
19 ABSTRACT (Continue on reverse if necessary and identify by block number) <p>The interaction of regional seismic phases with complex structure can lead to a significant modification of the seismic wavefield with the result of masking the characteristics of the source. A combination of theoretical, computational and observational studies have been directed to elucidating the effect of heterogeneity on regional phases.</p> <p>A new method has been developed for calculating the propagation of guided waves through a medium described by stochastic heterogeneity. This approach allows the estimation of the scattering contribution to the attenuation of Lg and Sn phases which can approach 30 percent for realistic heterogeneity structures.</p> <p>A ray based treatment has been devised to describe the way in which the Lg phase is affected by changes in the shape of the crustal waveguide due to topography at the surface and the Mohorovičić discontinuity.</p>				
20 DISTRIBUTION/AVAILABILITY OF ABSTRACT <input type="checkbox"/> UNCLASSIFIED/UNLIMITED <input checked="" type="checkbox"/> SAME AS RPT <input type="checkbox"/> DTIC USERS			21 ABSTRACT SECURITY CLASSIFICATION Unclassified	
22a NAME OF RESPONSIBLE INDIVIDUAL James F. Lewkowicz			22b TELEPHONE (Include Area Code) (617) 377-3028	22c OFFICE SYMBOL LWH

UNCLASSIFIED

19. Abstract

By mapping the ray paths and the reflection points of rays which set out with specified phase velocities a semiquantitative measure of the disruption of Lg propagation patterns by complex structure can be made. In addition it is possible to estimate the likely extent of conversion between Rayleigh and Love wave propagation. This method has been successfully applied to predicting patterns of Lg propagation in central Asia and the southwestern United States.

A recent sequence of earthquakes in the Northern Territory of Australia provided an opportunity to record regional seismic phases in a Pre Cambrian geologic environment (similar to a number of areas within the USSR).

The seismograms display a high Lg velocity (around 3.7 km/s) and the attenuation of the regional phases with distance is inconsistent with the geometric spreading relations commonly adopted for paths in the United States and Europe. This discrepancy appears to arise from the gradational character of the crust - mantle transition in central Australia.

It is therefore important that corrections for attenuation take account of the character of the crustal structure because inappropriate corrections could build in systematic error to estimates of source magnitude (and hence yields) derived from regional observations.

Accession For	
NTIS GRA&I	<input checked="" type="checkbox"/>
DTIC TAB	<input checked="" type="checkbox"/>
Unannounced	<input type="checkbox"/>
Justification	
By	
Distribution/	
Availability Codes	
Date	
A-1	



REGIONAL PHASE PROPAGATION IN THREE DIMENSIONALLY HETEROGENEOUS MEDIA

RESEARCH OBJECTIVES:

The aim of this work is to develop techniques which can be used to describe the propagation of regional seismic phases in three dimensionally varying media, in order to improve understanding of the nature of such phases and the way in which the characteristics of the seismic source can be modified by propagation to the receiver. Such information will be valuable in assessing the effects of geological structure on the behaviour of potential discriminants between nuclear explosions and earthquakes.

The problem of discrimination becomes more difficult for small events recorded at considerable distances. The regional seismic phases, from which the discriminant properties are extracted, will have passed through regions of considerable horizontal variability in seismic properties in their passage from source to receiver.

We have therefore set out to find ways to improve the description of the interaction of regional phases with crustal structure via a combination of theoretical, computational and observational work.

RESEARCH STATUS AND ACHIEVEMENTS:

The crustal waveguide is a zone of complex variations in seismic wavespeeds. Although it is feasible to generate specific models of the heterogeneity structure it is more economical to use a stochastic description of the structure. However, with a stochastic model it is not possible to use the coupled modes techniques developed by Kennett (1984) for the description of regional S waves (the phases Lg, Sn). Fortunately it is possible to modify techniques originally devised for wave propagation in optical fibres to generate a new method for estimating the structural component of the apparent attenuation of guided waves with distance.

For a particular stochastic model of crustal and mantle heterogeneity it is now possible to calculate the attenuation of different modes as a function of distance, including intrinsic attenuation and scattering loss by transfer to other modes of propagation. Such statistical estimates of attenuation can then be compared with observations of the attenuation of regional phases for many paths traversing a single region. For Lg and Sn scattering attenuation can represent nearly a third of the apparent attenuation.

A full description of the coupled mode technique for stochastic media and the resulting estimates of scattering attenuation are given in the attached paper: *Guided wave attenuation in laterally varying media.*

The Lg phase is one of the most prominent features of many regional seismograms in the frequency band from 0.5 to 3.5 Hz and its size makes it valuable for the detection of small events. However the amplitude of Lg is known to be sensitive to changes in crustal structure and this behaviour reduces its utility for discrimination purposes. Given a particular source location it is therefore highly desirable to be able to predict the effects of crustal heterogeneity on the characteristics of Lg propagation. A large part of the effect of 3-D structure arises in the shape of the crustal waveguide and by using a ray theoretical description of the Lg phases, topography at the surface and the Moho can be included. Rays are traced at different initial angles to the vertical depending on the phase velocity under consideration. The rays are monitored in plan view and by mapping the reflection points at the surface and Moho, a semiquantitative measure of the disruption of Lg can be made. Also, the tilt of the rays can be used to judge the degree of interconversion between Love and Rayleigh wave energy.

The development of the technique, testing on simple models and application to the complex structures in central Asia are described in the accompanying paper:

The effect of three dimensional structure on Lg propagation patterns.

Despite the relative simplicity of the method the major characteristics of Lg propagation are well predicted. By including the possibility of secondary sources scattering due to specific structural features can be included and this approach is exploited in the section:

Guided wave tracking in 3-D - a tool for interpreting complex regional seismograms

in which the Lg wave tracking procedure is applied to the southwestern United States. Predicted strong scattering from the Sierra Nevada, reflection from the ocean-continent transition and resonance within the narrow corridor of Baja California match up well with features on observed seismograms.

Available detailed observations of regional seismic phases cover a relatively limited range of tectonic environments and there is therefore the possibility that many well accepted observations may be specific to certain styles of crustal structure. The Tennant Creek earthquake sequence in the Northern Territory of Australia in an area of PreCambrian outcrop provided an opportunity to investigate regional phase propagation in a different context. Recordings were made on a roughly linear area along the highway running between the arrays at Warramunga and Alice Springs giving sparse but useful coverage over a 400 km distance span.

The apparent velocity of Lg is quite fast (3.7 km/s) and its decay pattern is not consistent with the conventional assumption of geometric spreading in the form $r^{-5/6}$. These unusual features appear to be related to the gradational character of the crust-mantle transition in this region. The accompanying report

The effects of crustal velocity gradients on the propagation of regional S phases describes the analysis of this data. Work continues on attempting to characterise the dependance of the parameters of the regional phases in the nature of the crust-mantle transition.

CONTENTS

GUIDED WAVE ATTENUATION IN Laterally Varying Media	1
Introduction	1
Coupled Mode Equations	2
Coupled Power Equations	4
Separation of Crust & Mantle Heterogeneity Contributions	8
Attenuation via Intermode Coupling	10
Estimates of Scattering Attenuation	12
References	15
THE EFFECT OF THREE-DIMENSIONAL STRUCTURE ON Lg PROPAGATION PATTERNS	21
Introduction	21
The Ray Diagram Method	23
Crustal Models	24
Simple Crustal Structures	25
Crustal Thinning	26
Central Asia	26
Sempalitinsk	28
Eastern Tien Shan	29
Discussion	31
References	32
GUIDED WAVE TRACKING IN 3-D - A TOOL FOR INTERPRETING COMPLEX REGIONAL SEISMOGRAMS	46
Introduction	47
Diablo Range Events	48
Northern Baja California Events	50
Discussion	51
References	52
THE EFFECTS OF CRUSTAL VELOCITY GRADIENTS ON THE PROPAGATION OF REGIONAL S PHASES	63
Introduction	63
Data and Geological Setting	64
Group Velocity	66
Lg Attenuation	66
Discussion	68
References	71

Guided Wave Attenuation in Laterally Varying Media

B.L.N. Kennett

*Research School of Earth Sciences, Australian National University,
G.P.O. Box 4, Canberra ACT 2601, Australia*

Summary

Coupled mode techniques for guided wave propagation are extended to two-dimensional stochastic heterogeneity superimposed on a stratified medium. This approach requires the variations to be smoothly varying and of modest size (less than ± 2 per cent). By averaging over an ensemble of statistically similar models coupled equations for the modal energy transport can be generated. The intermode coupling depends on the horizontal correlation functions for the heterogeneity in the crust and mantle, and the integrated effect of the vertical variations in velocity and the modal eigenfunctions.

For a particular stochastic model the attenuation of a single mode as a function of distance can be calculated as a superposition of intrinsic attenuation and scattering loss by energy transfer to other modes of propagation. These statistical estimates of attenuation can be compared with observations of regional phases travelling over a variety of paths in a single region. For Lg and Sn phases, intermode scattering may represent up to 30 per cent of the apparent loss.

Key Words: Attenuation, Guided wave propagation, stochastic heterogeneity, regional seismic phases

Introduction

Detailed studies of the structure of the crust and upper mantle show lateral heterogeneity on a wide variety of scales superimposed on a basic stratification with depth. Guided seismic waves travelling nearly horizontally through such structures are particularly vulnerable to scattering due to the presence of heterogeneity.

A convenient way of representing such guided waves is in terms of a superposition of surface wave modes whose eigenfunctions are largely confined to the

waveguide. Such a description has been used by Malin (1980), Wang & Herrmann (1988) in simulations of the coda of local earthquakes. For longer distance propagation Malichewsky (1987) has summarised the techniques for handling the interactions of surface waves with vertical interfaces or sharp transitions. These methods relate the amplitudes of the surface wave modes in the structure on one side of the boundary to those on the other side. In a similar way, for continuous heterogeneity the wavefield can be described in terms of surface wave modes if allowance is made for energy transfer between modes (Kennett 1984; Maupin 1988). These coupled mode methods have generally been formulated for deterministic velocity structures and much less work has been done on a stochastic description of guided wave propagation even though this has been extensively developed for body waves (see e.g. Aki & Richards 1980, chapter 13; Hudson 1982).

We here present an adaptation of the coupled mode procedure to a 2-D stochastic heterogeneous medium, and generate coupled equations for the modal energy transport averaged over an ensemble of statistically similar models. The approach is based on techniques developed for fibre optics (Marcuse 1974), but is extended to multiple waveguides e.g. the crust and upper mantle for regional seismic phases. For a specified stochastic model of the velocity heterogeneity we are able to estimate for each mode the contribution to the modal loss factor, $Q_m(\omega)$ induced by scattering into other modes of propagation. Such estimates can be compared with observations of guided waves over a variety of paths in a single geographic region, as e.g. the observations of Nuttli (1980) for Sn and Lg phases propagating across Iran.

Coupled Mode Equations:

Kennett (1984) has shown how the displacement and traction fields for guided seismic waves in 2-D laterally varying media can be represented as a sum of modal eigenfunctions with horizontally varying coefficients. When the variations in seismic parameters do not show a systematic trend horizontally, the expansion may be made in terms of the modes for a fixed reference structure. Maupin & Kennett (1987) have shown how the effect of inclined interfaces can be included in the scheme by modifying the matrix elements in the differential equations for coupling between the modal coefficients. When the structure has systematic horizontal variations a more effective representation is to work in terms of the local modes of the structure (Maupin 1987). Although the nature of the coupling coefficients differ, the two styles of modal representation lead to sets of coupled equations with similar structure.

The coupled mode equations give a representation in terms of a particular velocity structure. However, in considering different classes of heterogeneity it can be advantageous to adopt a stochastic treatment for the heterogeneity structure. We will consider the case where the heterogeneity has no more than ± 2 per cent variation in seismic parameters from those of a reference model. This provides a good representation of many situations in the crust and uppermost mantle and can be well treated using the coupled mode approach with a fixed set of reference modes (Kennett 1989).

At each point in the 2-D varying medium we represent the displacement field $w(x, z)$ as a sum of vertically varying modal eigenfunctions with coefficients which depend only on horizontal position (Kennett 1984). Thus

$$w(x, z) = \sum_r c_r(x) \exp\{ik_r x\} w_r^o(k_r, z), \quad (1)$$

where w_r^o is the eigenfunction for the r th mode with horizontal wavenumber k_r , and the sum is taken over both forward and backward travelling modes. The total number of modes must be chosen large enough to include all the propagation processes of interest (see Maupin & Kennett 1987). The eigenfunctions for the modes are normalised so that they have the same horizontal energy transport.

The horizontal evolution of the modal coefficients c_r is described by a set of ordinary differential equations

$$\frac{\partial}{\partial x} c_r(x) = \sum_s K_{rs}(x) \exp\{i(k_s - k_r)x\} c_s(x), \quad (2)$$

where the coupling matrix K depends on the deviations of the properties of the actual medium from those of the reference. Using the concise notation of Maupin & Kennett (1987), which is suitable for anisotropic media

$$\begin{aligned} K_{rs} = i \int_0^\infty dz & [\bar{t}_{1r}^o \Delta C_{11}^{-1} t_{1s}^o + \Lambda \rho \omega^2 \bar{w}_r^o \cdot w_s^o \\ & - \partial_z \bar{w}_r^o \Delta Q_{33} \partial_z w_s^o + \partial_z \bar{w}_r^o \Delta (C_{31} C_{11}^{-1}) t_{1s}^o - \bar{t}_{1r}^o \Delta (C_{11}^{-1} C_{13}) \partial_z w_s^o] \\ & + \sum_n h_n [\bar{w}_r^o \cdot t_{1s}^o]_n, \end{aligned} \quad (3)$$

where t_{1r}^o is the horizontal traction derived from w_r^o and we have written $\bar{w}_r^o = w_r^o(-k_r, z)$. In terms of the elastic modulus tensor c_{kij}

$$(C_{ij})_{kl} = c_{kijl}, \quad Q_{33} = C_{33} - C_{31} C_{11}^{-1} C_{13}.$$

The interface terms depend on the slope of the interface and the jumps in the horizontal traction t_{1r}^0 across the interface.

The set of equations (2) include the possibility of both reflection and transmission. However, direct calculations using the coupled mode equations show that reflected waves can be neglected without appreciable error, provided that deviations in the seismic parameters from the reference model are not too large (less than ± 2 per cent) and the scale of variation is not rapid compared with the horizontal wavelengths involved. This neglect of reflected waves can also be justified by using first-order Born scattering results in the wavenumber domain (Kennett 1972). For a heterogeneity pattern with wavenumber spectrum $f(k)$, the scattering between two wavenumbers k_a and k_b is proportional to $f(k_a - k_b)$. For reflected waves k_b is negative and so the difference $k_a - k_b$ will be large. Thus scattering into reflected waves will only be noticeable if $f(k)$ has significant amplitude for large k , i.e. if the heterogeneity itself varies on very small horizontal scales (or is discontinuous).

We will therefore restrict attention to transmitted waves and so consider the limited set of coupled equations

$$\frac{\partial}{\partial x} c_r(x) = \sum_{s=0}^N K_{rs}(x) \exp[i(k_s - k_r)x] c_s(x). \quad (4)$$

With the restrictions we have placed on the nature of the heterogeneity a good approximation for the modal coefficients after passage through a small horizontal distance h is given by

$$c_r(x+h) = c_r(x) + \sum_{s=0}^N c_s(x) \int_x^{x+h} dq K_{rs}(q) \exp[i(k_s - k_r)q], \quad (5)$$

the first term in a systematic expansion in terms of the coupling coefficients K_{rs} ; higher order interactions can be neglected since we have assumed weak heterogeneity. We are thus able to treat the set $\{c_r\}$ as the amplitude distribution across the modes at the horizontal position x .

Coupled Power Equations

The set of coupled mode equations (2) can be solved for a particular heterogeneity model and then provides a detailed description of the phase and amplitude behaviour of all the modes at each point x in the waveguide. By combining this information for many frequencies we can, in principal, construct theoretical seismograms but very substantial computational effort is required.

We can, however, get a measure of the energy redistribution between modes as a function of distance in propagating through a random heterogeneity by considering the average power over an ensemble of heterogeneity models. The resulting equations for the modal power contributions for each frequency are a coupled set of first order differential equations with constant and symmetric coefficients.

We will adopt a physically based approach to the derivation of the coupled power equations following Marcuse (1974). The results we derive can be justified formally using the techniques of stochastic differential equations described in Kohler & Papanicolaou (1977).

We have adopted a normalisation for modal eigenfunctions in which the horizontal energy transport is equal for each mode. As a result, for a particular heterogeneity model a measure of the power in an individual mode P_m is

$$P_m = |c_m|^2,$$

and from (4) satisfies the horizontal evolution equation

$$\begin{aligned} \frac{\partial}{\partial x} P_m &= c_m^* \frac{\partial}{\partial x} c_m + c_m \frac{\partial}{\partial x} c_m^* \\ &= c_m^* \sum_n K_{mn} c_n \exp\{i(k_n - k_m)x\} + c.c., \end{aligned} \quad (7)$$

where *c.c.* denotes the complex conjugate of the previous term. We now consider an ensemble average over a collection of statistically similar heterogeneity models, built according to the same prescription but not identical. In particular we assume that the phases of any periodic components in the heterogeneity are randomly distributed across the members of the statistical ensemble.

The averaged power in each mode

$$S_m = \langle |c_m|^2 \rangle, \quad (8)$$

and its change with horizontal position will be governed by the ensemble average of equation (7):

$$\frac{\partial}{\partial x} S_m = \sum_n \langle K_{mn} c_m^* c_n \rangle \exp\{i(k_n - k_m)x\} + c.c. \quad (9)$$

We will assume that each of the elements defining the heterogeneity $\Delta\rho$, ΔC_{11}^{-1} , ΔQ_{33} , $\Delta(C_{11}^{-1}C_{13})$, $\Delta(C_{31}C_{11}^{-1})$ have similar statistical properties and the heterogeneity values at widely separated points are uncorrelated. The coupling coefficients will be described by a stationary random process with a finite correlation length *D* in the horizontal direction. We will assume the average heterogeneity level across the

ensemble vanishes so that

$$\langle K_{mn}(x) \rangle = 0.$$

For the guided waves travelling in the direction of increasing x we anticipate that the modal amplitude $c_m(x)$ and the coupling matrix $K(x)$ will be uncorrelated if

$$x' - x \gg D,$$

and then

$$\langle c_m(x') c_n(x') K_{mn}(x) \rangle = \langle c_m(x') c_n(x') \rangle \langle K_{mn}(x) \rangle$$

with similar behaviour for products of coupling coefficients. We can exploit this result in (9) if we express the modal field at x in terms of that at x' using (5). Under the assumption that third order interaction terms of the type $\langle KKK \rangle$ can be neglected because the heterogeneity is small, we find

$$\begin{aligned} \frac{\partial}{\partial x} S_m = \sum_{n,r} [& \langle c_m^*(x') c_r(x') \rangle \exp\{i(k_n - k_m)x\} \int_x^{x'} dq \langle K_{mn}(x) K_{nr}(q) \rangle \exp\{i(k_r - k_n)x\} \\ & + \langle c_n(x') c_r^*(x') \rangle \exp\{i(k_n - k_m)x\} \int_x^{x'} dq \langle K_{mn}(x) K_{mr}^*(q) \rangle \exp\{-i(k_r - k_m)x\} \\ & + \text{c.c.}]. \end{aligned} \quad (10)$$

Since we have assumed a short correlation length we can extend the lower limit of integration to $-\infty$, and so recast the integrals in the form of half range Fourier transforms over the correlation between the coupling coefficients

$$\begin{aligned} & \exp\{i(k_n - k_m)x\} \int_x^{x'} dq \langle K_{mn}(x) K_{mr}^*(q) \rangle \exp\{i(k_m - k_r)q\} \\ & = \exp\{i(k_n - k_r)x\} \int_0^\infty du \langle K_{mn}(x) K_{mr}^*(x-u) \rangle \exp\{-i(k_m - k_r)u\}. \end{aligned} \quad (11)$$

The coupled power equations can therefore be written as

$$\begin{aligned} \frac{\partial}{\partial x} S_m = \sum_{n,r} [& \langle c_m^*(x') c_r(x') \rangle \exp\{i(k_r - k_m)x\} \int_0^\infty du \langle K_{mn}(x) K_{nr}(x-u) \rangle \exp\{i(k_n - k_r)u\} \\ & + \langle c_n(x') c_r^*(x') \rangle \exp\{i(k_n - k_r)x\} \int_0^\infty du \langle K_{mn}(x) K_{mr}^*(x-u) \rangle \exp\{i(k_r - k_m)u\} \\ & + \text{c.c.}]. \end{aligned} \quad (12)$$

We anticipate that the modal amplitudes will tend to have random phase so that

$$\langle c_n c_m^* \rangle = \langle |c_m|^2 \rangle \delta_{mn}$$

and this selection of diagonal elements will be reinforced by a situation akin to stationary phase: the main contribution from the right hand side of (12) will arise from non-oscillatory terms in the integrals. Hence we are able to drop one summation to give

$$\begin{aligned} \frac{\partial}{\partial x} S_m = \sum_n [& S_m(x') \int_0^\infty du \langle K_{mn}(x) K_{nm}(x-u) \rangle \exp\{i(k_n - k_m)u\} \\ & + S_n(x') \int_0^\infty du \langle K_{mn}(x) K_{mn}^*(x-u) \rangle \exp\{i(k_n - k_m)u\} \\ & + \text{c.c.}]. \end{aligned} \quad (13)$$

We have assumed that the modal coefficients are slowly varying in going from x to x' , and so S_m will be nearly constant over this interval. As a result, we can replace $S_m(x')$ by $S_m(x)$ on the right hand side of (13). Further, we require that the total power should be independent of x in a lossless medium so

$$K_{nm}(x) = -K_{mn}^*(x).$$

Thus

$$\frac{\partial}{\partial x} S_m = \int_{-\infty}^{\infty} du \{ \langle K_{mn}(x) K_{mn}^*(x-u) \rangle [S_n(x) - S_m(x)] \} \exp[i(k_n - k_m)u],$$

where we have used the fact that the term in braces is real to incorporate the complex conjugate term as an integral along the negative u axis. (Note that in this perfectly elastic situation after propagation through a very large distance the power in all the modes will equalise to the same level.)

Equation (14) covers the general case of weak heterogeneity but we can simplify further if we make specific assumptions about the form of the heterogeneity model. The near stratification within the Earth will impose different stochastic properties on the horizontal and vertical variations of the heterogeneity. The coupling coefficients K_{mn} are defined in terms of an integral over the full depth of the heterogeneity. After taking the ensemble average over the set of statistically similar models, the evolution equations for the average modal power will be dominated by the nature of the variations in the heterogeneity in the horizontal direction.

Separation of crust and mantle heterogeneity contributions

In general we expect the heterogeneity in the crust to have a different character to that in the mantle. Since we have assumed weak heterogeneity, we are able to extract a common functional dependence from each of the coupling coefficients K_{mn} for the horizontal behaviour of the heterogeneity in each of the crust and mantle zones

$$K_{mn}(x) = f^C(x)K_{mn}^C(x) + f^M(x)K_{mn}^M(x). \quad (15)$$

$f^C(x)$ is the horizontal variation function for the crustal heterogeneity and $K_{mn}^C(x)$ is an integral restricted to the crust. Similarly $f^M(x)$ is the horizontal variation function for the mantle and $K_{mn}^M(x)$ is defined by an integral over the span of the mantle. We do not require a complete separation of the horizontal and vertical dependence of the velocity and density perturbations from the reference. The part of the variation unaccounted for by $f^C(x)$, $f^M(x)$ remains in the crust and mantle coupling coefficients $K_{mn}^P(x)$, $K_{mn}^M(x)$ which depend on the properties as a function of depth at the location x . When we take the average over an ensemble of statistically equivalent models, we remove this dependence on location. The ensemble average

$$\begin{aligned} \langle K_{mn}(x)K_{mn}^*(x-u) \rangle &= \langle f^C(x)f^C(x-u) \rangle |\hat{K}_{mn}^C|^2 + \langle f^M(x)f^M(x-u) \rangle |\hat{K}_{mn}^M|^2 \\ &= R^C(u) |\hat{K}_{mn}^C|^2 + R^M(u) |\hat{K}_{mn}^M|^2, \end{aligned} \quad (16)$$

in terms of the autocorrelation functions R^C , R^M of the horizontal variation of the crust and mantle heterogeneity e.g. $R^C(u) = \langle f^C(x)f^C(x-u) \rangle$. \hat{K}_{mn}^C , \hat{K}_{mn}^M represent ensemble averages over the vertical variations. We have made the not unreasonable assumption that the horizontal variations in the crust and mantle heterogeneity are uncorrelated.

With the expression (16) for the heterogeneity contribution the evolution equations for the averaged modal power can be recast as

$$\begin{aligned} \frac{\partial}{\partial x} S_m = \sum_n [S_n(x) - S_m(x)] &\left[|\hat{K}_{mn}^C|^2 \langle |F^C(k_n - k_m)|^2 \rangle \right. \\ &\left. + |\hat{K}_{mn}^M|^2 \langle |F^M(k_n - k_m)|^2 \rangle \right] \end{aligned} \quad (17)$$

where $\langle |F^C|^2 \rangle$, $\langle |F^M|^2 \rangle$ are the power spectra of the crust and mantle correlation functions e.g.

$$\langle |F^C(k_n - k_m)|^2 \rangle = \int_{-\infty}^{\infty} du R^C(u) \exp\{i(k_n - k_m)u\}. \quad (18)$$

We have so far ignored the possibility of intrinsic attenuation of the modes as they propagate through the medium, but it is easy to compensate for the effect of Q by introducing a simple power loss term into (17). Thus for an attenuative medium

$$\frac{\partial}{\partial x} S_m = -k_m Q_m^{-1} S_m(x) + \sum_{n=0}^N H_{mn} [S_n(x) - S_m(x)], \quad (19)$$

where the power coupling coefficients

$$H_{mn} = |\hat{K}_{mn}^C|^2 \langle |F^C(k_n - k_m)|^2 \rangle + |\hat{K}_{mn}^M|^2 \langle |F^M(k_n - k_m)|^2 \rangle \quad (20)$$

and Q_m^{-1} is the intrinsic loss factor for the m th mode. The spatial loss factor Q_m^{-1} is related to the temporal loss factor ${}^t Q_m^{-1}$ for the same mode by the ratio of the group velocity (U_m) and phase velocity (c_m) for the mode

$${}^t Q_m^{-1} = (U_m/c_m) Q_m^{-1}.$$

The set of coupled equations (19) can be readily solved numerically for any given power distribution. Similar equations can be derived for other configurations of heterogeneity, the differences will lie in the form of the power coupling coefficients as e.g. where the mantle has to be subdivided into different zones.

For small perturbations of an interface

$$K_{mn}(x) = f^I(x) K_{mn}^I(x), \quad (21)$$

where $f^I(x)$ is the shape of the varying interface. The coupling integral K_{mn}^I will be confined to a depth band representing the extent of the interface variations, and will depend on the contrast in seismic properties across the interface. In this case, the equivalent to (16) is

$$\langle K_{mn}(x) K_{mn}^*(x-u) \rangle = \langle f^I(x) f^I(x-u) \rangle |\hat{K}_{mn}^I|^2 = R^I(u) |\hat{K}_{mn}^I|^2, \quad (22)$$

where R^I is the autocorrelation function of the interface shape and \hat{K}_{mn}^I the ensemble average over the coupling terms. The subsequent analysis will parallel equations (17-19) and the corresponding power coupling coefficients

$$H_{mn} = |\hat{K}_{mn}^I|^2 \langle |F^I(k_n - k_m)|^2 \rangle. \quad (23)$$

For interfaces with considerable contrast, e.g. the crust-mantle boundary the effect of random topography can be comparable to that of velocity perturbations. The present approach is not suitable for situations with a systematic variation in the depth of an interface.

Attenuation via intermode coupling

We can rewrite the coupled power equations (19) in a form which emphasises the behaviour of the m th mode

$$\frac{\partial}{\partial x} S_m = -(k_m Q_m^{-1} + b_m) S_m(x) + \sum_{n=0}^N {}' H_{mn} S_n(x), \quad (24)$$

where Σ' denotes a summation omitting $m=n$, and

$$b_m = \sum_{n=0}^N {}' H_{mn}$$

i.e. a sum over one column of the matrix of power coupling coefficients H excluding the diagonal element. Note that coupling a mode to itself will not affect the power distribution with the natural consequence of excluding the diagonal element.

For a given initial power distribution $S_{0m}(x_0)$, an equivalent integral equation to (24) is

$$S_m(x) = \exp\{-(k_m Q_m^{-1} + b_m)(x - x_0)\} S_{0m}(x_0) + \sum_{n=0}^N {}' \int_{x_0}^x dv \exp\{-(k_m Q_m^{-1} + b_m)(x - v)\} H_{mn} S_n(v). \quad (25)$$

Since we have assumed relatively weak heterogeneity the dominant behaviour can be seen from the first-order approximate solution

$$S_m(x) = \exp\{-a_m(x - x_0)\} S_{0m}(x_0) + \sum_{n=0}^N {}' \int_{x_0}^x dv \exp\{-a_m(x - v)\} H_{mn} \exp\{-a_m(v - x_0)\} S_n(x_0). \quad (26)$$

where we have introduced the effective decay rate with distance for energy in the m th mode

$$a_m = k_m Q_m^{-1} + b_m = k_m Q_m^{-1} + \sum_n {}' H_{mn}. \quad (27)$$

If we now consider an initial distribution $S_{0m}(x_0)$ concentrated solely in the m th mode, we see from (25,26) that the main part of the behaviour of the m th mode with distance will be decay as $\exp\{-a_m(x - x_0)\}$. There will be limited retransfer of energy to the m th mode by secondary scattering from other modes.

We can therefore characterise the energy decay rate for the m th mode by a_m and regard the intermode coupling as introducing a 'scattering' attenuation term for the m th mode

$$\begin{aligned}
{}_s Q_m^{-1} &= k_m^{-1} b_m \\
&= k_m^{-1} \sum_n \left[|\hat{K}_{mn}^C|^2 \langle |F^C(k_n - k_m)|^2 \rangle + |\hat{K}_{mn}^M|^2 \langle |F^M(k_n - k_m)|^2 \rangle \right], \quad (28)
\end{aligned}$$

where we have reinstated the explicit form (20) for the power coupling coefficients between the modes. Equation (26) represents the first term in an iterative solution in terms of H and since all elements of H_{mn} are positive the full solution will give a slightly larger value for $S_m(x)$ than estimated from (26). The loss factor ${}_s Q_m^{-1}$ defined by (28) is therefore a little too small, but gives a very useful indication of the behaviour. Equation (28) represents the spatial loss factor; the corresponding temporal loss factor for the m th mode will be $(U_m/c_m) {}_s Q_m^{-1}$.

For regional seismic phases, the scattering attenuation will be significantly different for the mantle phases than the crustally guided waves. The dominant term in (25) for Lg type modes will be $|\hat{K}_{mn}^C|^2 \langle |F^C(k_n - k_m)|^2 \rangle$ and since we anticipate the largest heterogeneity to be concentrated in the crust ${}_s Q_m^{-1}$ can be significant. For the Sn modes the main contribution will be from the mantle heterogeneity.

When we wish to compare the behaviour of a set of modes at fixed frequency ω , it can be advantageous to work with the energy decay factors a_m, b_m since these terms are directly comparable between modes.

The expressions for the scattering attenuation for individual modes derived in this section are dependent on our assumption of 2-D heterogeneity. For 3-D heterogeneity there is the additional complication that there is the likelihood of energy being scattered in directions other than forwards and backwards along the local direction of propagation. Once scattered out of a particular mode, energy is unlikely to return to it in the case of 3-D heterogeneity; thus attenuation will be stronger than the estimates based on our 2-D model.

However, when we consider a multimode seismic wavetrain, this directional scattering will work to reduce the reinforcement of modal amplitudes by cross-coupling. An average of the estimated scattering attenuation across a number of modes will therefore give a measure of the decay rate of the wavetrain with distance which can be compared with observations on attenuation. It should also be recalled that the derivation of the scattering attenuation depends on propagation occurring over distances which are long compared with the correlation length of the heterogeneity.

Estimates of Scattering Attenuation

The computational procedure which we have just derived enables us to generate a good estimate of the statistical loss factor for an individual mode as a combination of anelastic and scattering contributions. For direct comparison between different modes we can use the rate of energy decay with distance. We will here apply our results to the regional phases Lg, Sn travelling through heterogeneous earth models.

From equation (25), calculation of the scattering loss factor requires us to specify the statistical nature of the horizontal heterogeneity spectrum in the crust and upper mantle as well as estimate the ensemble averages of the intermode coupling terms \hat{K}^C , \hat{K}^M which depend on the modal eigenfunctions for the reference model. In figure 1 we show our reference model (ARANDA) together with the vertical component of displacement for Rayleigh modes at 1Hz. The modes clearly divide into two classes: firstly, those modes for which the displacement is largely restricted to the crust which will constitute the Lg wave train, and secondly, modes with little crustal displacement but significant energy transport in the mantle which represent the Sn phase. At 1 Hz the transition occurs at mode 11. The fundamental and first higher mode are confined to the sedimentary overburden and hardly interact with the other modes.

The ensemble averages \hat{K}^C , \hat{K}^M require an average of depth integrals over a combination of heterogeneity and eigenfunction terms. We have estimated these averages by a Monte Carlo simulation: random velocity perturbations (up to 1 per cent) were applied to the velocities at the top and bottom of each of the layers in the reference model ARANDA and linear interpolation was used to calculate intermediate velocity values. Densities were varied in proportion to the velocities and the depths of the interfaces were not varied. The coupling integrals (3) were then evaluated for both Love and Rayleigh waves for 300 different simulations of the vertical heterogeneity structure and averaged to give estimates of \hat{K}^C , \hat{K}^M . \hat{K}^C is calculated for an integral over the crust i.e. down to 30 km and \hat{K}^M over the mantle structure which is extended in the reference model to 200 km depth. This procedure gives quite stable estimates for \hat{K}^C and \hat{K}^M .

The model adopted for the autocorrelation of the horizontal variation of the heterogeneity was exponential

$$R(u) = h^2 \exp(-|u|/D),$$

for a horizontal correlation length D . This form has the advantage that it can allow the existence of discontinuities in velocity gradients. The corresponding Fourier transform appearing in the loss factor terms is

$$\langle |F(k)|^2 \rangle = 2h^2/D [k^2 + (1/D)^2].$$

We have scaled the amplitude factor h to be unity for the ± 1 per cent heterogeneity assumed in the calculation of the vertical averages R^C, R^M .

The dependence of the loss factor on heterogeneity will be quadratic over the ranges for which the present theory is valid (less than ± 2 per cent). At higher levels, local multiple scattering will become important and the rate of increase of the loss factor will drop below quadratic.

In figure 2, we show the behaviour of the scattering loss factor for three Rayleigh and Love modes at 1 Hz, with ± 1 per cent heterogeneity, as a function of the correlation length D_C for the crust. The mantle correlation length was fixed at 50 km. The modes were chosen to represent different aspects of the wavefield. At 1 Hz, mode 4 is sensitive to the upper and middle crust and forms part of the onset of Lg with a group velocity of 3.45 km/s. Mode 9 has greater sensitivity to lower crustal properties and represents waves travelling near critical incidence on the crust-mantle interface; at 1 Hz it is close to an Airy Phase with a group velocity of 3.2 km/s and so represents the coda of Lg. Mode 14 has a group velocity around 4.45 km/s and forms part of the Sn phase.

The solid triangles in figure 2 indicate the calculations for two-dimensional structure for Rayleigh waves and the open diamonds indicate the corresponding values for Love waves. The behaviour is generally similar although there is more difference for the Sn type mode (14). For this slowness the Rayleigh wave couples P waves propagating in the near surface with Sn type behaviour for S; the influence of the P wave velocity heterogeneity raise the loss factor for the mode.

For both of the crustal mode we see a tendency for the scattering loss factor to peak for correlation distances about 3 times the horizontal wavelength of the waves. For small scale heterogeneity there will be considerable scattering but loss and gain by intermodal interactions will tend to balance. For larger scale heterogeneity, scattering will be more infrequent and so loss will be reduced. The detailed behaviour depends on the mode and also the character prescribed for the vertical heterogeneity.

The loss factor for the mantle mode (14) is only less sensitive to the character of the crustal heterogeneity. There is considerable mixing between mantle modes giving a significant scattering component. However, the intrinsic attenuation is likely to be low so that the overall loss factor will normally be less than for crustal propagation.

In order to compare a number of different modes it is preferable to work with the rate of energy loss with distance h_m rather than the scattering loss factors. In

figure 3 we therefore display b_m as a function of mode number at 1 Hz, for both Love and Rayleigh waves and three different choices of crustal correlation length D_C . Mode 1 is confined to the sediments and has little interaction with other modes, so that its scattering attenuation is small. Attenuation for the other modes is of the same order of magnitude. As the horizontal correlation length shortens to less than 10 km, a reasonable value for crustal variation (Wu & Aki 1988), the decay rates of the various crustal modes tend to equalise which will give rise to a consistent decay rate for the Lg wavetrain.

The frequency dependence of the loss factor estimates is explicit through the dependence on ω , k in the coupling coefficients and correlation spectra, but also implicit through the shape of the eigenfunctions. For a crustally guided mode it is difficult to compare the Q^{-1} estimates at different frequencies because the character of the mode changes. However, we can compare modes with similar propagation characteristics at different frequencies and we find that our statistical estimates of Q^{-1} increase with frequency. The increase is not a simple power law and there is an indication of saturation at higher frequencies (around 2 Hz).

As pointed out by Hudson (1982) it is often difficult to find a direct relation between the results of stochastic calculations and observable features of the seismic wavefield. Fortunately, for guided wave attenuation we are able to find a very close correspondence between our estimate of energy loss with distance and observations of regional phase attenuation over a variety of paths within a single region (see e.g. Nuttli 1980, Herrmann 1980). Once the effects of dispersion and geometrical spreading are removed from the observations, the attenuation with distance is isolated and will include both intrinsic and scattering attenuation.

For a large number of different paths in Iran at 1 Hz, Nuttli (1980) found a broad spread of amplitude decay factors for both Lg and Sn with an average value around 0.0045 km^{-1} . To convert to energy loss coefficients we must multiply by a factor of two. Comparison with figure 3 shows that ± 1 per cent heterogeneity would account for about 10 per cent of the observed attenuation and this factor would rise to around 40 per cent for ± 2 per cent heterogeneity. The intrinsic attenuation is likely to be high in Iran, but the apparent Q of around 200 may well have a significant scattering component.

For the low attenuation zone in the Eastern United States, Herrmann (1980) has deduced an amplitude decay rate of 0.0009 km^{-1} , with an apparent Q of 1500, for many paths to the station BLA (Blacksburg, Virginia). This would be equivalent to an energy decay rate of 0.0018 km^{-1} . Nearly a third of this loss could be accounted for

by scattering due to ± 1 per cent heterogeneity, within a medium with low intrinsic loss ($Q_i \gg 2250$).

These results show that our estimate of the scattering loss for guided waves fit well with observations of guided wave attenuation. If, then, we have a measure of the heterogeneity structure and intrinsic attenuation for a region we can use our statistical approach to estimate and average effective loss factor which can be used as a reference against which to compare observations on different paths.

The seismic velocity distributions derived from tomographic inversion (e.g. Spakman 1989) often show higher levels of heterogeneity than have been assumed in the stochastic calculations (up to ± 5 per cent). However such heterogeneity has a horizontal scale length typically greater than 200 km and so will not be a significant contributor to scattering for higher frequency waves (1 Hz and above). The estimates of scattering attenuation due to small scale variations in seismic properties will therefore give a good guide to the behaviour in the presence of variability on much longer horizontal scales.

Acknowledgements

This work was supported in part by the Advanced Research Projects Agency of the U.S. Department of Defense under grant AFOSR-89-0330. The coupled power calculations were carried out on the Fujitsu VP-100 of the Australian National University Supercomputer Facility.

References

- Aki K. & Richards P.G. 1980,
Quantitative Seismology (2 vols), W.H. Freeman, San Francisco.
- Herrmann R.B. 1980,
Q estimates using the coda of local earthquakes, *Bull. seism. Soc. Am.* **70**, 447-468
- Hudson J.A. 1982,
Use of stochastic models in seismology, *Geophys. J. R. astr. Soc.* **69**, 649-657
- Kennett B.L.N. 1972,
Seismic waves in laterally inhomogeneous media, *Geophys. J. R. astr. Soc.* **23**, 301-325
- Kennett B.L.N. 1984,
Guided wave propagation in laterally varying media - 1. Theoretical development, *Geophys. J. R. astr. Soc.* **79**, 235-255

- Kennett B.L.N. 1989,
Lg wave propagation in heterogeneous media, *Bull. seism. Soc Am* **79**,
- Kohler W. & Papanicolaou G.C. 1977,
Wave propagation in a randomly inhomogeneous ocean, in *Wave Propagation and Underwater Acoustics*, (ed. J.B. Keller & S. Papadakis), Springer-Verlag, Berlin, 153-223
- Malichewsky P. 1987,
Surface waves and discontinuities, Akademie-Verlag/Elsevier, Berlin
- Malin P.E. 1980,
A first order scattering solution for modelling elastic wave codas - I the acoustic case, *Geophys. J. R. astr. Soc.* **63**, 361-380
- Marcuse D. 1974,
Theory of dielectric optical waveguides, Academic Press, New York
- Maupin V. 1988,
Surface waves across 2-D structures: a method based on coupled local modes, *Geophys. J. Int.* **93**, 173-185
- Maupin V. & Kennett B.L.N. 1987,
On the use of truncated modal expansions in laterally varying media *Geophys. J. R. astr. Soc.* **91**, 837-851
- Spakman W. 1989,
Upper mantle delay time tomography, Ph.D. thesis, University of Utrecht
- Wang C-Y. & Herrmann R.B. 1988,
Synthesis of coda waves in layered medium, *Pageoph* **128**, 7-42
- Wu R-S. & Aki K. 1988,
Introduction: seismic wave scattering in three-dimensionally heterogeneous Earth, *Pageoph* **128**, 1-6

Figure Captions:

1. ARANDA reference model and the vertical component of displacement for the first 18 Rayleigh modes at 1 Hz.
2. Variation of the scattering loss factor ${}_sQ_m^{-1}$ for different Rayleigh and Love modes at 1 Hz as a function of horizontal correlation length in the crust. Rayleigh waves are indicated by solid triangles and Love waves by open diamonds.
3. Variation of the energy loss with distance b_m with mode number for different horizontal correlation lengths in the crust. Rayleigh waves are indicated by solid triangles and Love waves by open diamonds.

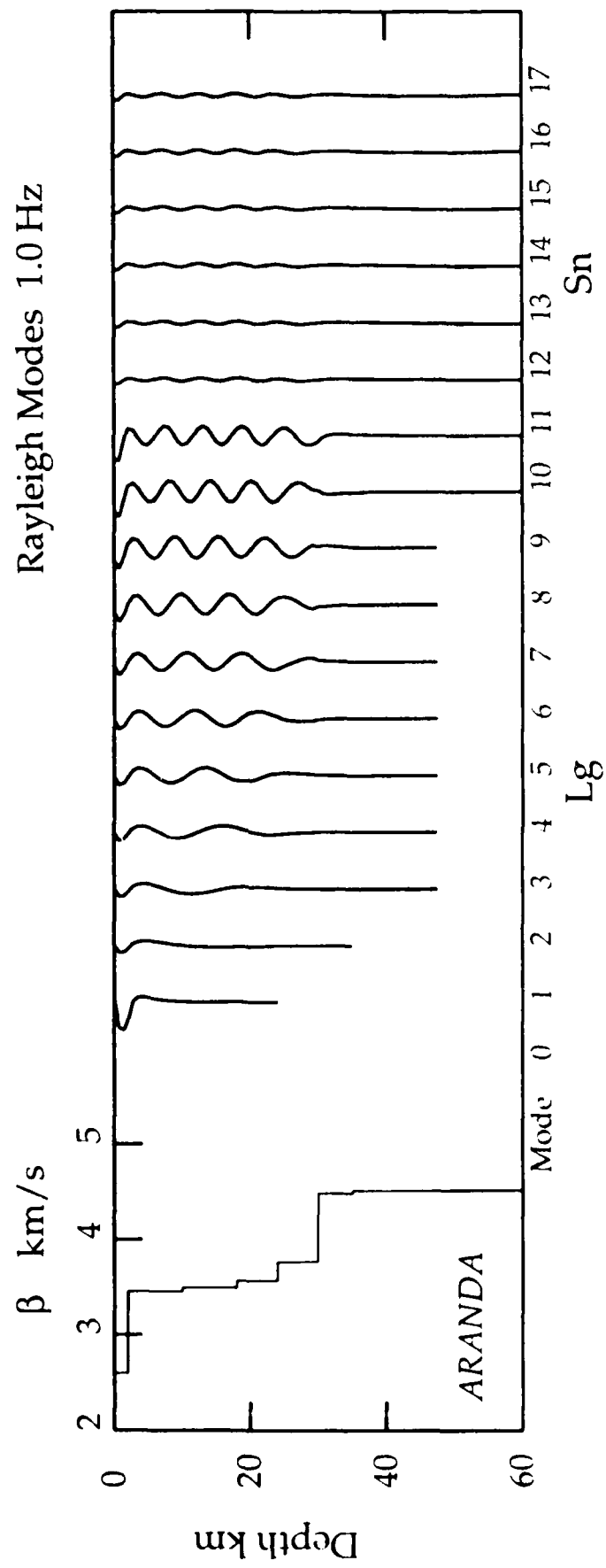


FIGURE 1

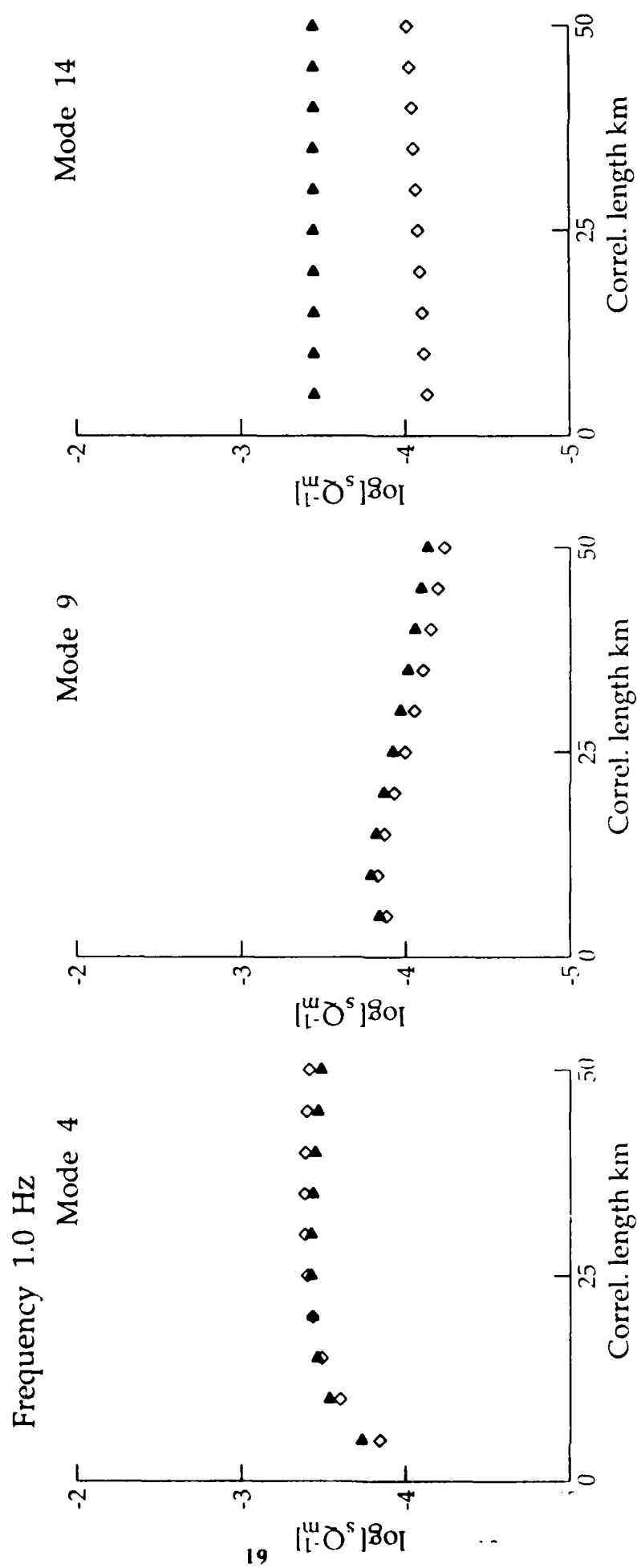


FIGURE 2

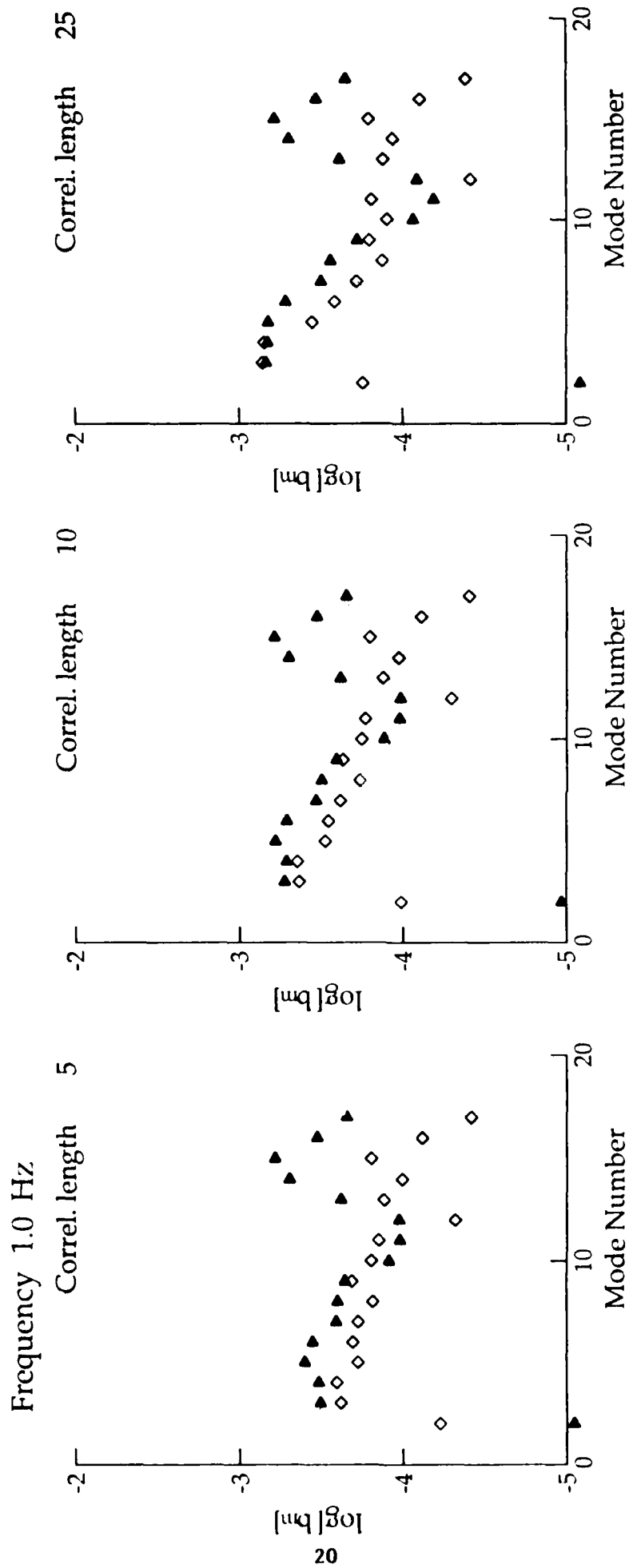


FIGURE 3

THE EFFECT OF THREE-DIMENSIONAL STRUCTURE ON LG PROPAGATION PATTERNS

M.G. Bostock and B.L.N. Kennett
*Research School of Earth Sciences,
Australian National University,
GPO Box 4, Canberra, ACT 2601, Australia*

SUMMARY

The Lg phase is one of the most prominent features of many regional seismograms and its amplitude is known to be sensitive to major changes in crustal structure. This sensitivity can be exploited to investigate the nature of crustal heterogeneity, but also reduces the utility of the analysis of Lg phases for characterizing seismic sources.

The method of ray diagrams, based on the constructive interference of multiple S reflections, gives a visual measure of the interaction of guided wave trains with variations in crustal structure. The technique is extended to three dimensional heterogeneity and by representing the S ray systems in plan view through their basement reflection points, a semiquantitative measure of the disruption of Lg at different phase velocities can be made. In addition, the tilt of the ray systems can be used as an indication of the degree of interconversion between Rayleigh and Love wave energy.

Two simple crustal models are examined to investigate the effects of oblique incidence and transverse topographic gradients on multiple S reflections using ray diagrams. The method is then applied to several real earth models of the crust in central Asia using topographic data and assuming isostasy. Interpretations of the ray diagrams for paths across the major tectonic features compare well with many of the observations from previous studies (Ruzaikan et al., 1977; Ni and Barazangi, 1983), and suggest that the gross characteristics of Lg propagation can be attributed to the shape of the crustal wave guide.

INTRODUCTION

The Lg phase propagates in the earth's crust and dominates seismograms at regional distances. It is characterized by frequencies between 1 and 5 Hz and is often of extended duration. Although the wavetrain does not exhibit a clear onset, it builds to an amplitude maximum at a group velocity close to 3.5 km/s and may, in regions of sedimentary cover, carry significant energy to group velocities of 2.8 km/s. Recently considerable attention has focussed on the signature of the Lg wavetrain in deducing crustal morphology and as an aid to nuclear discrimination;

in both instances an understanding of the manner in which Lg interacts with zones of crustal heterogeneity is a primary objective.

The sensitivity of Lg to major variation in crustal structure has been widely noted; early studies revealed that as little as 100 km of intervening oceanic crust is sufficient to eliminate Lg propagation across ocean basins (Ewing et al., 1957). The character of Lg propagation across certain continental areas where the crust is known to be complex, most notably central Asia, has been used to constrain structure and provide insight into the operative tectonic processes (Ruzaikan et al., 1977; Kadinsky-Cade et al., 1981; Ni and Barazangi, 1983). These studies have involved the interpretation of short period seismograms to qualitatively characterize broad geographical zones in terms of their amenability to Lg propagation. More quantitative analysis is possible with increased raypath coverage; Kennett et al. (1985) inverted a comprehensive set of Lg attenuation data for paths in NW Europe to delineate crustal heterogeneity in the North Sea region.

Two different descriptions, which are equivalent in the case of a stratified medium, can be made for the physical nature of Lg in a heterogeneous crust: the phase can be considered as a sum of higher mode surface waves whose energy is mostly confined to the crust, or alternatively, as the result of constructive interference between S-waves multiply reflected between the free surface and the crust-mantle boundary. For heterogeneous zones, two methods have evolved to model the propagation of Lg based on these different views of the propagation process.

The coupled mode technique (Kennett, 1984) is based on the modal interpretation and solves the boundary value problem exactly; however in zones of exaggerated heterogeneity and variable layer thickness it can become computationally intractable. The method of ray diagrams is a simpler means of assessing the propagation of Lg in a semi-quantitative manner and is not limited by the same circumstances. It involves tracing a set of rays at fixed slowness through a crustal layer of variable thickness, and the disruption in the pattern of the ray system (or equivalently the reflection points) is used as a measure of modal coupling and scattering. Kennett (1986) compared the visually descriptive ray diagrams with coupled mode solutions for simple 2D earth models and established the validity of the ray based technique.

Our objective in this study is to extend Kennett's (1986) approach to 3D heterogeneity. After describing a basis for the interpretation of ray diagrams we examine two simple earth models and investigate the effects of oblique incidence on Lg propagation. We then shift our focus to a central Asia to compare our predictions of Lg propagation with observations from previous studies.

THE RAY DIAGRAM METHOD

Kennett (1986) provided a basis for the interpretation of ray diagrams by comparing them with coupled mode solutions for a suite of 2D earth models and noting some simple and consistent relationships. The coupled mode technique describes Lg as a sum of modal eigenfunctions, associated with a laterally homogeneous reference model, and weighted by modal coefficients which vary with position. In 2D these coefficients satisfy a system of non-linear differential equations which can be solved exactly in principle. In practice, however, the method becomes computationally intractable in zones of exaggerated heterogeneity (greater than 5% velocity perturbation or 2 km in boundary perturbation for 1 Hz waves) as consideration of intermode coupling among an increasing number of modes becomes necessary. Maupin (1988) has made use of coupled local modes to give a more direct treatment of variable boundaries; however changes in position of interfaces require extensive recomputation of modal eigenfunctions. Ray diagrams, in contrast, are most useful where the shape of the crustal waveguide varies and become more difficult to interpret if a non-uniform velocity structure is imposed. The analysis of Kennett (1986) included models amenable to both methods, and demonstrated the close correspondence between the coupled mode and ray diagram results.

The correspondence between the two methods is most easily explained by noting that for a given frequency the Lg wave train will comprise a finite number of modes. Each mode is characterized by a specific phase velocity which can be associated with an S-wave ray system at a particular angle to the vertical. This suggests that the geometrical regularity of a system of rays launched in some systematic fashion may be used as an indication of the coherence and sustained amplitude of a given mode in addition to a measure of the S-wave constructive interference condition.

At fixed frequency, the angle of S-wave propagation to the vertical increases as the phase velocity decreases. For a given angle to the vertical, determined by the choice of incident mode, the behaviour after interaction with heterogeneity can be conveniently characterized by the spread in propagation angles. Increased angles to the vertical correspond to conversion to lower order modes with the change in angle proportional to the spread in intermode coupling. Similarly steeper propagation corresponds to conversion to higher order modes. In general waves incident with higher phase velocities tend to show a larger variation in ray angle after transmission through the heterogeneity due to increased multiple reflections in the complex zone. In those cases where caustics develop in the ray diagrams the equivalent coupled mode solutions show considerable variation in the amplitudes of the modal coefficients with position.

The crustal models presented in the following analysis exhibit 3D heterogeneity. It is no longer possible to construct ray patterns from a system of plane waves in cross section as in the 2D case. Rather, we have resorted to plan views representing surface/Moho topography via contours and consider a single point source emitting rays at a given angle to the vertical (modal slowness) through a range of azimuths. Regularity in plotted surface/Moho reflection points and the horizontal projection of raypaths provide a measure of the constructive interference condition in a manner analogous to the pattern of 2D ray systems considered by Kennett (1986). An added feature of the 3D analysis is that we are able to examine the way in which the wavefronts tilt as they encounter features oblique to the line of propagation. This 'ray tilt' will lead to a rotation of the polarization of the S waves between the vertical and horizontal planes. As a result energy having an explosive source lying purely in a vertical plane (i.e. represented solely by higher mode Rayleigh waves), may after encounter with the heterogeneity have some component in the horizontal plane, which would be interpreted as conversion to higher mode Love waves. Zones of the model where the ray patterns exhibit a consistent change in tilt can be expected to produce significant conversion.

CRUSTAL MODELS

We have investigated Lg propagation in two simple models of crustal structure and in reconstructions of the crustal structure in central Asia based on world topography data, using ray diagrams. All of these models are characterized by simple variation in surface and basement (Moho) topography; physical properties remain constant throughout the crust.

Although a more sophisticated analysis incorporating crustal stratification might be implemented with slight modification, this has not been done for several reasons. Ray diagrams are at best semiquantitative and are meant to provide a simple means of assessing Lg propagation through crustal structure. Moreover, although the shape of the crustal waveguide is the dominant factor influencing Lg, other factors such as small scale heterogeneity in crustal velocities cannot be entirely ignored. In addition, when we construct a crustal model from just the surface topography we are forced to make a number of assumptions which may not be well founded, and so a very complex model is not warranted.

Shear velocities of 3.5 km/s and 4.6 km/s were chosen to characterize the crust and upper mantle. For a given phase velocity rays were traced away from a point source with multiple reflections at the surface and the Moho. The character of the propagation patterns are indicated by plotting a plan section of the rays and marking the reflection points at the Moho. The magnitude of changes in ray tilt

are illustrated on separate ray diagrams by 'tics' located perpendicular to the ray at surface and Moho reflection points. This display enables the regular character of the Lg wavefront in the homogeneous regions to be compared with the disrupted pattern after passage through the heterogeneity.

SIMPLE CRUSTAL STRUCTURES

In this section we consider two structures for which the surface and Moho topography are represented as piecewise smooth surfaces and the zones of variation are of limited spatial extent. The ray patterns resulting from these simple configurations are intended to demonstrate the effects of simple changes in topography and aid in the interpretation of more complicated ray diagrams for central Asia presented in the following section.

Crustal Thickening

The first case is of a linear mountain chain and a section across the model along the profile A-B is shown. Ray diagrams were examined for the full range of phase velocities associated with Lg propagation (3.5 to 4.6 km/s) and several general features were observed to characterize the wavefield emergent from the structure. In figure 1 we show the ray diagrams for phase velocities of 3.7 km/s and 4.3 km/s which illustrate the major features of the wavefield. Perpendicular to the axis of the range we note a central corridor marked by a continuous and regular arrangement of bottom reflection points and little variation in ray density with azimuth (even though the angle to the vertical is increased). This corridor is flanked by zones of alternating high and low ray density as the angle between the axis and the wavefront increases.

For particular combinations of source location and phase velocity, some zones may exhibit regularity in both ray density and reflection pattern, and, therefore represent windows through which a significant fraction of the initial Lg wave energy can pass. As ray incidence becomes increasingly oblique to the mountain range axis, rays become trapped within the range and few rays penetrate the structure to the crust outside. Thus we might expect linear zones of crustal thickening to act as lateral waveguides, especially for earthquakes in close proximity.

Rays which impinge on the surface at angles to the surface normal less than the critical angle defined by Snell's law will undergo transmission into the upper mantle and are distinguished by filled diamonds marking the Moho reflection points. Kennett (1986) notes that this situation represents a coupling to modes constituting the Sn phase. As observed in the equivalent 2D model (Kennett, 1986), refraction after emergence from the mountain range occurs most prominently near the maximum phase velocity for Lg (above 4.4 km/s). The

distribution of these emergent refracted rays is dependent on source location and displays little azimuthal preference. In figure 2 we show the polarization of the S rays for the same phase velocities as figure 1 by means of 'tics' which show the projection onto a horizontal plane of waves which left the source with energy confined to the vertical plane. Figure 2 reveals that changes in ray tilt develop in the zones flanking the central corridor where topographic gradients become increasingly transverse to the direction of propagation. Thus we expect some transfer of energy between vertical and horizontal planes which would be interpreted as a conversion between Love and Rayleigh waves. This feature introduces further complexity to what is already seen to be a very complicated wavefield.

Crustal Thinning

The second case represents a region of crustal thinning simulating a zone of localized crustal extension and is designed to illustrate the effect of local transverse gradients in topography. In cross section it is characterized by flanks rising from 30 km to 20 km depth to a plateau at the Moho; its configuration in the horizontal plane is elliptical. Kennett (1986) noted in an analogous 2D model that constriction of the crustal waveguide had a more severe effect on transmission of Lg than increase in thickness. This is also apparent in the 3D model (see figure 3) where we again display ray patterns for phase velocities of 3.7 and 4.3 km/s. The effect of the crustal thinning is to steer rays away from the angular window defined by the lateral boundaries of the structure and the source position. This effect, due to the presence of strong gradients in topography oblique to the ray path, gives rise to caustics in the ray pattern, and is particularly noticeable at higher phase velocities as in figure 3c. The constriction of the waveguide can also lead to waves travelling across the top of the structure being refracted into the mantle, and hence the low density of emergent rays is complemented by an additional energy loss through conversion to Sn.

In figure 4, we show the ray tilt representation of the S wave polarisation for this crustal thinning model. The three dimensional character of the crustal heterogeneity leads to polarization changes for a larger proportion of the rays than for the linear mountain chain of figure 2. At the higher phase velocities the polarization rotation is particularly strong at the lower margin of the heterogeneity where the gradients in Moho topography are nearly transverse to the ray path.

CENTRAL ASIA

The propagation of Lg is of considerable interest in determining the nature of the earth's crust in central Asia. Extreme variations in topographic relief over the region shown in figure 5 testify to a complex and heterogeneous waveguide. To the

north of the Indian shield (average elevation 200 m), the Himalayas rise above 6000 m and form the southern perimeter of the Tibetan Plateau, a remarkable physiographic feature covering some $2.5 \times 10^6 \text{ km}^2$ and characterized by an average elevation of about 5000 m. The Tarim Basin separates the Tibetan Plateau to the northwest from a second major mountain range, the Tien Shan.

The pattern of Lg propagation varies significantly over the region (see Figure 5; Ruzaikan et al., 1977; Ni and Barazangi, 1983). Specifically, Lg propagates very efficiently across the more tectonically stable areas: the Indian Shield, Tarim Basin and Eurasian Platform. The phase is also present for paths along the Himalayas and Tien Shan (although less clear); however it is generally weak or absent for paths crossing the Tibetan Plateau. These observations bear important implications for the interpretation of the tectonic evolution of the region. Additional interest in the nature of Lg propagation across central Asia is prompted by the presence of both Soviet and Chinese nuclear test sites. The prominence of Lg waves on regional seismograms makes the phase valuable for the detection of small events, but the sensitivity of Lg to the variation in crustal structure across the region reduces its utility for discrimination and a better knowledge of the effects of heterogeneity on propagation is necessary.

Surface topography for the following models of the crustal structure was constructed by smoothing (25 point average) digital elevation data supplied at 5' intervals from a world topography data base (ETOPO5 compiled by the National Geophysical Data Center, Boulder, Colorado). The depth to the Moho was determined by further smoothing (81 point average) of the surface topography and assuming 90% isostatic compensation occurs within the crust. This assumption, although simplistic, is thought to be reasonable within the limitations of the ray method for a uniform crust.

The choice of a suitable phase velocity in representing Lg propagation in the real earth by ray diagrams deserves some discussion. In typical crustal situations the higher modes constituting Lg propagate at a range of phase velocities. Within this range certain modes within loosely defined phase velocity windows will dominate at different group velocities. The onset of Lg on short period seismograms is determined by modes at phase velocities of 3.4 to 3.6 km/s (i.e. crustal shear velocities). The amplitude maximum which follows is usually characterized by slightly greater phase velocities between 3.7 and 4.0 km/s whereas typical values for the late-arriving Airy phases reach 4.3 to 4.5 km/s. These latter phases play an important role in determining the character of regional seismograms especially in zones of heterogeneity where conversion to Sn is significant. An additional factor to consider is the effect of velocity variation within the crust. Although the shape of the crustal wave guide is a major

influence on Lg propagation, a positive crustal velocity gradient in depth will have some effect on the configuration of the ray systems, flattening them and extending the distances between reflection points. In our simple single layer crustal model this is equivalent to a decrease in phase velocity. By examining the horizontal distance between reflections for single layer and multilayered crustal models based on equivalent total traveltime, we note that the actual magnitude of the decrease is only significant at very low phase velocities (i.e. within a few percent of the crustal shear velocity). Therefore in modelling effects on the early arrivals it may be appropriate to compensate by reducing the phase velocity parameter for crustal models of uniform velocity. As the overall character of the Lg wavetrain is dependent on modal contributions at a full range of phase velocities we have attempted to select model values which both illustrate the general disruption in Lg propagation due to changes in the shape of the crustal wave guide, and are pertinent to observations made in previous studies.

Although the major topographic features in the area exist at a larger lateral scale than those in the two simple structural models, the ray patterns can nonetheless be quite sensitive to source position. Attempts have been made in the following analysis to restrict interpretation to those features which remain stable over small changes in source location.

Semipalitinsk

For our first study, we examine Lg propagation in the vicinity of the Soviet nuclear test sites located in eastern Kazakhstan, approximately 400 km northeast of Lake Balkhash, near Semipalitinsk. Seismic stations at Novosibirsk (NSB) and Talgar (TLG) are shown as triangles to the north and southeast of the source at Semipalitinsk in figure 6. The rather moderate and consistent topography over much of this region permits an assessment of our modelling procedure in what is presumably a relatively uniform portion of the crustal waveguide.

The ray diagrams shown in figure 6 are generated at a phase velocity of 4.3 km/s since anomalous propagation patterns are most pronounced at velocities above 4.0 km/s. The character of the patterns can be discussed in terms of three broad geographic zones. To the north, elevation decreases very gradually, consequently the ray patterns are very regular and experience a slight increase in phase velocity with distance from the source. For initial phase velocities above 4.45 km/s, this results in energy loss through conversion to Sn, however Lg transmission through this zone for lower phase velocities is likely to be extremely efficient. It is worth noting that Lg recorded at NORSAR would propagate through this region. The general topography in Kazakhstan to the west of the test sites remains relatively constant although there are minor local fluctuations. Ray patterns in this zone are slightly less coherent but still suggest efficient Lg

transmission. The Tien Shan and Altai chains, mountain ranges rising over 5000 m, border the region to the south and east. Changes in relief are extreme and ray patterns are severely distorted especially at higher phase velocities. The character of Lg recorded at stations along these paths beyond the mountainous regions will undoubtedly be very complex; there is likely to be considerable variability with position and significant attenuation due to conversion to Sn and scattering.

In the corresponding ray tilt diagram (figure 6b), as expected, rays passing through mountainous areas, where elevation gradients transverse to direction of propagation are likely to be most pronounced, show the greatest degree of tilt. Also of interest and perhaps of greater significance to the interpretation of source parameters from regional seismograms are the tilt patterns to the north and west. The slight but relatively uniform north-south gradient in elevation over these areas causes a very regular and obvious tilt pattern in eastern Kazakhstan; whereas north of Semipalitinsk, where rays lie subparallel with the gradient, virtually no tilt is evident. This implies that Lg recorded at stations within these two distinct windows might differ markedly in the relative energy distribution among transverse, radial and vertical components. An explosive source at Semipalitinsk generating shear energy primarily on vertical and radial components might nonetheless give rise to Lg in south and central Europe with a dominant transverse component, while Lg recorded further north, at NORSAR for example, would retain much of its Rayleigh-type energy.

Eastern Tien Shan

We now turn our attention to a more complicated region comprising the Tarim Basin, the Altai chain, much of the Tien Shan and the northern fringe of the Tibetan Plateau. Ruzaikan et al. (1977) noted that earthquakes in the eastern Tien Shan radiate clear Lg phases to station NSB whereas at TLG the phase is often very weak.

Figures 7a displays the reflection patterns at phase velocities of 3.7 and 4.3 km/s for a source in this area of interest. The lower velocity diagram reveals a more consistent and uniform ray pattern at NSB than TLG even though the former station is some 500 km further from the source. This observation would tend to support the explanation of Ruzaikan et al. that the difference between signal at TLG and NSB results from different path lengths within the complicated structure of the Tien Shan. The higher phase velocity used to generate the diagram in figure 7b has produced a more severely distorted pattern due to an increased number of multiple reflections. Several specific points are worthy of note. Although the ray density and patterns are still somewhat consistent at NSB, rays in the vicinity of TLG are funnelled into two arms of the Tien Shan in a manner similar to that described for the simple crustal thickening model. Rays in

the northern subsidiary arm rapidly lose energy through transmission to the mantle whereas those in the southern arm remain trapped. This funnelling behaviour first becomes apparent at a phase velocity of 3.9 km/s and suggests that the main arm may act as a lateral wave guide, trapping and guiding energy within a zone of relatively narrow width (100-200 km). The observations of Ruzaikan et al. would tend to suggest that the station at TLG may lie just outside the borders of such a guide.

Ni and Barazangi (1983) note that Lg propagation in the Himalayas is less efficient across strike than along strike. This and studies in other mountainous regions (e.g. along the Andes [Chinn et al., 1980]) suggest that mountain chains may play an important role in influencing patterns of Lg propagation by focussing and guiding energy along quasi-linear zones of increased crustal thickness.

Kunlun

Lg propagation across the Tibetan Plateau has been the focus of many studies into the nature of the crust near the continental collision margin. Several authors have noted the absence of Lg for paths crossing the plateau and the peculiar pattern of propagation for sources within and on its boundaries. In the latter case there appear to be well defined geographic boundaries to effective propagation, notably the 36° line of latitude to the north (Ruzaikan et al., 1977) and the Indus Tsangpo suture to the south (Ni and Barazangi, 1983). Lg is rarely recorded from sources within these boundaries.

Ray diagrams at phase velocities of 3.7 and 4.3 km/s for a source just above the northern boundary in the Kunlun are shown in figure 8. At higher phase velocities (figure 8b), a large proportion of rays are confined to the plateau by lateral reflection along its borders, and those which do escape have undergone so many vertical reflections at subcritical angles as to be of no significance. In contrast, diagrams at lower phase velocities maintain regular ray patterns through most of the area. Certainly, patterns are fairly regular across the Tarim Basin where propagation is observed to be reasonably efficient (Ruzaikan et al., 1977). Ray systems emerging from the Himalayas are also fairly coherent but lose energy through transmission to the mantle. Our assumptions regarding the structure of the Moho are no longer valid in this region (see Molnar, 1988), where the crust is quite certainly not isostatically compensated; however a rapid transition in crustal thickness does exist and should complicate Lg propagation in a similar fashion. Efficient propagation across the Tarim Basin for this particular source location ceases above a phase velocity of approximately 4.0 km/s where the effects of source position, with phase velocity, relative to the crustal transition zone (discussed by Kennett [1986]) become manifest. The ray diagram approach agrees with suggestions of previous authors (Ruzaikan et al., 1977) that the absence of Lg along

paths crossing the Tibetan Plateau is due to changes in the crustal waveguide, notably constriction along its margins. Discriminating between natural and artificial sources from locations within Tibet using Lg is rendered exceedingly difficult, if not impossible, by this propagation effect.

DISCUSSION

We have seen how the simple device of ray diagrams can be extended to three dimensions and used to provide insight into the nature of the interaction of the Lg phase with heterogeneity. The interpretation of ray diagrams for crude constructions of the crust in central Asia, based on isostatic compensation, agree with observations from previous studies and indicate that much of the general character of Lg propagation can be attributed to changes in the shape of the crustal waveguide. Zones of regular reflection patterns, such as those in Kazakhstan for sources at Semipalitinsk, characterize a waveguide of uniform thickness and generally correspond to zones of efficient Lg propagation. Rapid decreases in crustal thickness, as for example the margins of the Tibetan Plateau, form boundaries which severely restrict Lg propagation especially at higher phase velocities. Where such changes occur over narrow, quasi-linear zones of crustal thickening (mountain ranges such as the Tien Shan, or the Himalayas), the possibility exists for the development of lateral wave guides. The three dimensional ray representation also affords a simple means of assessing the transfer of energy between horizontal and vertical planes through examination of the change in ray tilt with propagation. Over areas with transverse gradients in surface and Moho topography oblique to the direction of propagation, we expect there to be significant energy transfer corresponding to an interconversion between Love and Rayleigh modes. This feature may be of some value in separating propagation and source effects in the problem of nuclear discrimination where energy at the explosive source is predominantly P-SV.

By incorporating detailed information on gravity anomalies and crustal structure where these are available it may be possible to further improve the accuracy of the technique. However, caution should be exercised not to over extend the limits of its usefulness; internal crustal structure undoubtedly plays a significant and complicated role in the propagation of Lg as is made evident in its effect on dispersion. The value of the ray approach lies in assessing the main effects of crustal shape on Lg.

ACKNOWLEDGEMENT

This work was supported in part by the Advanced Research Projects Agency of the U.S. Department of Defense under Grant AFOSR-89-0330.

REFERENCES

- Chinn D., Isacks B., and Barazangi M. (1980) High-frequency wave propagation in western South America along the continental margin, in the Nazca plate, and across the Altiplano, *Geophys. J. R. astr. Soc.*, **60**, 209-244.
- Ewing M., Jardetsky W.S. and Press (1957) *Elastic Waves in Layered Media*, McGraw-Hill, New York.
- Kadinsky-Cade K., Barazangi M., Oliver J. and Isacks B. (1981) Lateral variations of high-frequency seismic wave propagation at regional distances across the Turkish and Iranian Plateaus, *J. Geophys. Res.*, **86**, 9377-9396
- Kennett B.L.N. (1984) Guided wave propagation in laterally varying media, I. Theoretical development, *Geophys. J. R. astr. Soc.*, **79**, 235-255
- Kennett B.L.N. (1986) Lg waves and structural boundaries, *Bull. Seism. Soc. Am.*, **76**, 1133-1141
- Kennett B.L.N., Gregersen S., Mykkeltveit S., and Newmark S. (1985) Guided wave propagation in laterally varying media - II. Lg waves in north-western Europe, *Geophys. J. R. astr. Soc.*, **79**, 257-267
- Maupin V. (1988) Surface waves across 2D structures: a method based on coupled local modes, *Geophys. J. R. astr. Soc.*, **93**, 173-185
- Molnar P. (1988) A review of geophysical constraints on the deep structure of the Tibetan Plateau, the Himalaya and the Karakoram, and their tectonic implications, *Phil. Trans. R. Soc. Lond.*, **A 326**, 33-88
- Ni J. and Barazangi M. (1983) High frequency seismic wave propagation beneath the Indian shield, Himalayan Arc, Tibetan Plateau, and surrounding regions: high uppermost mantle velocities and efficient Sn propagation beneath Tibet, *Geophys. J. R. astr. Soc.*, **72**, 655-689
- Ruzaikan A. I., Nersesov I.L., Khalturin V.I. and Molnar P. (1977) Propagation of Lg and lateral variation in crustal structure in Asia, *J. Geophys. Res.*, **82**, 307-316

FIGURE CAPTIONS

Figure 1. Reflection patterns for a linear zone of crustal thickening, simulating a mountain range. A vertical cross section through A-B is shown in a), while b) and c) show ray diagrams generated at phase velocities of 3.7 and 4.3 km/s. Moho reflection points are plotted as open squares; filled diamonds indicate leakage out of the crustal waveguide.

Figure 2. Tilt patterns for the same configuration as figure 1. The effects of transverse gradients in topography are evidenced through the development of ray tilt at angles oblique to the axis of the zone of thickening. The magnitude of a tick corresponding to a 90° change in tilt is indicated.

Figure 3. Reflection patterns impinging on an elliptical zone of crustal thinning.

Figure 4. Tilt patterns for the same configuration as figure 3.

Figure 5. Central Asia. a) Topography and epicentral data from Ruzaikan et al. (1977) illustrating characteristics of Lg propagation to Talgar (TLG) are plotted as circles (Lg clear), diamonds (Lg weak), and triangles (Lg absent). b) Reference map identifying major topographic features in a) and relative positions of maps in figures 6, 7 and 8. Note that there is some systematic distortion in this and the following figures due to conversion from spherical to rectangular coordinates.

Figure 6. Reflection (a) and tilt (b) patterns for a source at the Soviet nuclear test site near Semipalatinsk at a phase velocity of 4.3 km/s. Rays in the northwestern quadrant represent energy propagating toward western Europe and show very regular patterns indicative of efficient Lg propagation. The slight but regular, north-south gradient in topography causes rays over the western half of the map in (b) to exhibit significant tilt, indicating a transfer of energy between horizontal and vertical planes. The magnitude of a tick corresponding to a 90° change in tilt is indicated.

Figure 7. Reflection patterns for a source in the eastern Tien Shan at phase velocities of (a) 3.7 km/s and (b) 4.3 km/s. Note distortion in reflection pattern eastwards toward Talgar in (a). Energy is guided into two arms of the Tien Shan near Talgar in (b), a feature which first becomes apparent at a phase velocity of 3.9 km/s.

Figure 8. Reflection patterns for a source in the Kunlun, northern Tibet at phase velocities of 3.7 and 4.3 km/s. Rays south of the Himalayas in (a) are characterized by increased phase velocities and widespread transmission into the mantle due to constriction of the crustal wave guide. The reflection pattern in (b) is highly distorted; both transmission into the mantle and reflection along the margins of Tibet contribute to very little coherent energy actually exiting through the crustal waveguide.

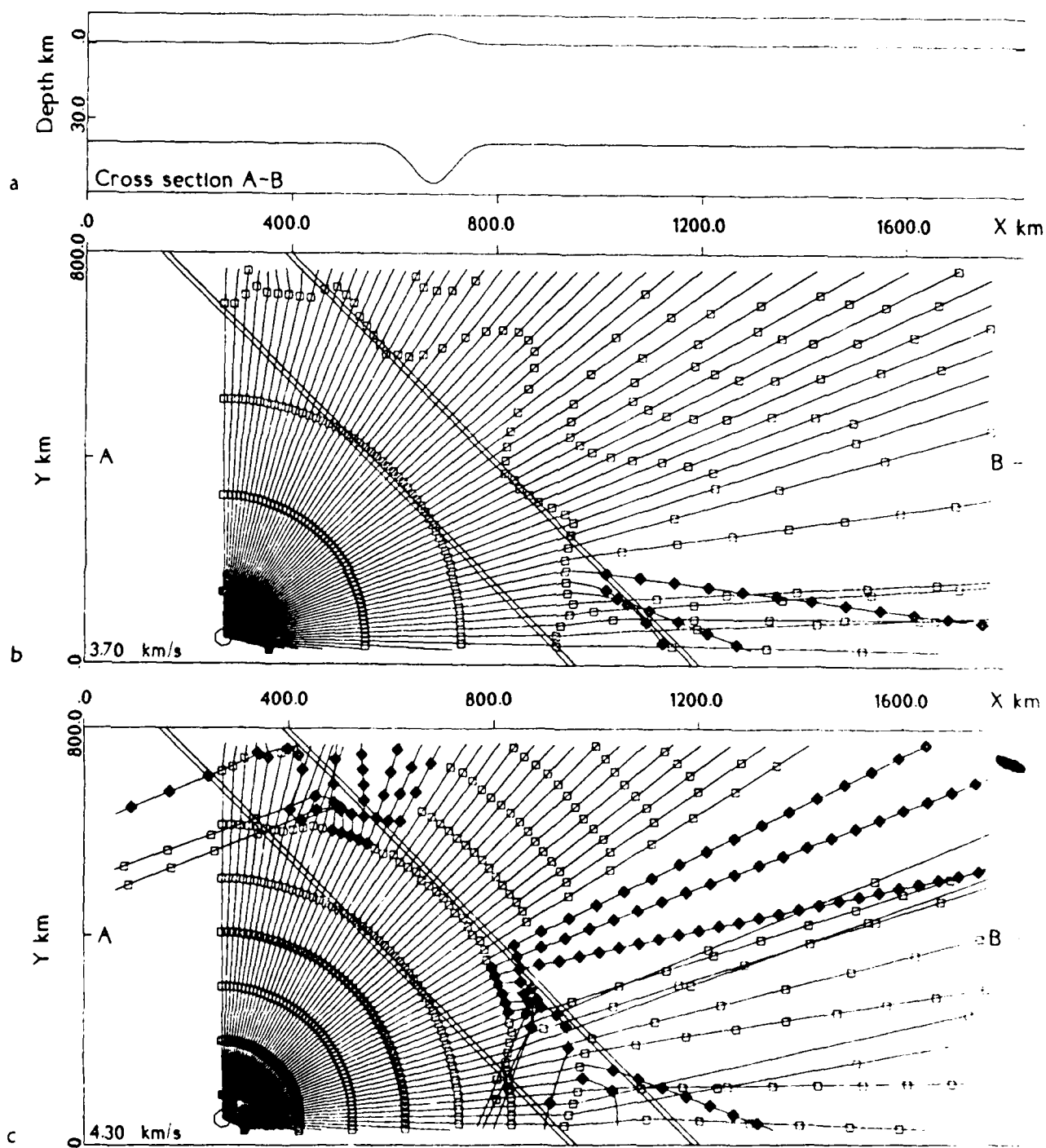


FIGURE 1

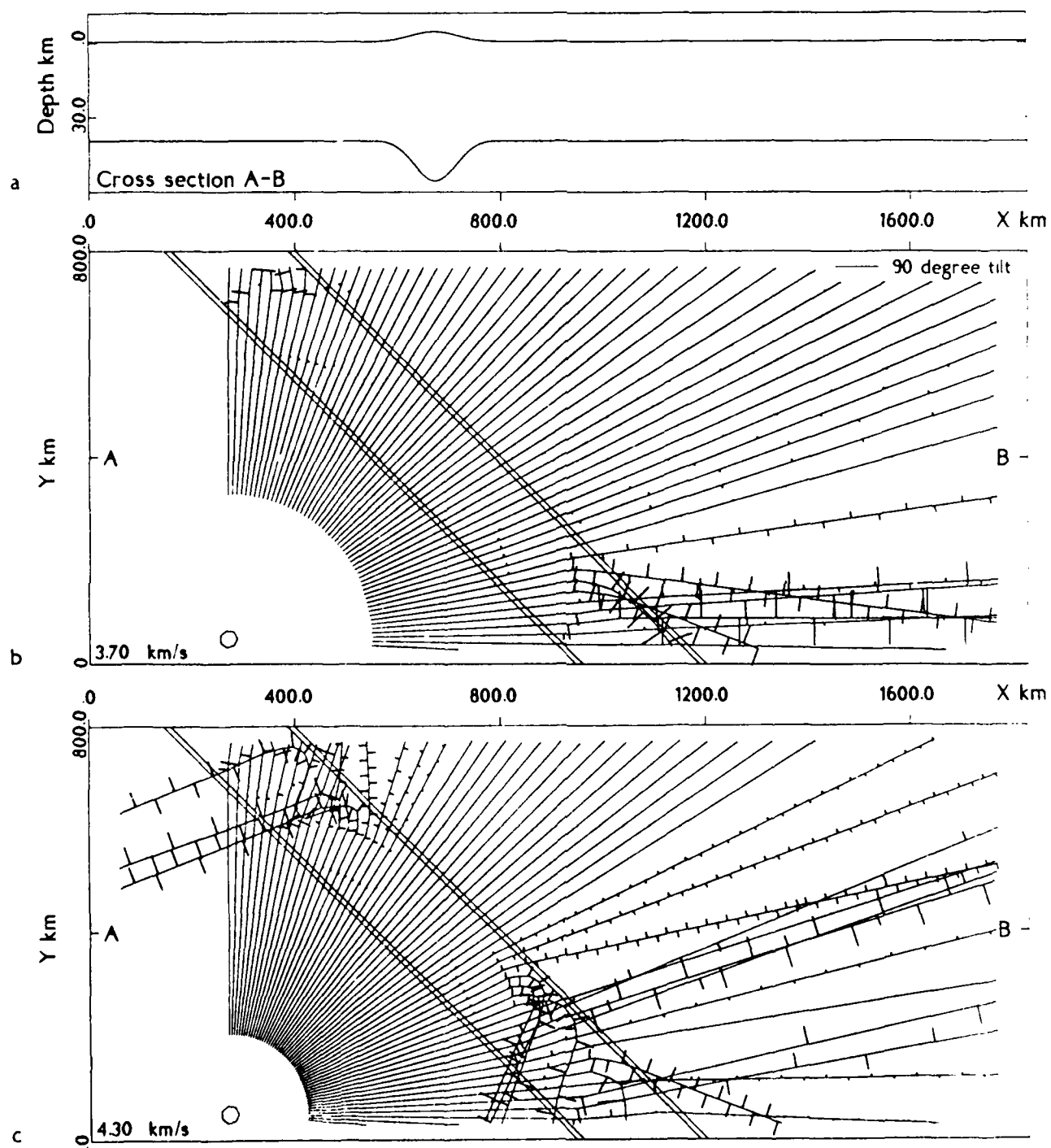


FIGURE 2

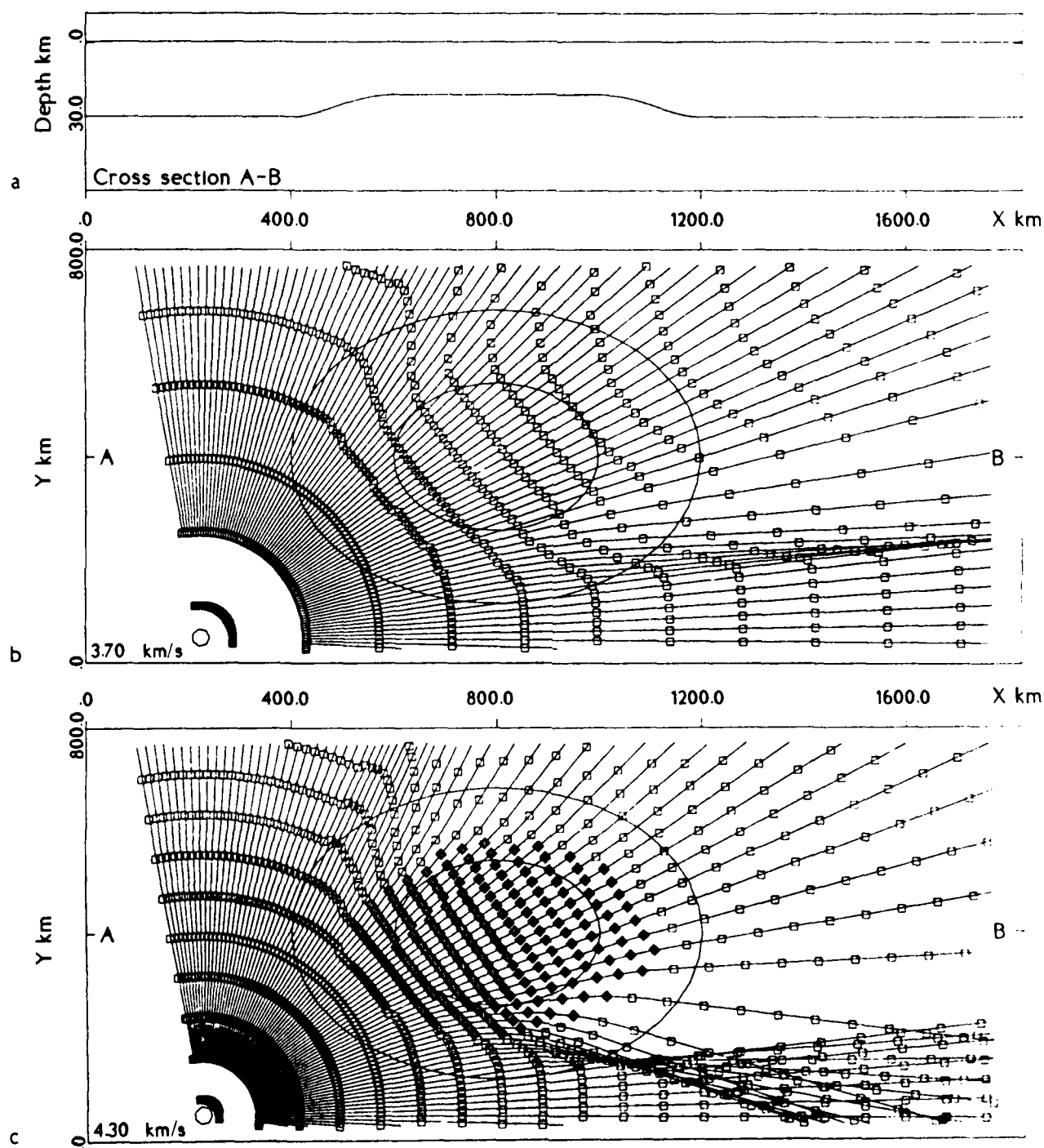


FIGURE 3

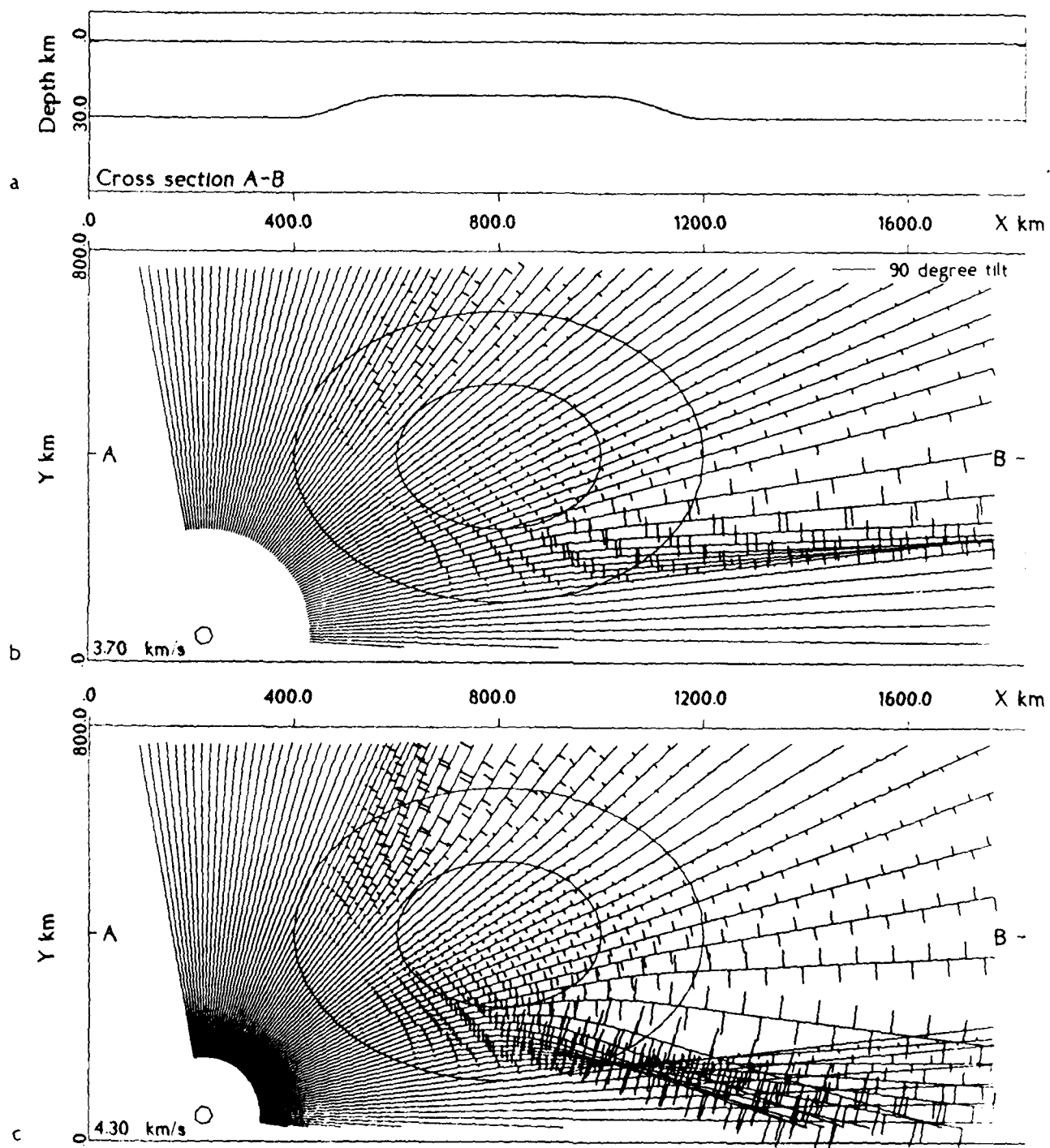
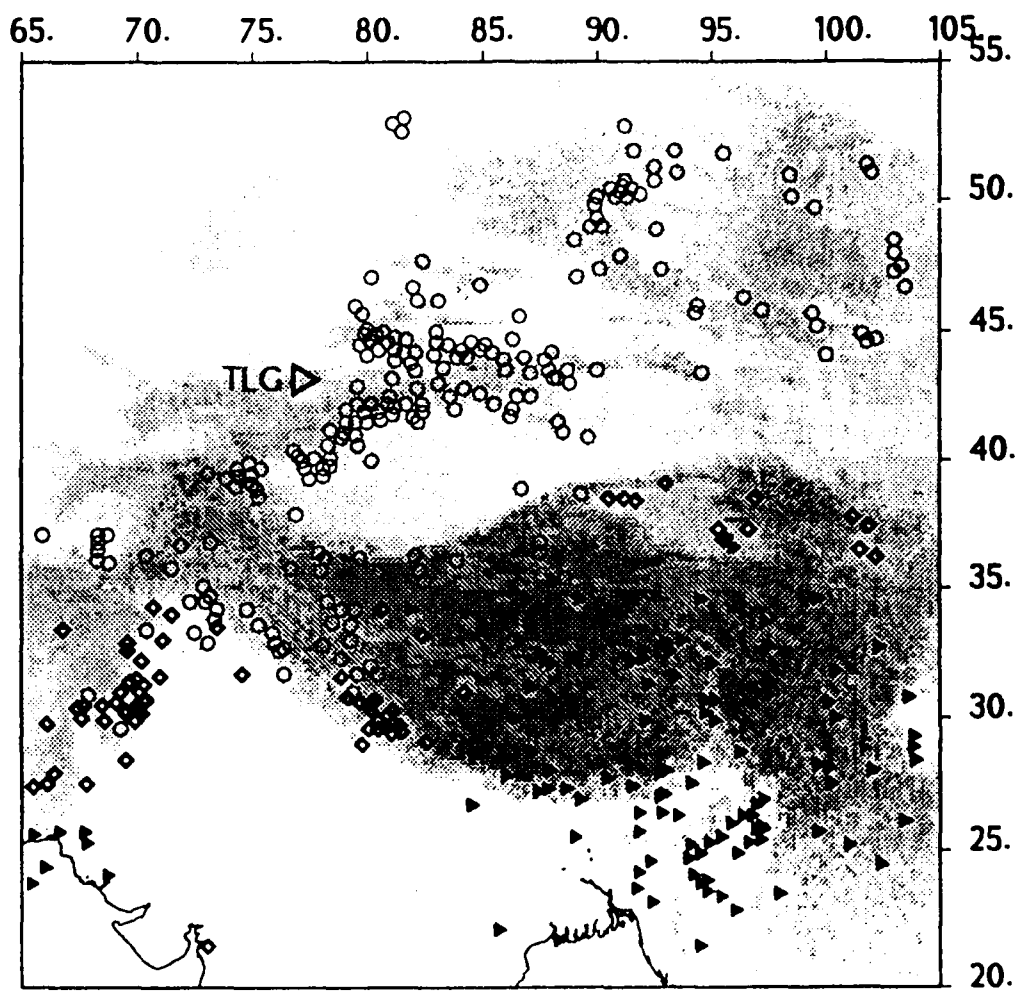
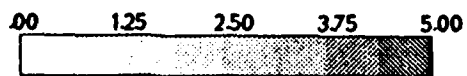
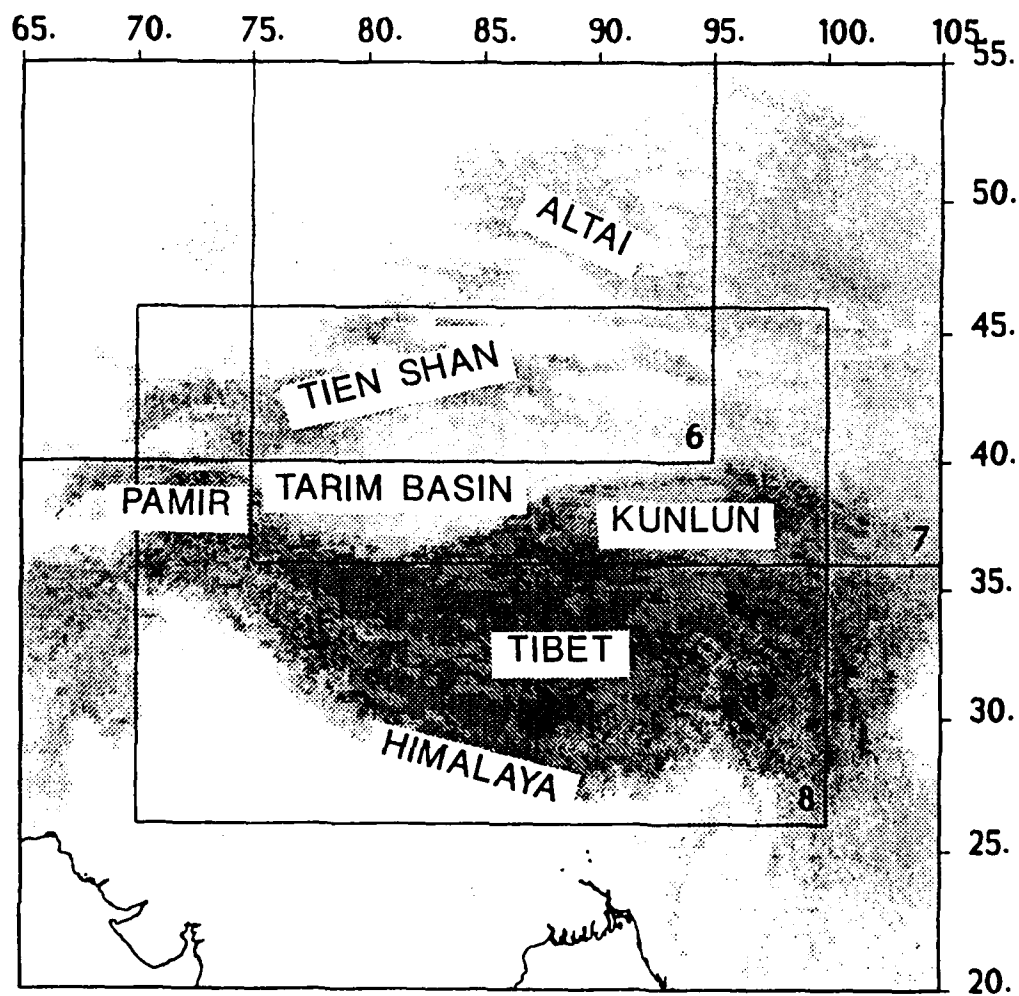


FIGURE 4



- a
- Lg clear
 - ◇ Lg weak
 - ▴ Lg absent

FIGURE 5 (a)



b Height km above msl

FIGURE 5 (b)

Lg Rayplot

Semipalitnsk

PHASE VELOCITY

4.30 km/s

WINDOW

65. - 95. E

40. - 60. N

SOURCE

79. E 50. N

SCALES

Horizontal - km as marked

Vertical - km above msl

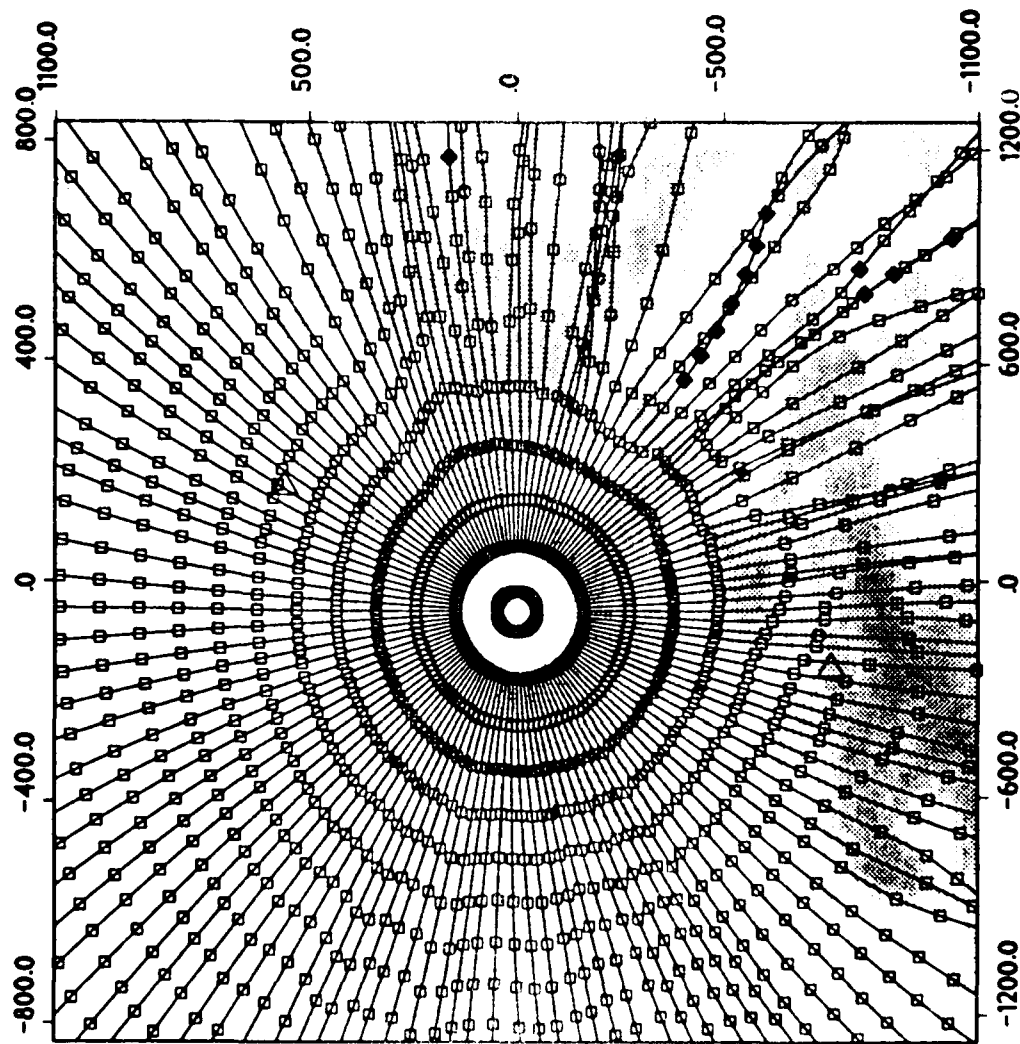
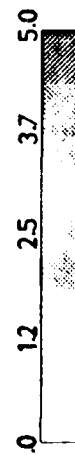


FIGURE 6 (a)

a

Lg Rayplot

Semipalitsinsk

PHASE VELOCITY

4.30 km/s

WINDOW

65. - 95. E

40. - 60. N

SOURCE

79. E 50. N

SCALES

Horizontal - km as marked

Vertical - km above msl



— 90 degree tilt

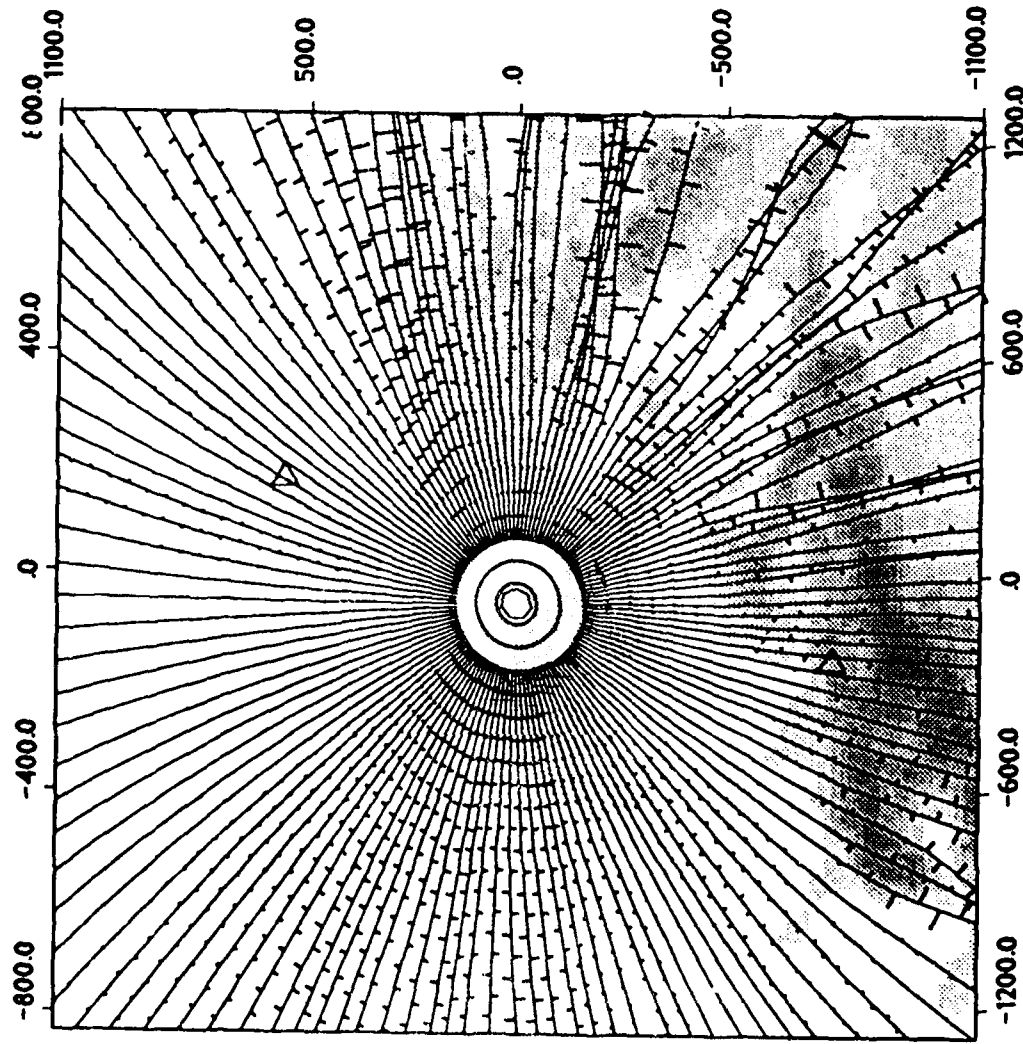


FIGURE 6 (b)

Lg Rayplot

E Tien Shan

PHASE VELOCITY

3.70 km/s

WINDOW

75. - 105.E

36. - 56. N

SOURCE

89. E 43. N

SCALES

Horizontal - km as marked

Vertical - km above msl

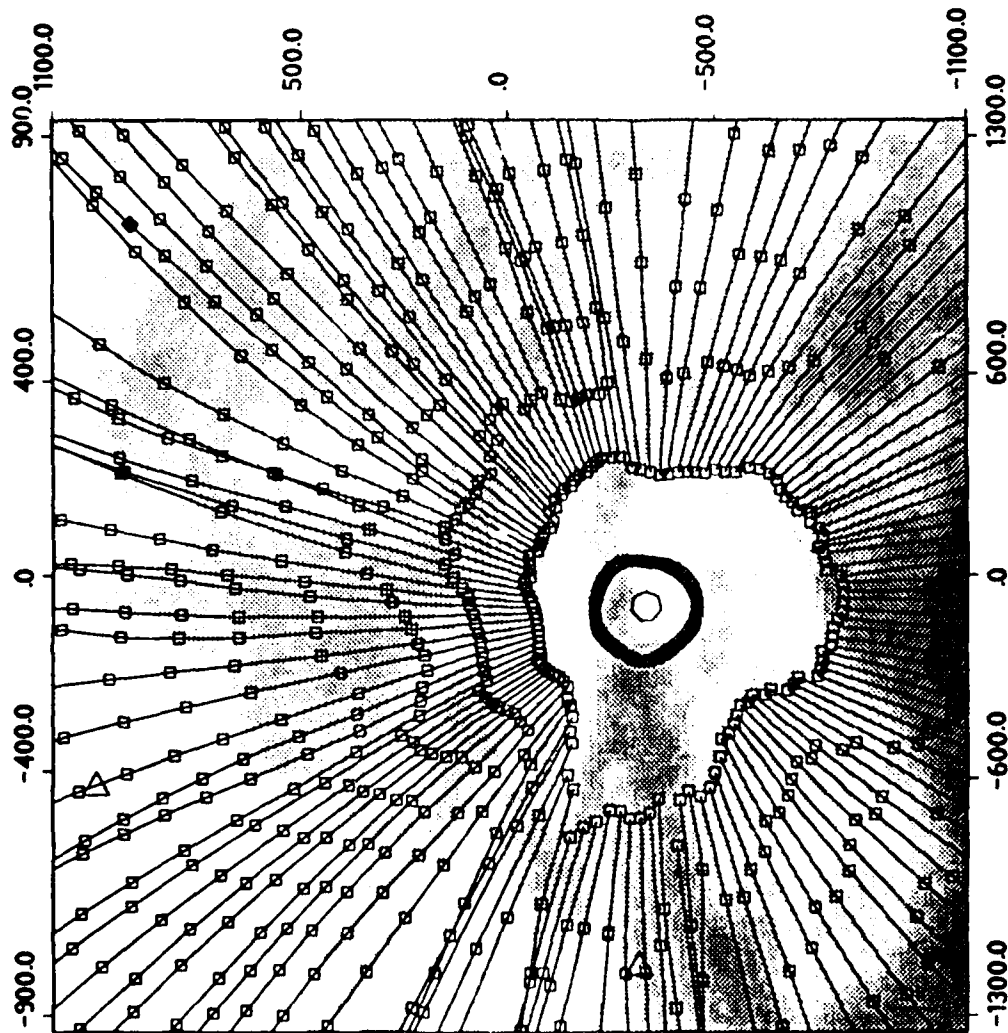
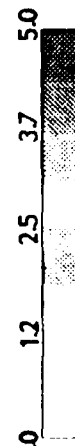


FIGURE 7 (a)

a

Lg Rayplot

E Tien Shan

PHASE VELOCITY

430 km/s

WINDOW

75. - 105.E

36. - 56. N

SOURCE

89. E 43. N

SCALES

Horizontal - km as marked

Vertical - km above msl

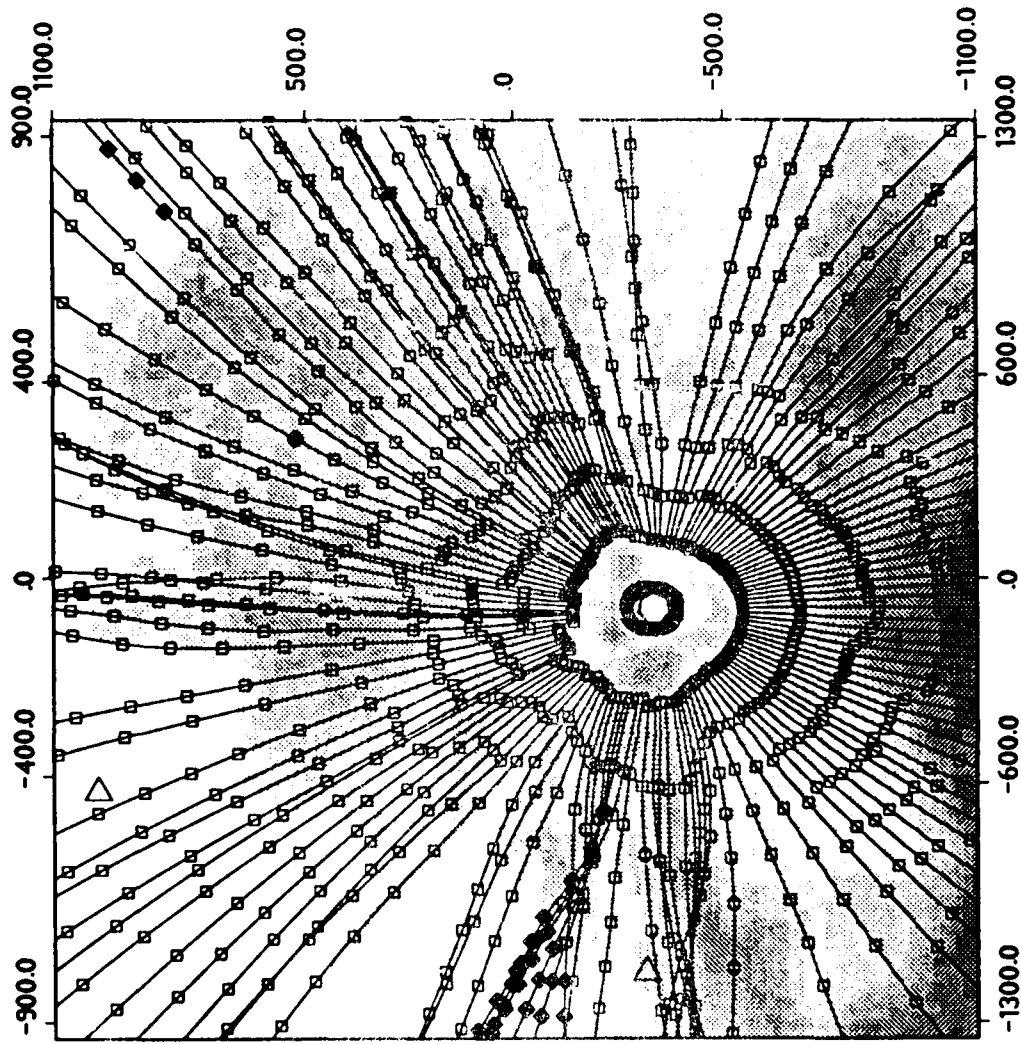


FIGURE 7 (b)

b

Lg Rayplot

Kunlun

PHASE VELOCITY

3.70 km/s

WINDOW

70. - 100E

26. - 46. N

SOURCE

30. - 36. N

SC

Horizontal - km

Vertical - km

0 12 25 37 50

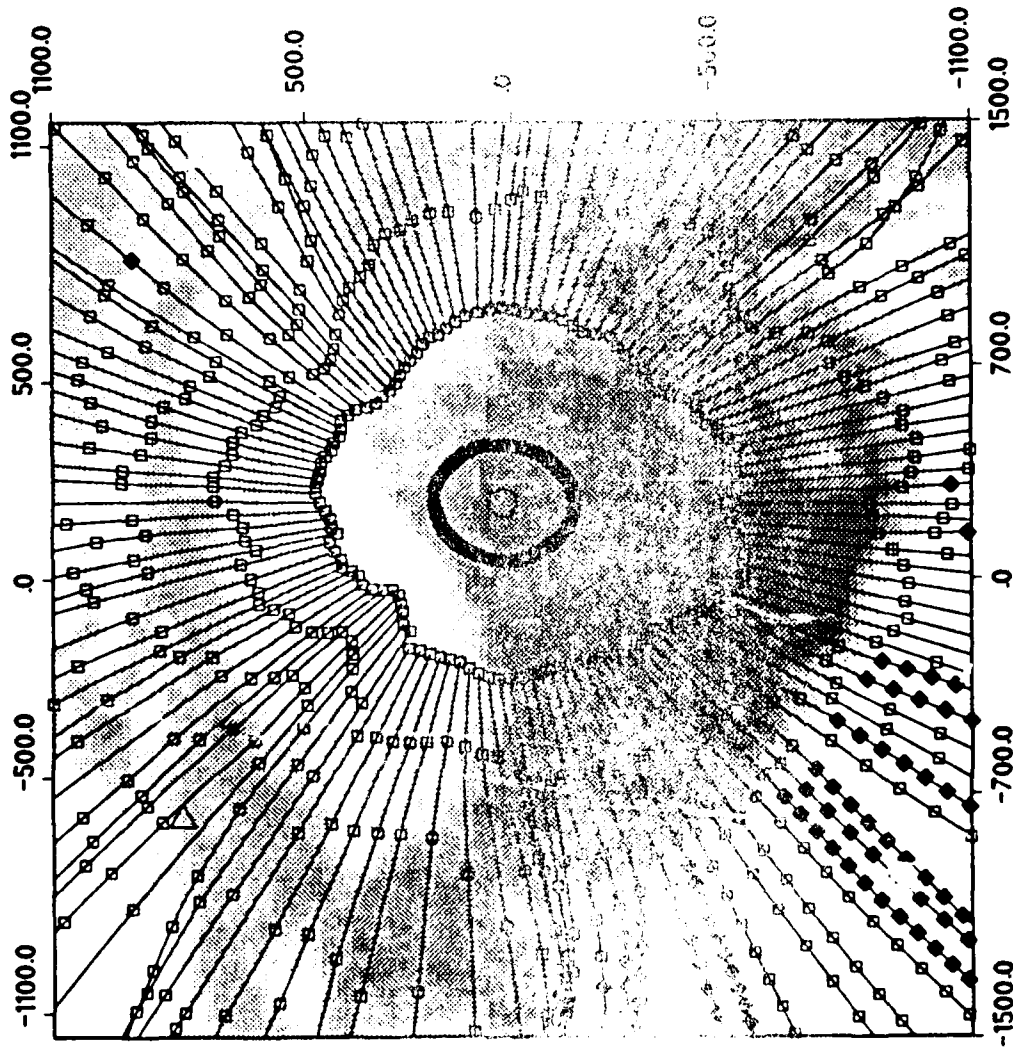


FIGURE 8 (a)

a

Lg Rayplot

Kunlun

PHASE VELOCITY

4.30 km/s

WINDOW

70. - 100E

26. - 46. N

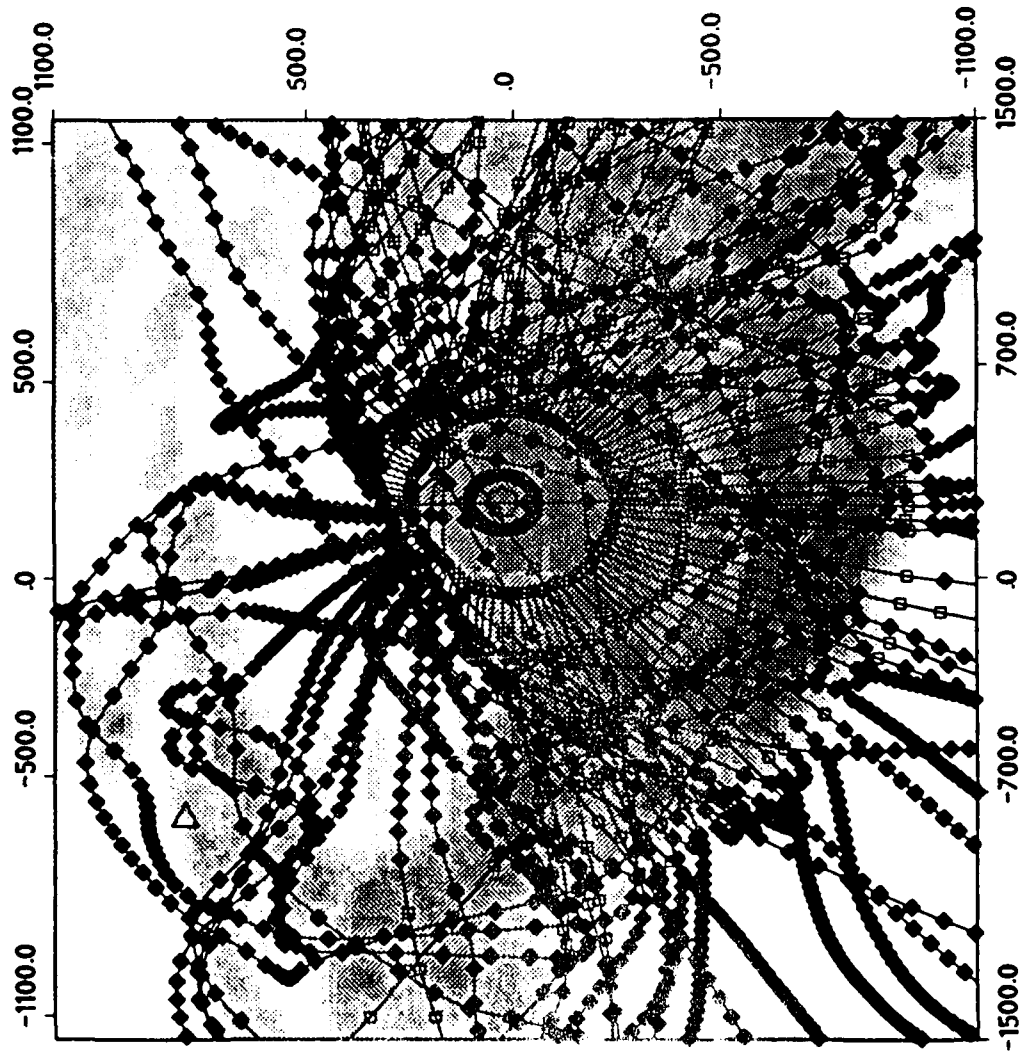
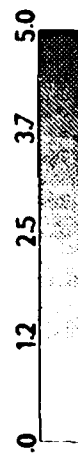
SOURCE

88. E 36. N

SCALES

Horizontal - km as marked

Vertical - km above msl



b

FIGURE 8 (b)

GUIDED WAVE TRACKING IN 3-D - A TOOL FOR INTERPRETING COMPLEX REGIONAL SEISMOGRAMS

B.L.N. Kennett, M.G. Bostock

*Research School of Earth Sciences, Australian National University,
G.P.O. Box 4, Canberra ACT 2601, Australia*

J-K Xie

*Department of Earth and Atmospheric Sciences, St Louis University,
3507 Laclede Avenue, St. Louis MO 63103, U.S.A.*

ABSTRACT

The tracking of guided wave trains by ray tracing in 3-D structures can provide a means of interpreting complex seismograms at regional distances. The method relies on the interpretation of Lg as the constructive interference of multiple S reflections within the crust, and strong scattering can be simulated by the inclusion of secondary sources.

This approach has been applied to Californian events observed in the southwestern United States whose records at regional distances frequently exhibit an extended and complex Lg coda with significant late energy arriving with group velocities of 2.5 km/s or less. The general character of this energy precludes an interpretation as the result of stochastic scattering processes or dispersion in low velocity surface sediments; and so some alternative explanation needs to be sought.

The observed wavetrains of events from two sites in southwestern California (Coalinga and North Baja) at stations LAC, MNV, ELK have been compared with the predictions from tracking guided wave patterns. Multipathing of energy by major changes in the thickness of the crustal wave guide is consistent with the extended and often "pulse-like" nature of the Lg coda. Examples of plausible multipathing mechanisms include reflection from the ocean-continent transition, scattering associated with topographic features such as the Sierra Nevada, and resonance within the narrow corridor of Baja California.

INTRODUCTION

Bostock & Kennett (1990) have recently introduced a simple scheme for modelling the main characteristics of guided wave trains in three-dimensionally varying structures by tracking the behaviour of multiply reflected waves. This technique has been able to match the general character of Lg wave propagation in central Asia. We show here how the method can be adapted to examine the nature of the propagation paths which may contribute to the Lg wave coda in the southwestern United States, by including secondary sources to simulate scattering as well as guided wave propagation.

The stations of the digital seismic network operated by the Lawrence Livermore National Laboratory lie at regional ranges from earthquakes in California and the northern part of Baja California. The most prominent part of the seismic record is usually the Lg phase (with frequencies of 1 Hz or above), although lower frequency Rg waves (around 0.25 Hz) are sometimes the largest feature (Xie & Mitchell 1990). For a number of events the structure of the Lg coda is quite complex with distinct packets of energy which arrive at rather low apparent group velocities (less than 2.5 km/s). In deriving coda Q models for the southwestern United States, Xie & Mitchell (1990) excluded such records from their analysis since this class of arrivals cannot be explained by a stochastic scattering model. We therefore seek a more direct physical interpretation.

We have built an approximate model of the crustal structure in California and Nevada based on the 5' by 5' digital topography database (ETOPO5). The shape of the Moho was derived from the surface topography by assuming that there was locally approximately 80 per cent isostatic compensation and that the Moho surface was smooth. This compensation factor reproduces the Moho depths of 30-35 km found by Hadley & Kanamori (1977) beneath the Transverse Ranges of southern California, but may overestimate crustal thicknesses for offshore structures. Since we wish to reproduce the main features of the propagation we do not attempt to make a full allowance for the seismic velocity distribution but rather impose a single constant velocity of 3.5 km/s in the crust and a velocity of 4.6 km/s beneath the crust-mantle boundary. We then concentrate on the way in which the guided S waves are affected by the gradients in surface and Moho topography.

The character of the guided wavefield for different phase velocities can be predicted by changing the take-off angles of the rays at the source. The propagation pattern is then most easily followed by mapping the reflection points at the surface and at the base of the crust. We also calculate the transit times along each ray so that group velocities can be calculated along the propagation paths. We consider here two groups of earthquakes. The first group of events is a cluster near Coalinga, in the Diablo Range of central California, recorded at stations MNV (315 km) and ELK (675 km) in Nevada. The records at these stations show a complex elongated coda with a few distinct later arrivals which

may be associated with back reflection from the continent-ocean transition. The second group of events lies in northern Baja California recorded at station LAC (300 km) and MNV (775 km). The relatively complex records suggest significant multipathing and possibly some sort of resonator effect within the peninsula of Baja California. The locations of the sources and receivers are given in Table 1 and illustrated in fig. 1 superimposed on the topography of the southwestern United States.

DIABLO RANGE EVENTS:

The character of the events from near Coalinga in the Diablo Range of central California is illustrated by the records at MNV and ELK of three events in 1983 with similar epicentres (Table 1). These displays show 300 seconds of bandpassed seismograms (corners 0.5, 1.5 Hz) which cover the Lg phase and coda, this frequency window is designed to emphasize Lg type energy. The three events have significant variation in frequency content which is reflected in the different waveforms for Lg in the band passed seismograms. The times corresponding to group velocities of 3.5 and 2.5 km/s are indicated by markers. We note that there is still substantial energy arriving very late in the coda.

The two stations lie along the same great circle and the propagation path crosses the San Joaquin Valley and the Sierra Nevada. There is the possibility of some energy being delayed by trapping in the sediments of the San Joaquin Valley but this would not be expected to produce late discrete pulses such as are seen at both MNV and ELK. It is more likely that such pulses would be produced by scattering or reflection mechanisms giving rise to arrivals reaching the stations along many different paths.

The great circle paths for the three Coalinga events are very close, and so the records should reflect similar propagation processes. However, the significance of different processes can be modified by the character of the radiation pattern for the event, which will be affected by both the source mechanism and depth.

We have investigated the nature of the propagation processes which might contribute to the character of the observed records using the ray-based method of Bostock & Kennett (1990). In figure 3 we show the propagation pattern, from the source, to the two receivers for both direct arriving waves and waves reflected back from the continent-ocean transition just off-shore. The phase velocity has been chosen to be 4.0 km/s to give a good general representation of the propagation behaviour. The ray paths through the model are shown and superimposed on these are small squares marking the reflection points for the multiply reflected S waves at the base of the crust. The squares are filled where reflection is subcritical to indicate the possibility of energy escaping from the waveguide.

In the case of direct propagation, the wavefronts marked by the patterns of reflection points are coherent for the first two crustal reflections but become more distorted after surface reflections have occurred within the Sierra Nevada. At station ELK the pattern of reflections for nearby rays shows considerable variation and this would lead to a spread in the apparent group velocities for the main energy.

The Coalinga events are not very far from the coast and the sharp contrast between continental and oceanic structures can lead to reflection of the guided waves. Because of the way we have built our crustal model the details of the transition may be somewhat simplified but the general character of the reflection process can be quite well represented. Energy can be returned from the coastal zone to both MNV and ELK from a number of different locations. We have considered the full range of phase velocities which might be regarded as of significance for the Lg waves and we find that the reflected arrivals would be expected to arrive at MNV with apparent group velocities from 1.8 km/s to 1.6 km/s. For ELK the corresponding group velocity range is from 2.3 km/s to 2.2 km/s (since the station is further away the additional path length to the reflection point and back is a smaller fraction of the whole). The spread of times predicted for such reflections is indicated on each of the seismograms in fig. 2 in a grey bar. For both MNV and ELK there is an interruption of the decay pattern for the Lg coda in the predicted time span on the band-passed records, with, in most cases, a distinct increase in amplitude. It is difficult to model the strength of such a reflection from the continent/ocean transition in detail because of strong dependence on the character of the source radiation, but the reflectivity is unlikely to exceed 0.20 at the angles of incidence in fig. 3. The reflection would therefore only be expected to be recognized when the general amplitude level is low. At MNV the predicted time interval on the unfiltered records is masked by low frequency Rg. However at ELK the interval lies in the coda of Rg and there is a distinct arrival at this time (fig. 4) on the unfiltered records, which is most pronounced for the event of 1983 July 9.

We have already noted that the pattern of the guided waves becomes disrupted on passage through the Sierra Nevada. The complex topography and structure in this zone will also generate scattered waves which would tend to extend the coda of the guided waves. We have introduced a simple model of a number of fixed secondary scatterers along the Sierras and then look at the time relations and propagation paths required to get energy from the source to the receivers via the secondary scattering centres. The process is illustrated in figure 4 for the Coalinga source and a receiver at ELK. For waves travelling with a true group velocity of 3.5 km/s, the scattering process can easily extend the train to 3.0 km/s. For MNV the contribution of the scattered wave legs is much larger and the apparent group velocity can be reduced to 2.5 km/s. Similar stretch factors

will occur for other group velocities. The corrugated surface topography in the Basin and Range province is also likely to contribute to scattering processes.

As has often been suggested (see e.g. Aki (1982), Herraiz & Espinosa (1987)) scattering is a powerful mechanism for fueling energy into the latter parts of the seismogram. Stochastic modelling of such scattering depends on an ensemble average over many models and can therefore predict envelope decay rates averaged over many seismograms but not the details of a single record (Hudson 1982). More specific modelling is therefore needed to try to unravel the nature of the Lg coda.

NORTHERN BAJA CALIFORNIA EVENTS

The second group of events occurred in northern Baja California and were recorded at the stations LAC (near Palm Springs) and MNV which lie close to a great circle through the event. Whereas the Coalinga events showed fairly consistent records, there is more variability from this group of events. At LAC, in particular, the event character seems to vary between relative rapid decay and a more extended coda. But when examined in detail the similarity between different events of the second group is somewhat greater; the coda includes short bursts of energy which continue with diminished amplitude for 150 seconds.

In figure 6 we show 300 s of bandpassed seismograms for the Lg wave and its coda for the event of 1985 May 10 at MNV and LAC, with again the times for apparent group velocities of 3.5 km/s and 2.5 km/s marked. The striking features of the records at MNV are the complex nature of the main arrivals and the persistence of the coda to very long times. Similarly at LAC, although the main coda decay is quite rapid the level remains sustained at a moderate level for nearly 50 s (from 200 to 250 s) before declining further.

The application of the Bostock & Kennett technique to this class of event showed that the propagation patterns were quite sensitive to the location of the event, which would fit with the variations in the character of the seismograms from different events. We illustrate in figure 7 the propagation pattern for the direct arrivals and for waves reflected at grazing incidence from the continent/ocean transition, as well as a few waves that get trapped in the narrow corridor of Baja California.

The spine of the Sierras tends to trap waves travelling in the general direction of MNV, these waves can then scatter to give many possible paths by which energy can arrive at MNV within the group velocity window from 3.5 km/s to 3.0 km/s. In addition there is a group of ray paths to MNV corresponding to reflection from offshore in the neighbourhood of the Channel Islands: such waves would arrive with an apparent group velocity around 2.4-2.3 km/s. The predicted time interval for these reflections is marked in grey on figure 5 and does indeed correspond to a distinct later arrival at MNV. For a single event such agreement might be accidental. However in fig.

8 unfiltered records at MNV for two Baja events with similar locations are shown, both have distinct arrivals in the predicted time interval. Since the reflection is near-grazing, quite high reflection amplitudes would be feasible. For station LAC the required angle of reflection from the offshore structure is too acute to enable a consistent pattern of rays to be established, and so pulse like arrivals would not be expected.

The sources lie at the northern end of the narrow peninsula of Baja California and it is tempting to suggest that the persistence of coda energy on the records is due to some kind of resonance phenomenon akin to a organ-pipe mode within the peninsula returning energy over a long time span as can be clearly seen in fig. 8. Ray tracing calculations (as in figure 7) confirm that it is indeed possible to trap energy within Baja California but that the configuration depends strongly on the assumptions used in building the crustal model. In addition to the rays presented in this study some scattering may occur where the trend of the structure alters and such waves would arrive at about the right time to give the extended main arrivals seen in figure 5.

DISCUSSION

We have shown that it is possible to explain much of the character of observed regional S wave seismograms in a complex region such as the southwestern United States using calculations based on Bostock & Kennett's (1990) treatment of guided-wave propagation in three-dimensionally varying media for a simple crustal model. The inclusion of scattering and reflection phenomena as well as direct propagation help to provide the classes of paths needed to span the observed ranges of group velocity. The continent/ocean transition is a very effective barrier to Lg wave propagation and can give rise to quite efficient reflections. Mountain ranges tend to encourage ducted wave propagation and where such a feature is coupled with efficient reflecting margins such as in Baja California it is possible to build up a strong trapped wavefield, which may act as a resonator feeding energy back into the external seismic waves over a fairly long time span.

The guided wave tracking procedure can be used to predict the character of regional phases given a knowledge of crustal structure. Indeed such modelling had suggested the resonator character of Baja California before any observations were sought to check the result.

ACKNOWLEDGEMENT

This work was supported by the Advanced Research Projects Agency of the U.S. Department of Defense under grant AFOSR-89-0330 and contract F19628-89-K-0021 monitored by the Air Force Geophysics Laboratory (research support for J.K. Xie).

TABLE 1. Locations of seismic stations and events studied

Location of LLNL Stations:

ELK	115.2388° W	40.7448° N
MNV	118.1544° W	38.4322° N
LAC	116.4115° W	34.3898° N

Events:

Group 1: Coalinga, Diablo Range

83 vii 09	7:40:50.90	120.41° W	36.24° N	depth 10 km mb 5.3
83 vii 22	3:43:00.60	120.41° W	36.21° N	depth 10 km mb 5.3
83 ix 11	11:48:08.00	120.39° W	36.23° N	depth 8 km mb 5.0

Group 2: Northern Baja California

85 v 08	23:40:18.20	115.80° W	31.70° N	depth 5 km mb 5.1
85 v 10	5:39:36.30	115.77° W	31.70° N	depth 6 km mb 4.6

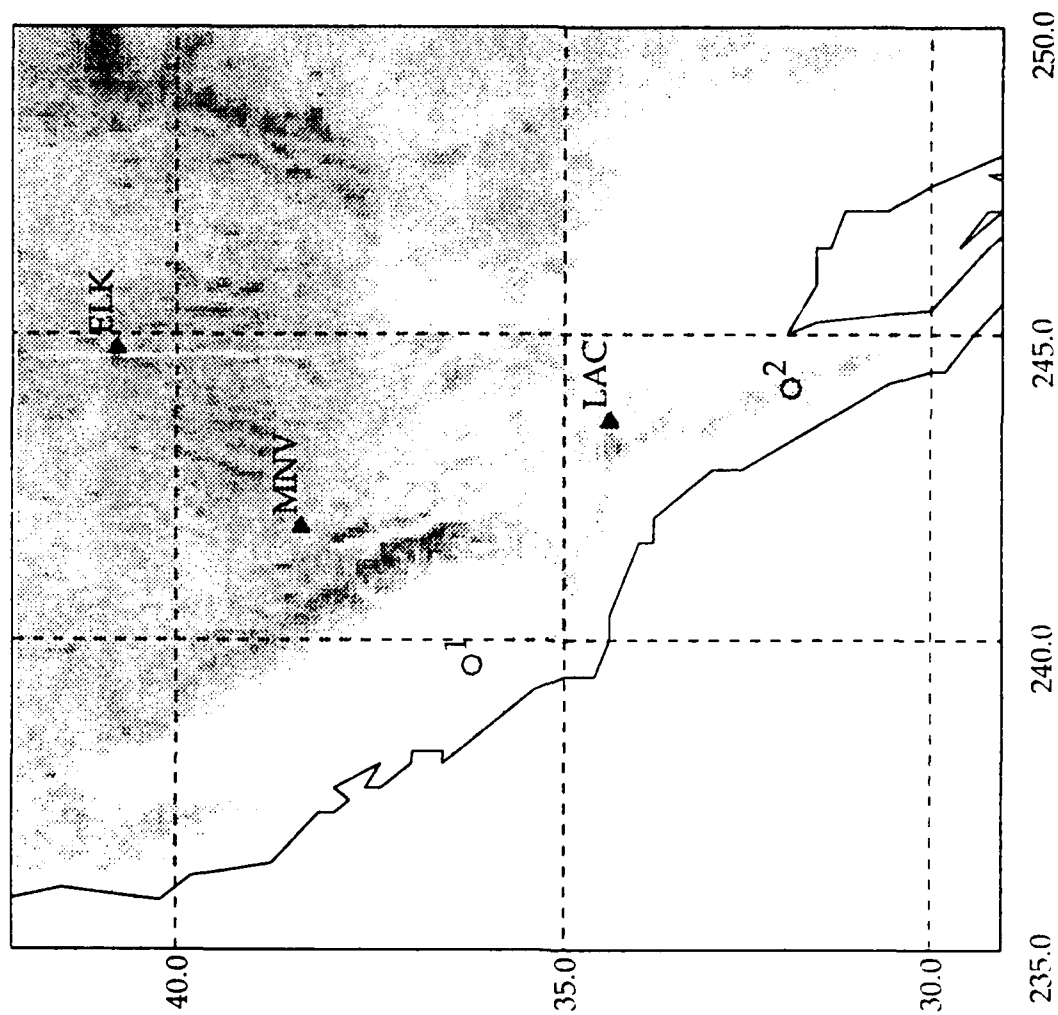
REFERENCES

- Aki K. 1982, Scattering and attenuation, *Bull. Seism. Soc. Am.*, **72**, 319-330.
- Bostock M.G. & Kennett B.L.N. 1990, The effect of three-dimensional structure on Lg propagation patterns, *Geophys. J. Int.* (in press).
- Hadley D. & Kanamori H. 1977, Seismic structure of the transverse ranges, California, *Bull. Geol. Soc. Am.*, **88**, 1469-1478.
- Herraiz M. & Espinosa A.F. 1987, Coda waves a review, *Pageoph*, **125**, 499-577.
- Hudson, J.A. 1982, The use of stochastic models in seismology, *Geophys. J. R. astr. Soc.*, **69**, 649-657.
- Xie J. & Mitchell B.J., 1989, Attenuation of multiphase surface waves in the Basin and Range Province, Part I: Lg and Lg coda, *Geophys. J. Int.* (in press)

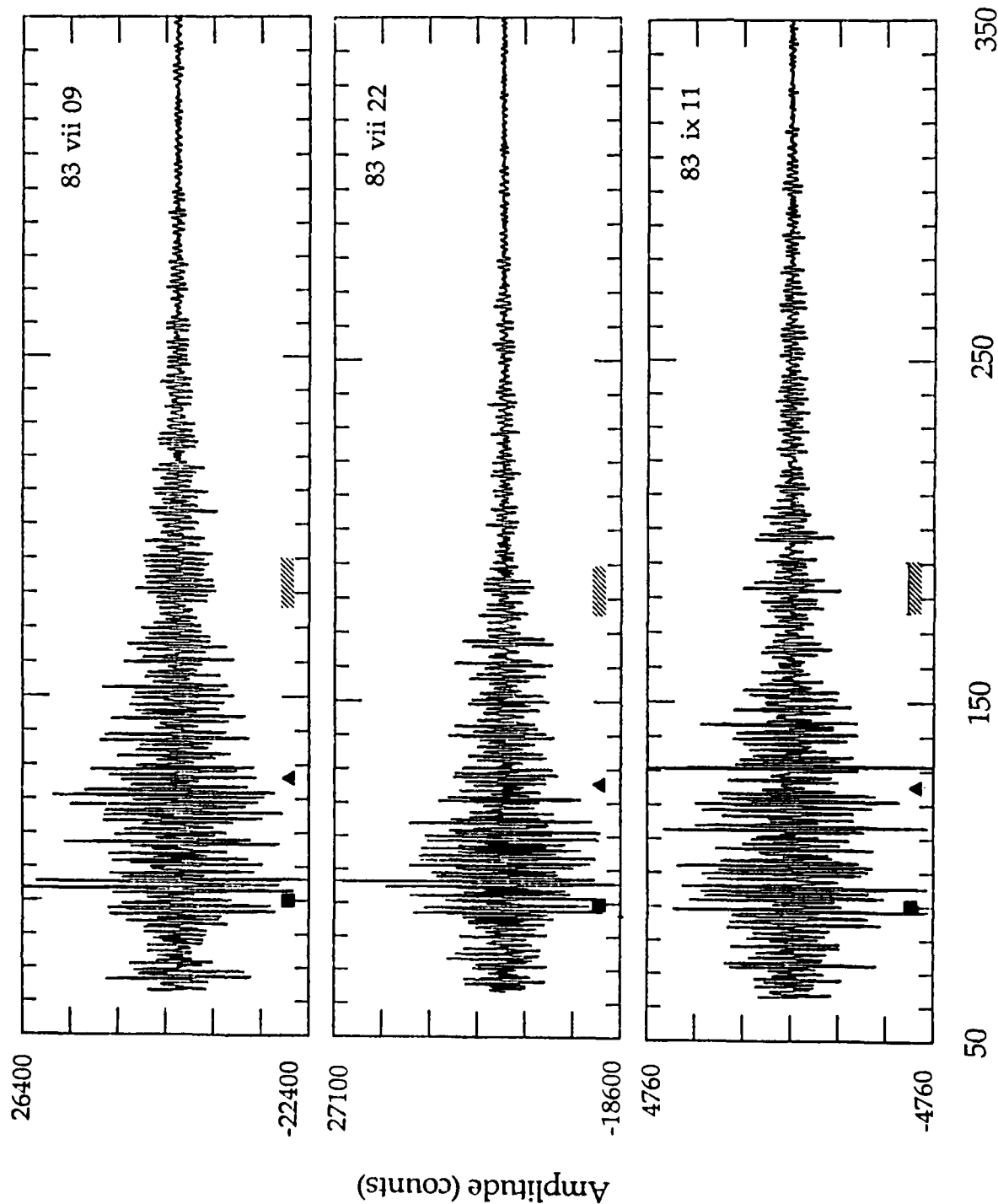
FIGURE CAPTIONS:

1. Reference map of southwestern United States with locations of the stations of the LLNL network and events used in this study.
2. Bandpassed seismograms of the Lg wave and coda for the group of events in the coastal range of central California at the stations MNV and ELK in Nevada. The passband (0.5, 1.5 Hz) is designed to enhance the Lg wave. The time corresponding to a group velocity of 3.5 km/s is marked by a square and 2.5 km/s by a triangle. The predicted time span for reflections from the continent ocean transition are marked by a grey bar.
3. Propagation diagram for guided S waves from a source near Coalinga at a phase velocity of 4.0 km/s. Both direct propagation and reflection from the continent/ocean transition are illustrated. The location of MNV and ELK are shown by solid triangles and the source by a hexagon.
4. Unfiltered seismograms for the group of Coalinga events at ELK. The predicted time span for reflections from the continent/ocean transition are marked by a grey bar and correspond to distinct arrivals in the coda.
5. Simulation of scattering by inclusion of secondary sources along the Sierra Nevada, the propagation patterns shown are for a receiver at ELK.
6. Bandpassed seismograms of the Lg wave and coda for the event of 1985 May 8 in the northern Baja California at the stations LAC (near Palm Springs) and MNV in Nevada. The passband (0.5, 1.5 Hz) is designed to enhance the Lg wave. The time corresponding to a group velocity of 3.5 km/s is marked by a square and 2.5 km/s by a triangle. The predicted time span for reflections from the continent ocean transition are marked by a grey bar.
7. Propagation diagram for guided S waves from a source in northern Baja at a phase velocity of 4.0 km/s. Direct propagation and grazing reflection from the continent/ocean transition are illustrated, as well as the propensity for rays to get trapped within Baja California. The location of LAC and MNV are shown by solid triangles and the source by a hexagon.
8. Unfiltered seismograms for two northern Baja events at MNV. The predicted time span for reflections from the continent/ocean transition in the neighbourhood of the Channel Islands are marked by a grey bar and correspond to distinct arrivals in the coda.

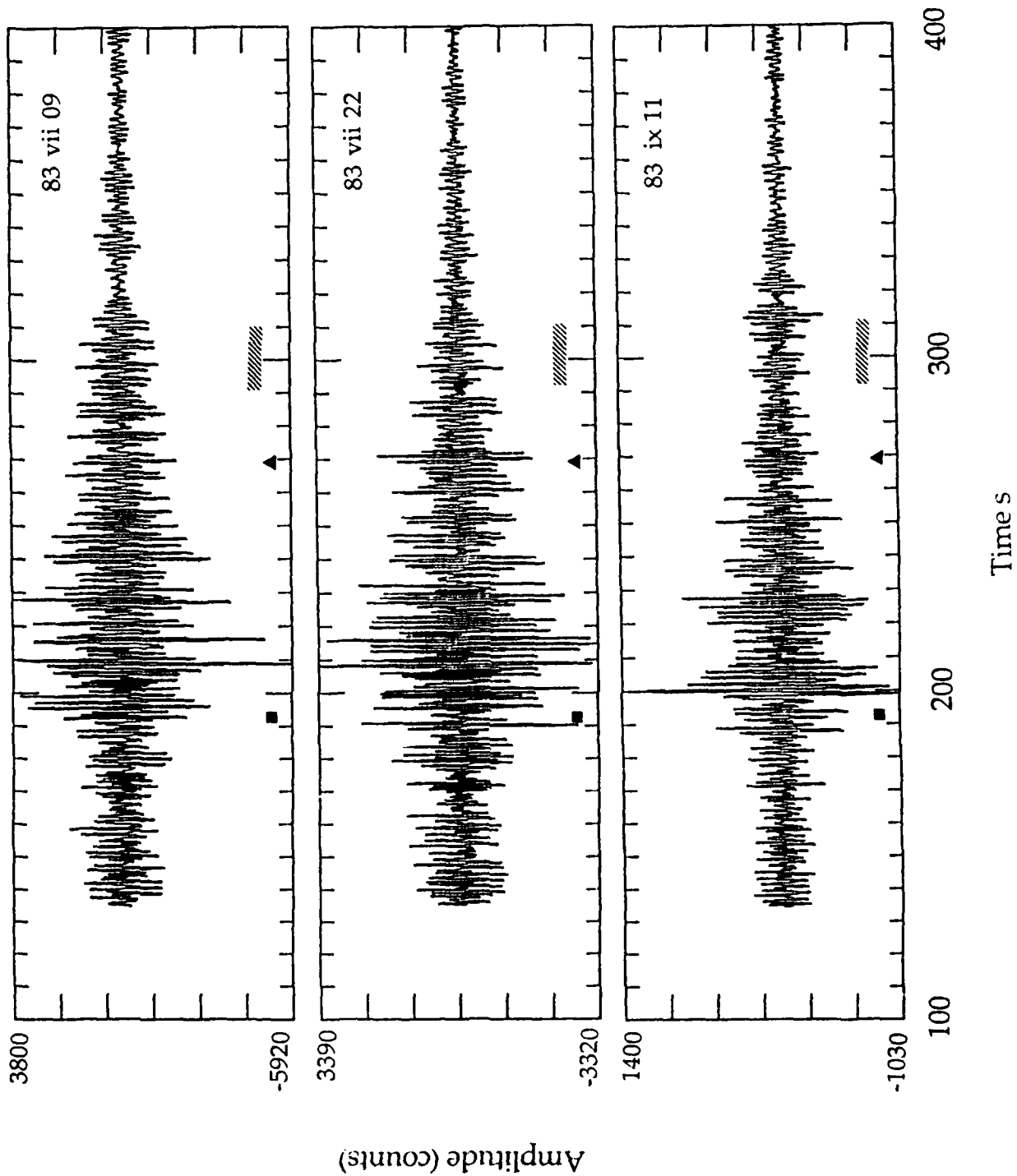
Southwestern United States



MNV 315 km



ELK 675 km



Lg Rayplot

Coalinga Events

PHASE VELOCITY

4.00 km/s

WINDOW

231. - 251.E

30. - 46. N

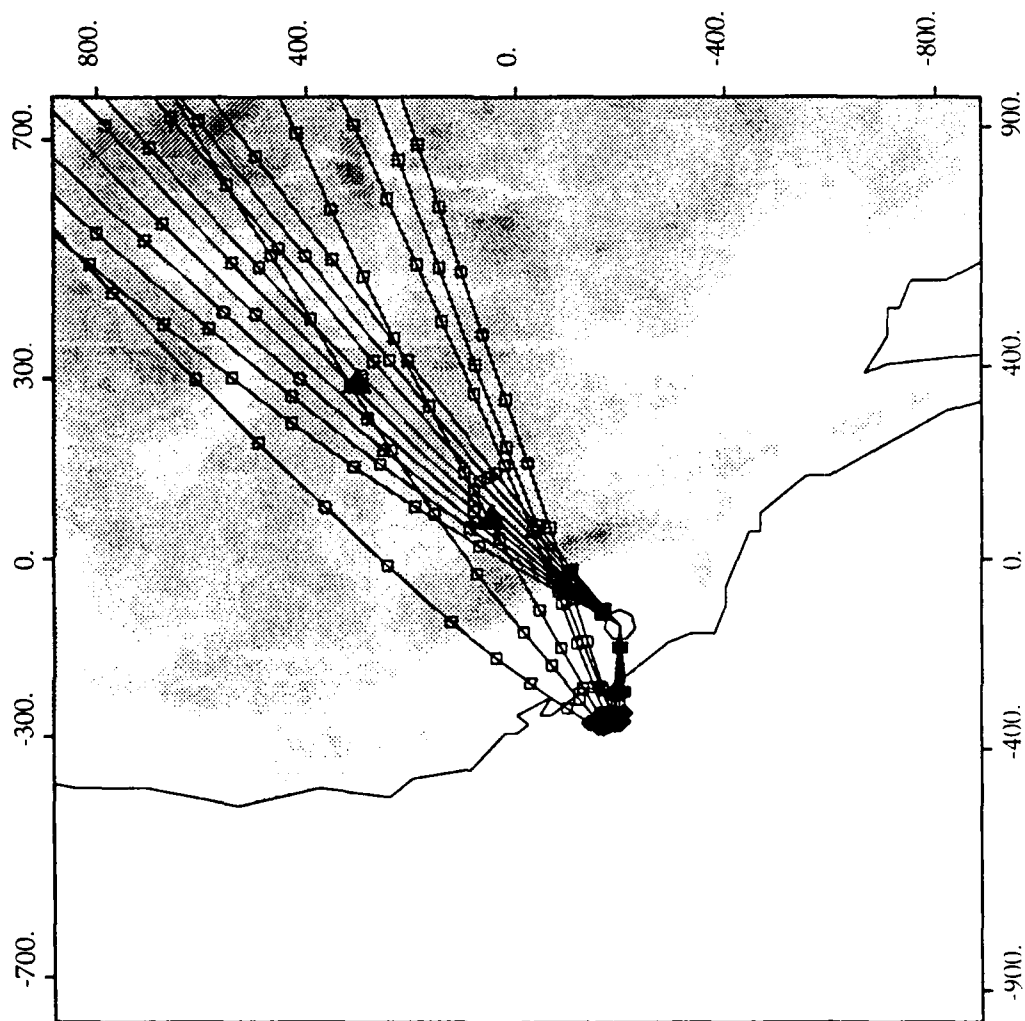
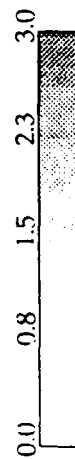
SOURCE

240.E 36. N

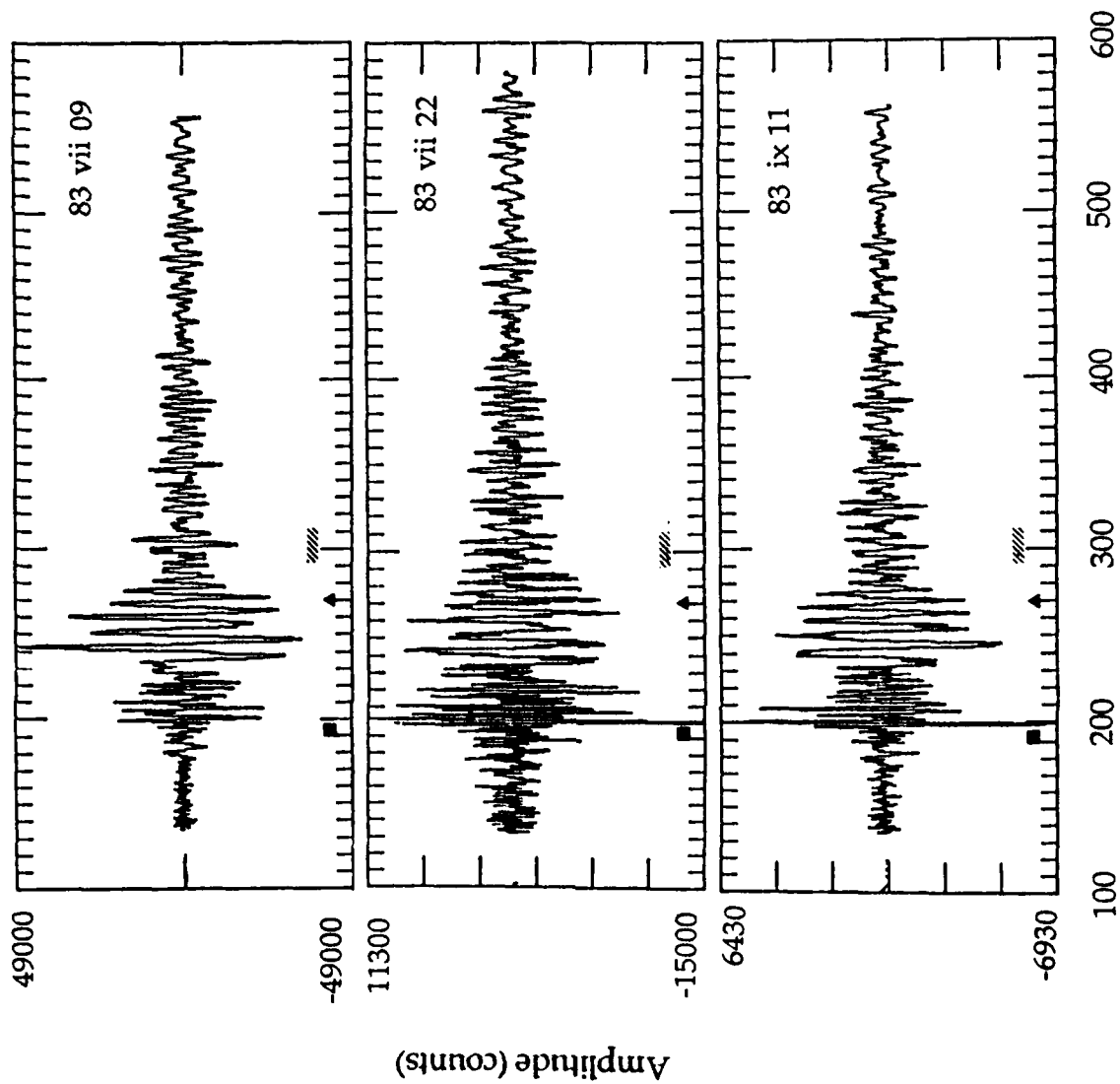
SCALES

Horizontal - km as marked

Vertical - km above msl



ELK 675 km



Time s

Lg Rayplot Coalinga Scatter Model

PHASE VELOCITY

4.00 km/s

WINDOW

231.- 251.E

30. - 46. N

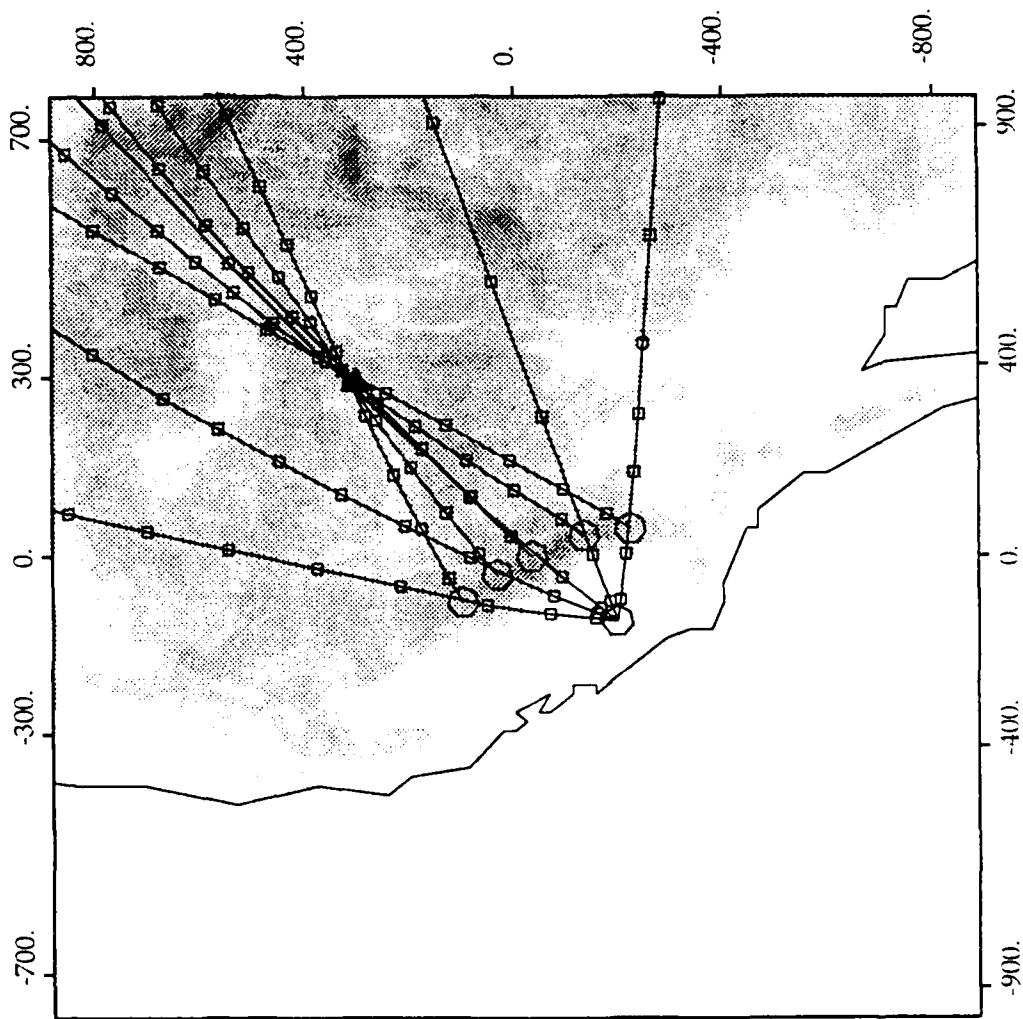
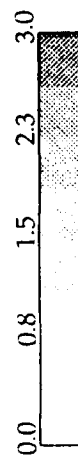
SOURCE

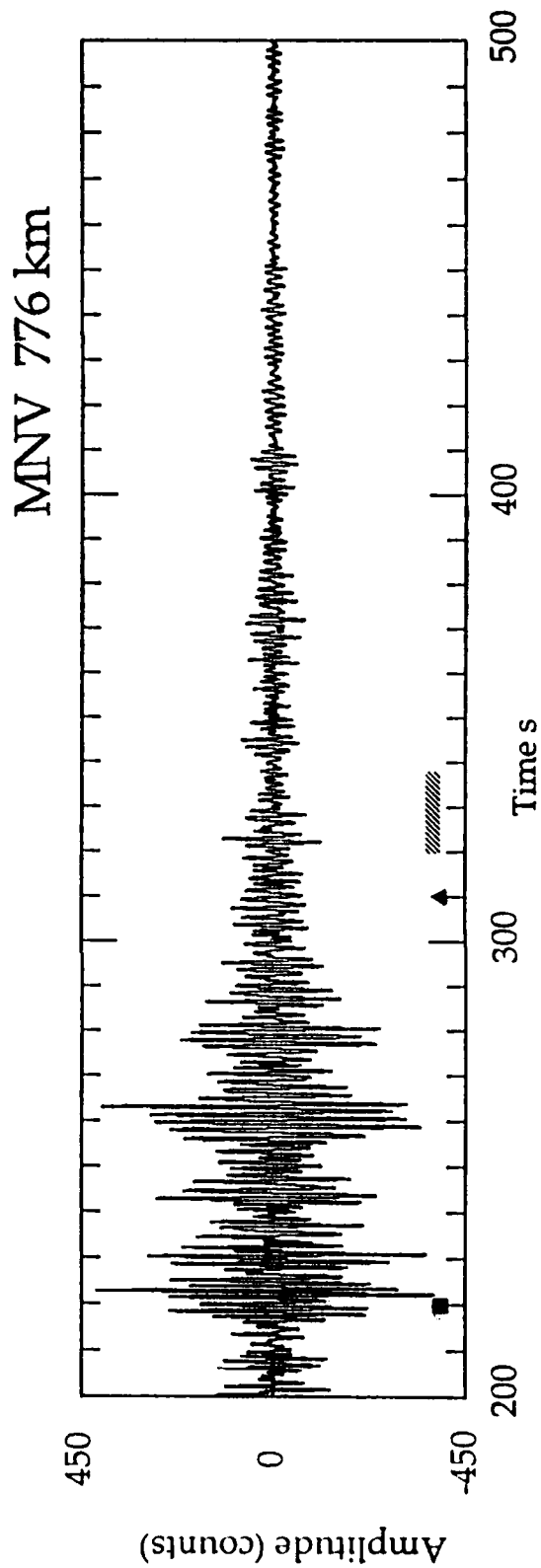
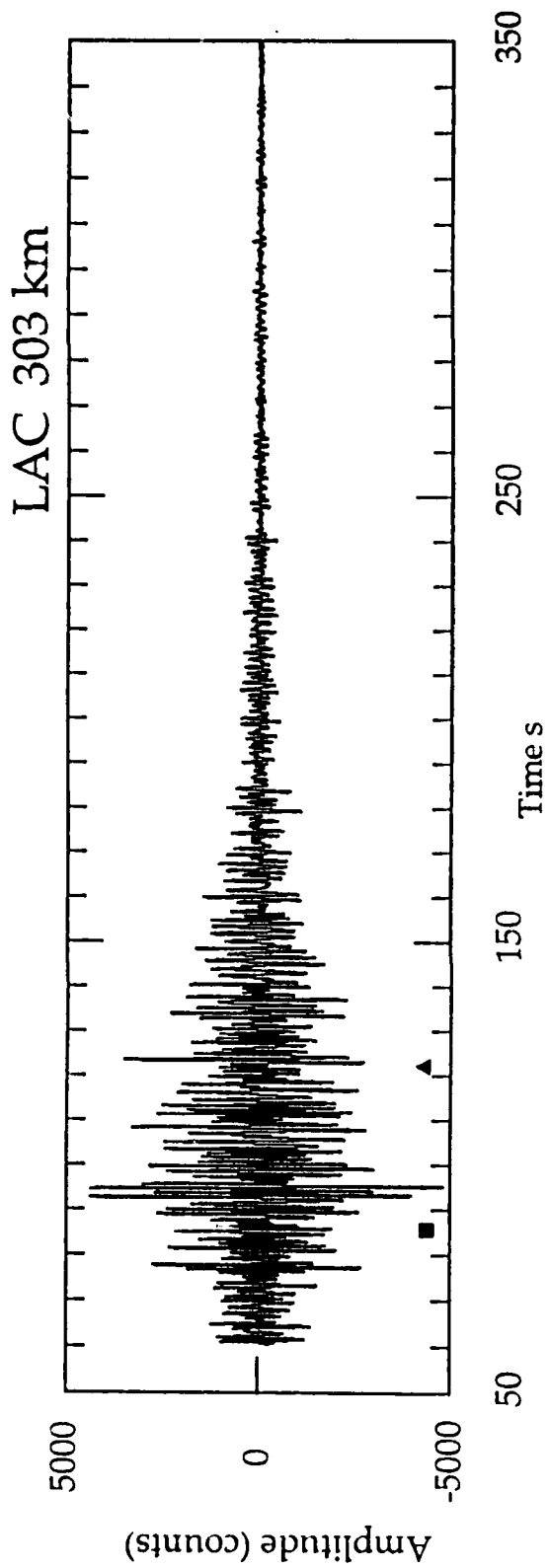
242.E 36. N

SCALES

Horizontal - km as marked

Vertical - km above msl





Lg Rayplot
Northern Baja Events

PHASE VELOCITY

4.00 km/s

WINDOW

235.- 252.E

22. - 39. N

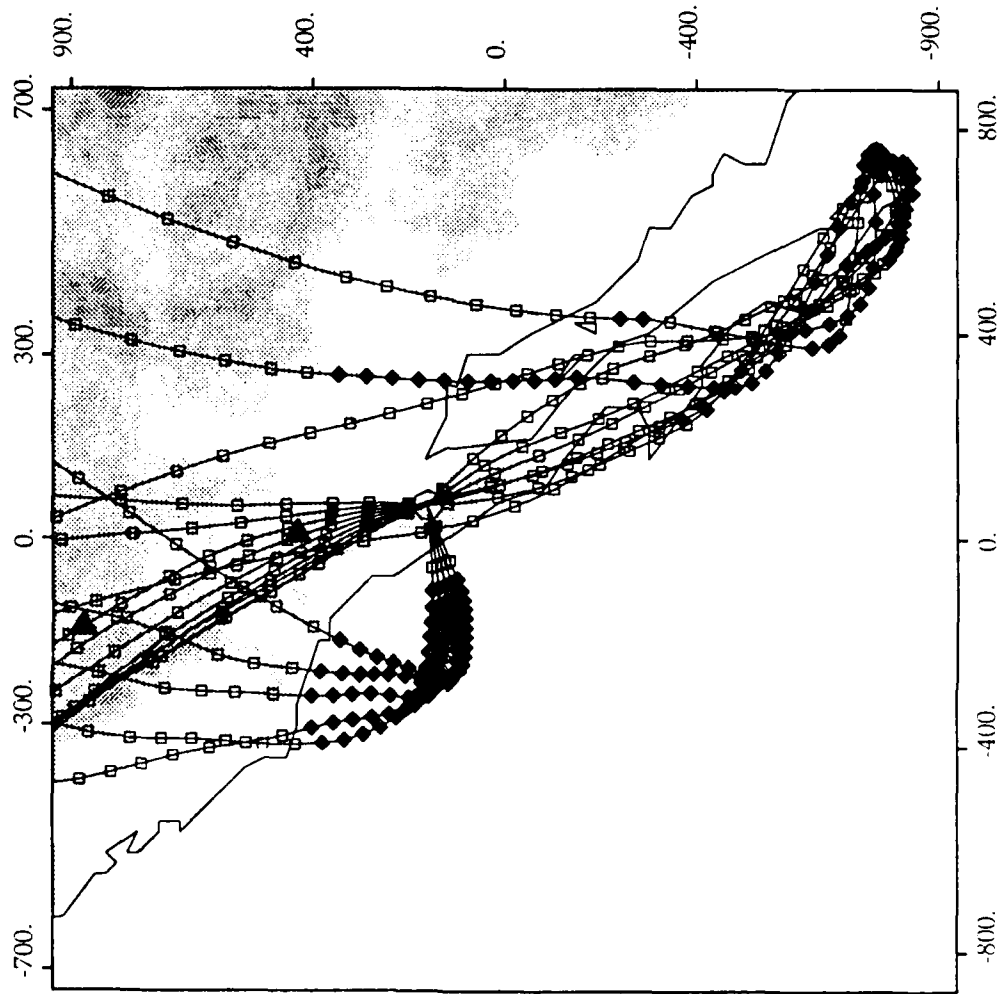
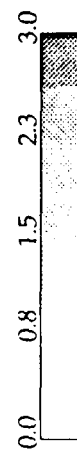
SOURCE

244.E 32. N

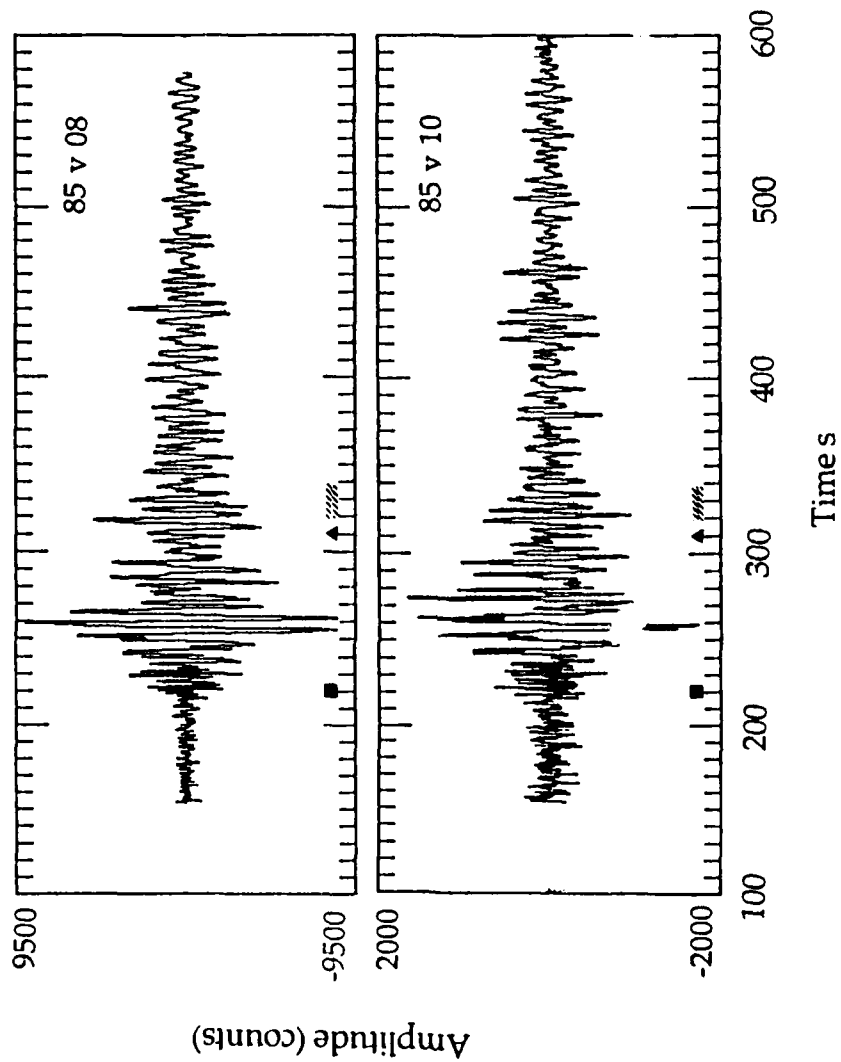
SCALES

Horizontal - km as marked

Vertical - km above msl



MNV 775 km



THE EFFECTS OF CRUSTAL VELOCITY GRADIENTS ON THE PROPAGATION OF REGIONAL S PHASES

J. Roger Bowman and B.L.N. Kennett
*Research School of Earth Sciences,
Australian National University
GPO Box 4, Canberra, ACT 2601
Australia*

INTRODUCTION

Lg waves are the dominant feature of seismograms at regional distances and are therefore quite useful for estimating earthquake magnitudes and for the detection and estimation of the yields of nuclear explosions. However, the accuracy of magnitude and yield estimates is dependent on the correct estimation of Lg amplitude decay with distance. In this paper we present results of a study of Lg attenuation in the Precambrian shield in Central Australia that demonstrate the effect of regional crustal structure on the rate of Lg amplitude decay.

Aftershocks of the 22 January 1988 Tennant Creek, Northern Territory earthquakes provide a localized source of radiation for an analysis of regional phases recorded by a 425 km linear array of portable seismographs between Tennant Creek and Alice Springs (Figure 1). The three Tennant Creek mainshocks (M_S 6.3, 6.4 and 6.7) produced two scarps of 32 km combined length (Bowman, 1988) and were followed by thousands of aftershocks in a 10 km x 40 km zone (Bowman et al., 1990) and in a complex geometry that suggests faulting on conjugate planes (Choy and Bowman, 1990).

Most previous studies of Lg propagation have relied on broadly distributed sources and receivers and, as a consequence, estimates of phase velocity and attenuation represent averages over the region sampled by the paths available. Moreover, there is seldom redundant data for the same paths, so no direct measure of errors in the estimates is available. We take advantage of the abundant aftershocks of the Tennant Creek earthquakes to examine Lg propagation along a simple path in the North Australian Craton.

Several lines of evidence suggest that the North Australian craton has low seismic attenuation. There is a large positive bias in M_L estimates for regional and teleseismic earthquakes recorded at stations located on the Australian craton that may be attributed to low attenuation (e.g., Gaull et al., 1989). Also, deep seismic reflection data from central Australia is unusually rich in high frequencies (Goleby et al., 1989). Furthermore, the isoseismal areas of earthquakes in the Australian craton are comparable to those in other stable continental regions with low

attenuation. However, in the present study, we find that estimates of attenuation are anomalously high when we correct the observed Lg wave amplitudes for geometrical spreading with a factor commonly used in North America and Western Europe. Crustal studies in central Australia suggest that the crust-mantle transition consists of a gradient zone rather than an abrupt discontinuity (Finlayson, 1982). We have therefore investigated the effect of the character of the crust-mantle transition on the apparent attenuation of Lg waves using synthetic seismogram modelling. Incomplete trapping of Lg waves in the presence of a gradient zone is likely to be responsible for the relatively rapid decrease in Lg amplitude with distance from the source.

DATA AND GEOLOGICAL SETTING

Eight portable seismographs were operated on a profile between Tennant Creek and Alice Springs for one week in March, 1988 (Figure 1). These stations consisted of vertical-component Willmore Mark III seismometers with 1 s natural periods and 9-track digital instruments recording continuously at 25.6 samples/s. A tripartite array consisting of station N1 situated west of the fault zone, three-component station B2 (operated at 16 samples/s) at the Warramunga (WRA) array and the northernmost station H1 of the linear array was used for determination of aftershock epicenters. Data from station H2, which had a partially clamped seismometer, and station H4, which had numerous tape errors, were not used for the attenuation analysis, but data from H2 were retained in the record section displays. In addition to the portable stations, we use data from the three-component, short-period station (SZ, SN and SE for vertical, north-south and east-west components) of the Alice Springs array (ASPA, Figure 1).

The propagation path from Tennant Creek to Alice Springs is in the North Australian Craton, which has formed a single relatively stable crustal block for 1700 m.y. (Plumb, 1979). The Tennant Creek fault zone is near the boundary between the Paleozoic Wiso Basin and the Early Proterozoic Tennant Creek "inlier". The inlier is a basement outcrop of a much larger feature and consists of sediments and metasediments of the Warramunga Group, which are intruded by lower Proterozoic granites. Stations H1-H3 were located on the Proterozoic Davenport geosyncline, stations H5 and H6 were situated on the western flank of the late Proterozoic-Devonian Georgina Basin and stations H7, H8 and ASPA were on the Proterozoic Arunta block. None of the stations is underlain by more than 50-100 m of sediment. All seismometers were emplaced in the Cenozoic aeolian and residual sand and gravel deposits that blanket most of the region with a thickness

generally less than 20 m. Therefore, there is no reason to expect large variations in site response.

Because of the high level of aftershock activity, we were able to select 11 earthquakes for analysis of sufficient size to be recorded at the most distant stations during the brief recording period (Figure 2, Table 1). Aftershock locations were determined using arrival time data from stations N1, B2 and H1, a simplified model (Table 2) based on refraction surveys (Finlayson, 1981, 1982), and the program HYPOELLIPSE (Lahr, 1980). Additional arrival times were available from triggered recorders in the source area for several of the larger events. Because only three stations were generally used in the solution and no station was located within two or three focal depths, all but one of the depths were fixed at 4 km, which is half the maximum focal depth observed in detailed aftershock studies (Bowman et al., 1990). Uncertainties in epicenter are generally less than 3 km.

For event 5 (Table 1) a sample record section of the regional data is shown in Figure 3 and a three-component record from Alice Springs is shown in Figure 4. In both displays each trace is normalized to its maximum amplitude. At Alice Springs the north-south component (SN) is very close to radial and the east-west component (SE), to transverse. The vertical component data in Figure 3 shows the evolution of the wavefield from 10 km to 430 km from the source. At ranges beyond 120 km, the seismograms consist of impulsive crustal P waves followed by emergent Lg wavetrains. The Lg arrival at station H6 is more impulsive and stronger than at neighboring stations. Record sections for the 11 events selected are remarkably similar, although there is some variation in the relative strengths of P and Lg, probably caused by differences in focal mechanism. The smaller earthquakes have the highest signal-to-noise ratio in the band 1.5-5 Hz.

The P-wave first arrivals have an apparent velocity of 7.7-7.8 km/s, which suggests that they are refractions from the lower crust. Finlayson (1982) used data from mine blasts near Tennant Creek recorded along a line extending 500 km to the east to interpret a Moho depth of 50 km and Pn velocity of 8.2 km/s. The crossover distance where Pn becomes a first arrival in Finlayson's model TCMI-2 is about 350 km for a surface source, and only stations H8 and ASPA lie beyond this distance. However, the differences between arrival times at these stations in our data are consistent with the velocities of 7.7-7.8 km/s observed at closer ranges. This suggests that the crust is thicker along this profile extending south of Tennant Creek than along a profile to the east, or that the Pn velocity is anomalously low. The apparent velocity of 7.7-7.8 km/s observed here is intermediate between the lower crustal (7.4 km/s) and Pn (8.2 km/s) velocities of TCMI-2.

On the vertical components along the profile (Figure 3), the initial P wave is followed by a coda of rather uniform amplitude without prominent, discrete phases such as Pg or Sn (except for a clear early Sn arrival at H8). On the radial (SN) component at ASPA (Figure 4), on the other hand, the first P is followed by a small pulse, then by a Pg phase, and on both the horizontal components, the Lg is preceded by a smaller pulse that may be an S counterpart to the initial P onset arrival. It should be noted that trace normalization exaggerates the strength of the Pg on the radial (SN) component.

The Lg phase dominates the seismograms at distances beyond 120 km with an average amplitude 3.3 ± 1.4 times that of the P wave in a group velocity window from 8-7 km/s (for seismograms filtered in a 3-8 Hz passband). Unless otherwise specified, amplitudes refer to the maximum sustained amplitude defined by Nuttli (1973), that is the amplitude equaled or exceeded by the three largest amplitude peaks in the wavetrain. The Lg/P ratio in northern Australia falls between that observed for earthquakes in eastern North America (10) and for earthquakes and explosions in the western USSR (1) (Pomeroy et al., 1982). At ASPA the ratios of radial and transverse components to the vertical component amplitudes are 0.8 ± 0.2 and 1.3 ± 0.3 , respectively, somewhat lower than the ratio of 2 between maximum horizontal and vertical sometimes assumed (e.g., Street, 1978).

GROUP VELOCITY

The Lg group velocity is estimated as 3.7 km/s by fitting a line to the maximum amplitudes recorded at stations H3 to ASPA for the 11 earthquakes in Table 1, and a similar velocity is estimated from the onsets of the Lg wavetrains. The group velocity in Central Australia is at the upper end of the range usually reported for stable continents (Pomeroy et al., 1982), and is somewhat higher than the only previous estimate of 3.5 km/s for Australia, based on paths crossing both Precambrian shield and the Phanerozoic region of eastern Australia (Bolt, 1957).

LG ATTENUATION

The Lg amplitude at frequency f for the i th earthquake ($i=1,n$) observed at the j th station ($j=1,m$) can be approximated by

$$A_{ij}(f) = A_{oi}(f) I_j(f) R_j(f) S_{ij} D_{ij} e^{-\gamma r_{ij}}, \quad (1)$$

where A_{oi} is a source factor, I_j is the instrument response, R_j is the site response, D_{ij} is a geometric spreading factor, S_{ij} is a source radiation term and $e^{-\gamma r_{ij}}$ is the attenuation factor for source-station separation r_{ij} . The coefficient of attenuation $\gamma = \pi f / QU$, where Q is the temporal quality factor and U the group velocity, and r_{ij} is the source-receiver distance. If the instruments are nominally identical

$$\log A_{ij} - \log D_{ij} - \log S_{ij} = \log A_{oi} - (\log_{10} e) \gamma r_{ij}. \quad (2)$$

where the site response has been taken as unity. Now, define A_{ij}^* as the logarithmic amplitude corrected for geometrical spreading and source radiation effects, and set $\gamma' = (\log_{10} e) \gamma$. Under the assumption that a single attenuation coefficient is adequate to describe the nearly coincident paths on the Tennant Creek profile, and variations in source radiation patterns can be ignored.

$$A_{ij}^* = \log A_{oi} - \gamma' r_{ij} \quad (3)$$

With a number of amplitude observations we can estimate the spatial attenuation coefficient γ' and the source excitation factors A_{oi} by a generalised least squares technique. The estimates are determined by minimising

$$\chi^2 = \sum_{j=1}^m \sum_{i=1}^n W_{ij} (A_{ij}^* - (A_{oi} - \gamma' r_{ij}))^2 \quad (4)$$

where W_{ij} is a weighting factor defined to reduce the influence of small arrivals (Dwyer et al 1983)

$$W_{ij} = \begin{cases} 1 & \text{SNR} > 4 \\ \text{SNR}/2-1 & 2 < \text{SNR} < 4 \\ 0 & \text{SNR} < 2 \end{cases} \quad (5)$$

and SNR is the ratio of Lg amplitude to the noise level before the first P arrival.

The geometrical spreading factor for Lg is frequently approximated by the simple power law

$$D = r^{-n} \quad (6)$$

Nutti (1973) suggested that $n = 5/6$. This is the predicted amplitude decay with distance for an Airy phase trapped in the crustal waveguide (p 145, Ewing et al 1957). However, Lg is not a single Airy phase, but rather a superposition of Airy phases of different modes with a range of phase and group velocities. As the observed amplitude will depend on the details of interference of the constituent modes, the amplitude decrease may not follow such a simple relationship. Although, results of numerical experiments by Campillo et al. (1984) and Shin and Herrmann (1987) are consistent with an average trend close to $r^{-5/6}$, it is noteworthy that both of these studies focused on velocity models with sharp discontinuities at the Moho. Because of the difficulty in simultaneously estimating geometric spreading and attenuation owing to absorption and scattering, we initially assume $r^{-5/6}$ spreading and arrive at an unexpectedly low value for Q in Central Australia.

We have Lg amplitudes in four discrete bands with center frequencies f_c of 1 Hz, 2 Hz, 3 Hz and 8 Hz and lower and upper corner frequencies of $f_c/\sqrt{2}$ and $\sqrt{2} f_c$.

respectively. For the smaller events, the 8 Hz frequency band had a poor SNR, so we concentrate on the three lower frequency bands. The solution to equation (4) gives an intercept for each earthquake, proportional to the size of the event, and an estimate of γ consistent with the assumed geometrical spreading. Maximum amplitude, maximum sustained amplitude and RMS amplitude in the group-velocity window 3.7-3.1 km/s were used as measures of the amplitude and found to give consistent results. An example of the least squares solution for the 1.41-2.82 Hz passband for RMS amplitudes is shown in Figure 5 and implies a Q of 302 for $n=5/6$.

Such a relatively low Q value is inconsistent with the frequency content of the seismograms, and so it is appropriate to examine the validity of the assumptions on which the attenuation estimate is based. In order to extract the loss coefficient we have to make an allowance for the main propagation effects of wavefront spreading. Figure 6 illustrates the trade-off between the attenuation coefficient γ and the index n in the power law representation of the spreading (6). An appropriate choice of spreading relation is clearly critical for an accurate estimate of attenuation.

In the following section we show how the pattern of Lg amplitudes variation with distance is influenced by the character of the crust-mantle transition. A simple power law relation for the amplitude variation with distance underestimates the complexity of the Lg propagation process, and in those cases where focussing effects give localised high amplitudes is a very poor representation of the behaviour.

DISCUSSION

As noted above, crustal models for the Tennant Creek inlier suggest that the crust-mantle transition is a gradient zone rather than an abrupt discontinuity (Finlayson 1981, 1982). Estimates of the spatial attenuation coefficient for Lg are strongly dependent on the assumptions made in correcting for the major geometric spreading component. The choice of $r^{-5/6}$ gives a noticeable discrepancy between the low estimated Q values and the propagation of high frequencies to considerable distances.

In order to investigate the influence of the nature of the crust-mantle transition on the character of the Lg phase we have constructed synthetic seismograms for a number of simple models of the crust-mantle transition. The reference model SJ0 has a sharp Moho discontinuity at a depth of 38 km and two classes of models were constructed based on replacing the single discontinuity by a set of three steps.

In the sequence SG1 to SG3 (Figure 7a) the discontinuity is replaced by a velocity gradient, covering the full span of the original Moho jump, extending over a progressively larger depth interval.

In the second sequence SJ1, SJ2, SG3 (Figure 7b) a partial jump at the base of the crust at 38 km is retained and the remainder of the velocity increase to mantle velocities is in the form of a gradient. The models SJ0 and SG3 can be regarded as the limits of both sequences.

Theoretical seismograms were calculated using a wavenumber integral approach for each of the models (Kennett 1983, 1988). A common set of source and integration parameters were employed to allow direct comparison between the results. The calculations were carried out for an explosive source at 15 km (to avoid source radiation effects), with a P wave Q of 1000 and an S wave Q of 500. A frequency interval of 0.5-4 Hz and a phase velocity interval of 3.0-5.0 km/s were used in the integration, and all P and S wave crustal multiples were included. The resulting seismograms for the two sequences of models are displayed in Figure 8 in a true amplitude display with a reduction velocity of 4 km/s.

At the head of each panel we display the seismograms for the reference model SJ0 with the sharp Moho transition. S_n is seen as a weak arrival at 200 km with a reduced time of 5 s which decreases to -2 s at 400 km. S_n is followed by a similar arrival with an extra leg reflected above the source. Such a free surface 'ghost' also helps to add to the complexity of the energy propagating in the crust. The sequence of packets of multiply reflected S wave energy within the crust build up to form the Lg wave train. The interference phenomena leading to the generation of Lg do not lead to a monotonic decay of amplitude with increasing range. The largest amplitudes occur for near critical reflection.

In the sequence of gradient models (Figure 8a) the general pattern of the seismograms is maintained but the locus of the maximum amplitude of Lg is shifted to greater range as the gradient that has replaced the Moho discontinuity is reduced. Because of the reduced gradient, the reflected S waves from the crust-mantle transition spend longer in this region and so require a greater distance to return to the surface. A further consequence is that these waves travel faster than before and so the locus of maximum amplitude in Lg shifts to higher group velocities.

The theoretical seismograms for the sequence of models with progressively smaller velocity jump at 38 km depth are displaced in Figure 8b. In model SJ1 the large velocity jump at 38 km means that critical reflections are important even though S_n is enhanced from model SJ0 by the increased gradient below 38 km. For model SJ2 with a smaller velocity jump but increased gradient below 38 km, the S_n

phase is very prominent at the shorter ranges. The interference of reflected and refracted energy gives a broad locus of increased amplitude as a function of distance. However once the velocity jump at 38 km is largely eliminated as in model SG3, sharper amplitude maxima occur dominated by the return from the crust-mantle gradient zone.

The amplitude behaviour of these theoretical seismogram calculations as a function of range is summarised in Figure 9. The maximum amplitudes are displayed together with a dashed line corresponding to $r^{-5/6} e^{-\gamma r}$ decay, including the effects of attenuation in the model at the 2 Hz centre frequency ($\gamma = 0.0028$). As would be expected from the character of the record sections in Figure 8, the calculated amplitude patterns are somewhat erratic and cannot be fit by any simple power law model. The model SJ0 with a sharp Moho transition predicts a mean amplitude decay which is closest to $r^{-5/6} e^{-\gamma r}$, but even in this case the application of a simple geometrical spreading correction would inevitably impose a systematic pattern of amplitude anomalies on the corrected data being used to estimate Lg wave attenuation coefficients. For those models with even a partial gradient zone the rate of Lg amplitude decay with distance is enhanced because of leakage of energy from the crustal waveguide, in the phase velocity range contributing to Lg.

An additional prediction for a crust-mantle transition composed almost entirely of a gradient zone is that the amplitude maxima for Lg are sharply peaked as a function of distance. Model SG3 predicts very strong Lg amplitude near 220 and 440 km and it is interesting to note that in the normalized seismograms of Figure 3 the Lg arrivals are most clear at just these distances. The crustal models of Finlayson (1982) designed to match the character of refraction data between Tennant Creek and Mt. Isa, Queensland show lower crustal velocities exceeding 7 km/s and gradients rather than a sharp crust-mantle transition. Model TCMI-3, in particular, has an average gradient (0.058 s^{-1}) between 35 and 60 km which is close to that for SG3 (0.064 s^{-1}). The character of the recorded seismograms along the recorded profile and the observed Lg decay rates are therefore consistent with the pattern expected for a gradient zone between crust and mantle.

However, our comparison of different crustal structures has shown the limitations of simple corrections for geometric spreading in estimating attenuation coefficients for Lg. Even for a single path a somewhat erratic trend of amplitude with distance can be expected, albeit with a superimposed decay. Such decay behaviour is a strong function of the character of the crust-mantle transition.

Although the commonly adopted geometric spreading power law for $r^{-5/6}$ is seen to give a reasonable representation of the behaviour for a sharp Moho, it cannot be universally applied. In many areas, the assumption of an abrupt crust-

mantle transition is well founded but beneath Precambrian terrains (which are well represented in the Soviet Union) a gradational crust-mantle transition seems to be quite common.

The principal application of Lg attenuation coefficients lies in applying path corrections to estimate the magnitude of a source (and in the case of an explosion to thereby estimate the yield). The use of inappropriate amplitude corrections could lead to misleading estimates of source parameters.

ACKNOWLEDGEMENTS

We thank J. Hulse for installing the portable seismographs, P. Cummins for programs to read field tapes, S. Ingate and K. Muirhead for supplying data from the Alice Springs array, and J. Lahr for a copy of HYPOELLIPSE. This work was supported in part by the Advanced Research Projects Agency of the U.S. Department of Defence under Grand AFOSR-89-0330.

REFERENCES

- Bolt, B.A. (1957). Velocity of the seismic waves Lg and Rg across Australia, *Nature*, **180**, 495.
- Bowman, J.R. (1988). Constraints on locations of large intraplate earthquakes near Tennant Creek, Northern Territory, Australia from observations at the Warramunga seismic array, *Geophys. Res. Lett.*, **15**, 1475-1478.
- Bowman, J.R., G. Gibson, and T. Jones (1990). Aftershocks of the 22 January 1988 Tennant Creek, Australia intraplate earthquakes: Evidence for a complex thrust fault geometry, *Geophys. J. Int.*, **100**, 87-97.
- Choy, G. and J.R. Bowman (1990). Rupture process of a multiple main shock sequence: analysis of teleseismic, local and field observations of the Tennant Creek, Australia earthquakes of 22 January 1988, in press, *J. Geophys. Res.*
- Dwyer, J.J., R.B. Herrmann and O.W. Nuttli (1983). Spatial attenuation of Lg waves in the central United States, *Bull. Seism. Soc. Am.*, **73**, 781-796.
- Finlayson, D.M. (1981). Reconnaissance of upper crustal seismic velocities in the Tennant Creek block, Northern Territory, *BMR J. Aust. Geol. Geophys.*, **6**, 245-252.
- Finlayson, D.M. (1982). Seismic crustal structure of the Proterozoic north Australian craton between Tennant Creek and Mount Isa, *J. Geophys. Res.*, **87**, 10,569-10,578.
- Gaull, B.A., P.J. Gregson and K. Malafant (1989). New magnitude scales in Western Australia, *Aust. Bur. Min. Resour. Record* 1989/6.

- Goleby, B.R., R.D. Shaw, C. Wright, B.L.N. Kennett and K. Lambeck (1989). Geophysical evidence for "thick-skinned" crustal deformation in central Australia, *Nature*, **337**, 325-330.
- Jones, T.D., G. Gibson, K. McCue, D. Denham, P.J. Gregson, and J.R. Bowman (1990). Three large earthquakes rupture the Australian Precambrian shield near Tennant Creek, Northern Territory on 22 January 1988, *Geophys. Res. Lett.*, in press.
- Kennett, B.L.N. (1983). *Seismic Wave Propagation in Stratified Media*. Cambridge University Press, Cambridge, pp. 342.
- Kennett, B.L.N. (1988). Systematic approximations to the seismic wavefield, in *Seismological Algorithms*, edited by D.J. Doornbos, Academic Press, London, 237-259.
- Lahr, J.C. (1980). HYPOELLIPSE/MULTICS; A computer program for determining local earthquake hypocentral parameters, magnitude, and first motion pattern, *U.S. Geological Survey Open-File Report 80-59*, 31 p.
- Nuttli, O.W. (1973). Seismic wave attenuation and magnitude relations for eastern North America, *J. Geophys. Res.*, **78**, 876-885.
- Plumb, K.A. (1979). The tectonic evolution of Australia, *Earth Sci. Rev.*, **14**, 205-249.
- Pomeroy, P.W., W.J. Best and T.V. McEvilly (1982). Test ban treaty verification with regional data--a review, *Bull. Seism. Soc. Am.*, **72**, S89-S129.
- Street, R.L. (1978). A note on the horizontal to vertical Lg wave-amplitude ratio in eastern United States, *Earthquake Notes*, **49**, 15-20.

TABLE 1. Earthquakes used in this study

No	Origin time			latitude (°S)	longitude (°E)	depth (km)*	M _L
1	3/27/88	8 51	45.1	19.853	133.933	4.0	
2	3/27/88	12 51	1.2	19.785	133.894	4.0	3.2
3	3/28/88	0 27	12.6	19.908	134.030	6.7	5.0 (m _b 4.9)
4	3/28/88	0 58	14.0	19.913	134.028	4.0	3.5
5	3/28/88	2 6	35.8	19.795	133.878	4.0	
6	3/28/88	19 1	10.7	19.858	133.934	4.0	3.0
7	3/29/88	13 22	40.3	19.824	133.923	4.0	
8	3/30/88	15 54	39.5	19.880	134.004	4.0	3.1
9	3/31/88	7 33	14.5	19.827	133.980	4.0	
10	3/31/88	10 46	52.6	19.899	134.046	4.0	
11	4/ 1/88	5 9	58.1	19.864	134.101	4.0	

* constrained to 4 km unless additional local data were available

TABLE 2. Crustal velocity model*

Depth (km)	V _p (km/s)
0.00	4.50
0.17	5.00
0.34	5.50
2.14	6.06
6.00	6.20
13.00	6.27
27.00	6.85
40.00	7.30
47.40	7.40
50.50	8.16
58.00	8.18
61.00	8.29

* Modified from Finlayson (1981, 1982)

FIGURE CAPTIONS

1. Map of the source (diamonds) and receiver (triangles) locations used for studying Lg propagation. Portable stations (N1 and H1-H8) recorded the vertical component only at 25.6 samples/s and the Alice Springs array recorded three-component data at 20 samples/s. Stations of the Warramunga (WRA) seismic array are shown as plus signs. Station B2 at the intersection of the two arms of the WRA array recorded three-component data at 16 samples/s.
2. Locations of the aftershocks used for the Lg study with symbols corresponding to event numbers in Table 1. The thrust fault scarps (Bowman et al., 1990) are shown as heavy lines with hatch marks on the upper plate.
3. Seismograms for event 5 at stations on the line between Tennant Creek and Alice Springs. Each trace is normalized to its maximum amplitude which is shown above in digital counts for stations for which it is reliable. Locations of stations are shown in Figure 1, and station SZ is the short-period, vertical-component of station ASPA. The Lg arrival is the largest phase at regional distances.
4. Three-component, short-period seismograms for event 5 from the Alice Springs array. Each trace is normalized to its maximum amplitude, which is shown on the right in digital counts.
5. RMS amplitude for 2 Hz center frequency and corrected for $r^{-5/6}$ geometric spreading are shown as a function of source-receiver distance and labeled by event number as in Figure 2. Lines show the consistency of the least squares fit to the data.
6. Attenuation coefficient γ as a function of the power n assumed for geometrical spreading for 1 Hz (circles), 2 Hz (triangles) and 4 Hz (diamonds). RMS amplitudes in the 3.7-3.1 km/s group velocity window were used.
7. Velocity models used for synthetic seismogram calculations. Heavy solid lines show reference model SJ0. a) Moho discontinuity replaced by a gradient in SG1, SG2 and SG3. b) Moho discontinuity reduced in models SJ1, SJ2 and SG3.
8. Vertical-component synthetic seismograms calculated with the wavenumber integral method (Kennett, 1983, 1988) for frequencies 1- 4 Hz, with explosive source at 15 km and a constant Q of 500 for S waves. Reduction velocity is 4 km/s. a) Gradient models. b) Moho jump models.
9. Maximum amplitude of synthetic seismograms shown in Figure 8 for the velocity models in Figure 7 as a function of source-receiver distance. Dashed lines show predicted behaviour for an Airy phase and heavy solid lines show amplitudes for model SJ0. a) Amplitudes for gradient models SG1, SG2 and SG3. b) Amplitudes for jump models SJ1 and SJ2.

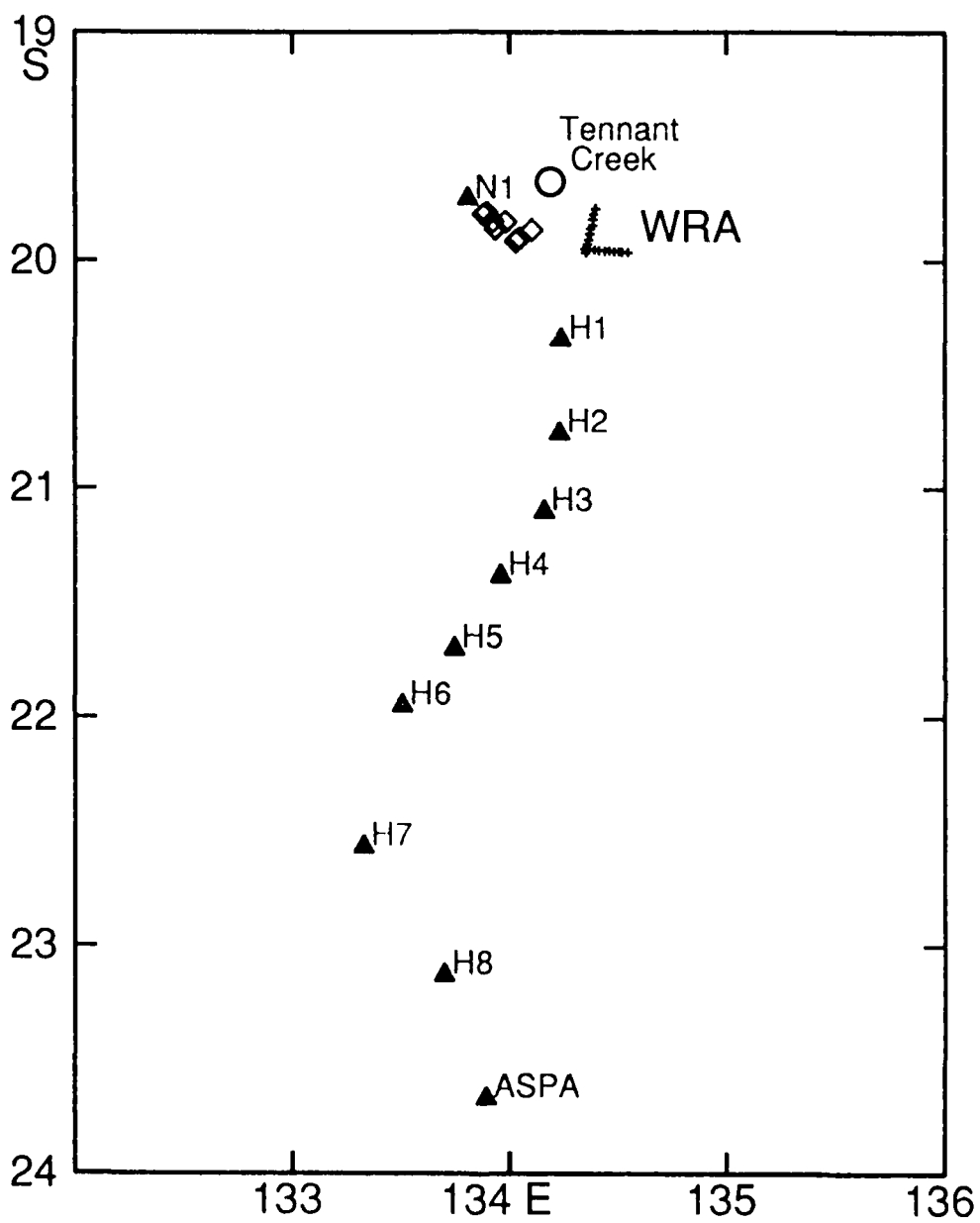


FIGURE 1

SHA sources

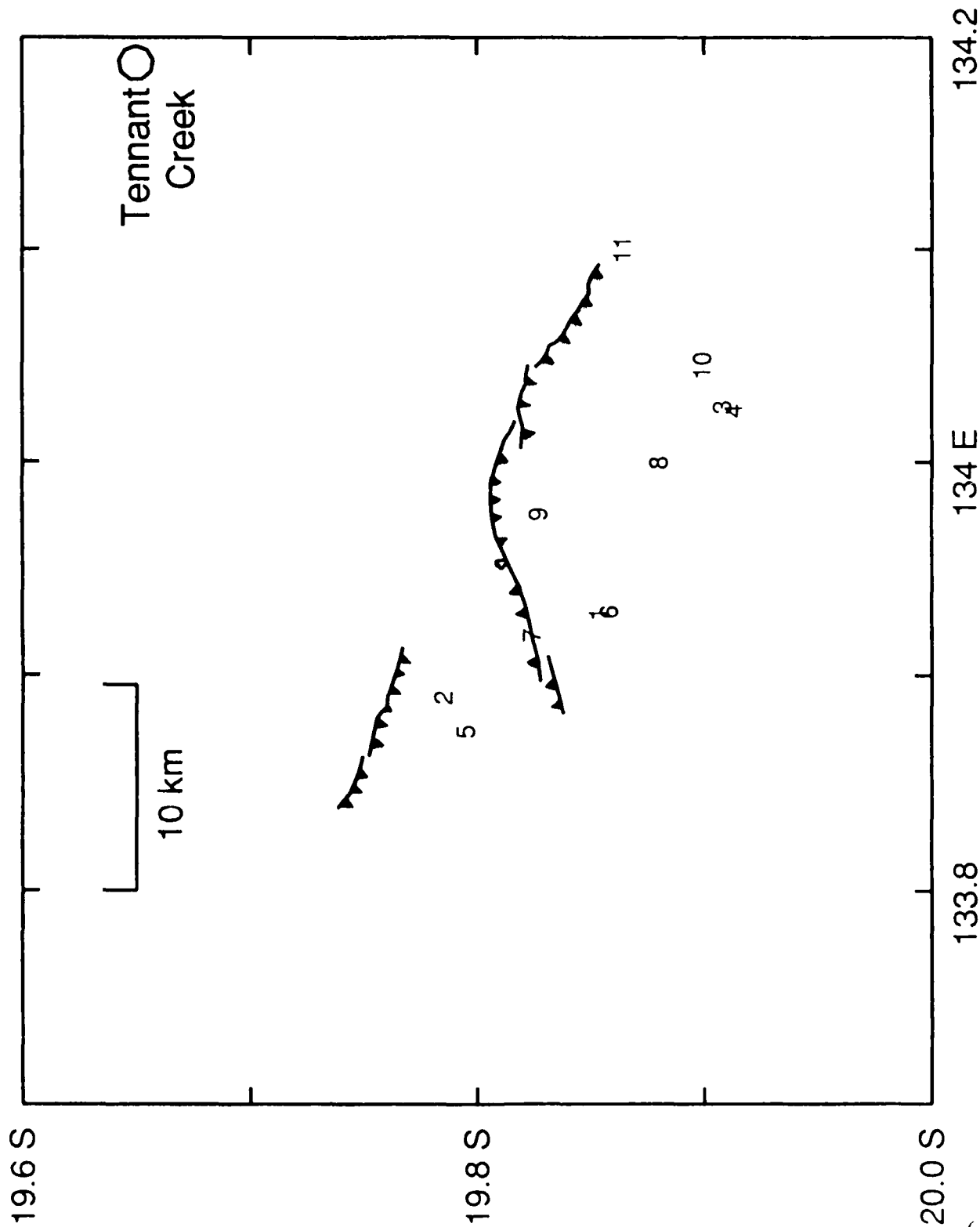


FIGURE 2

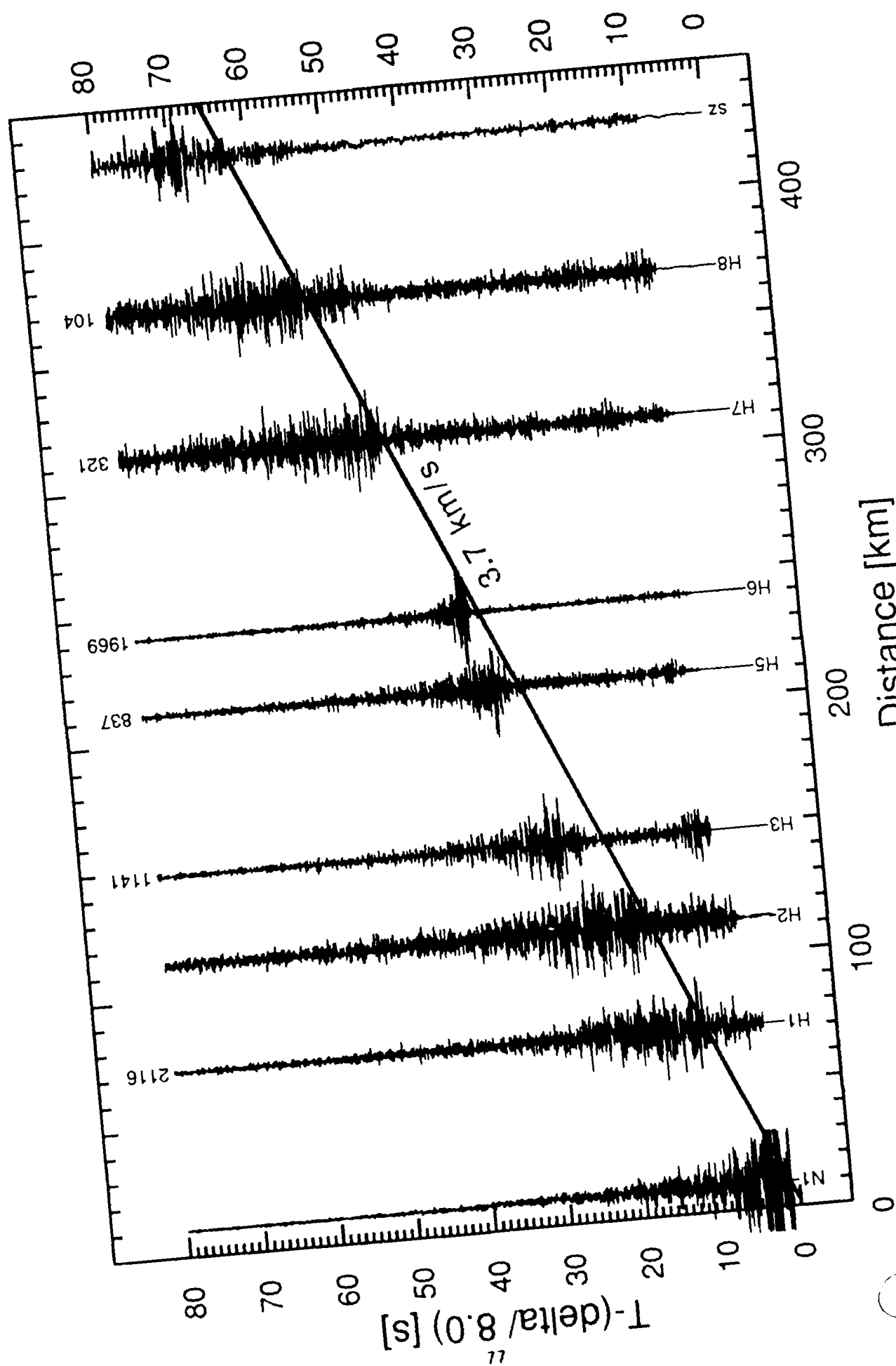


FIGURE 3

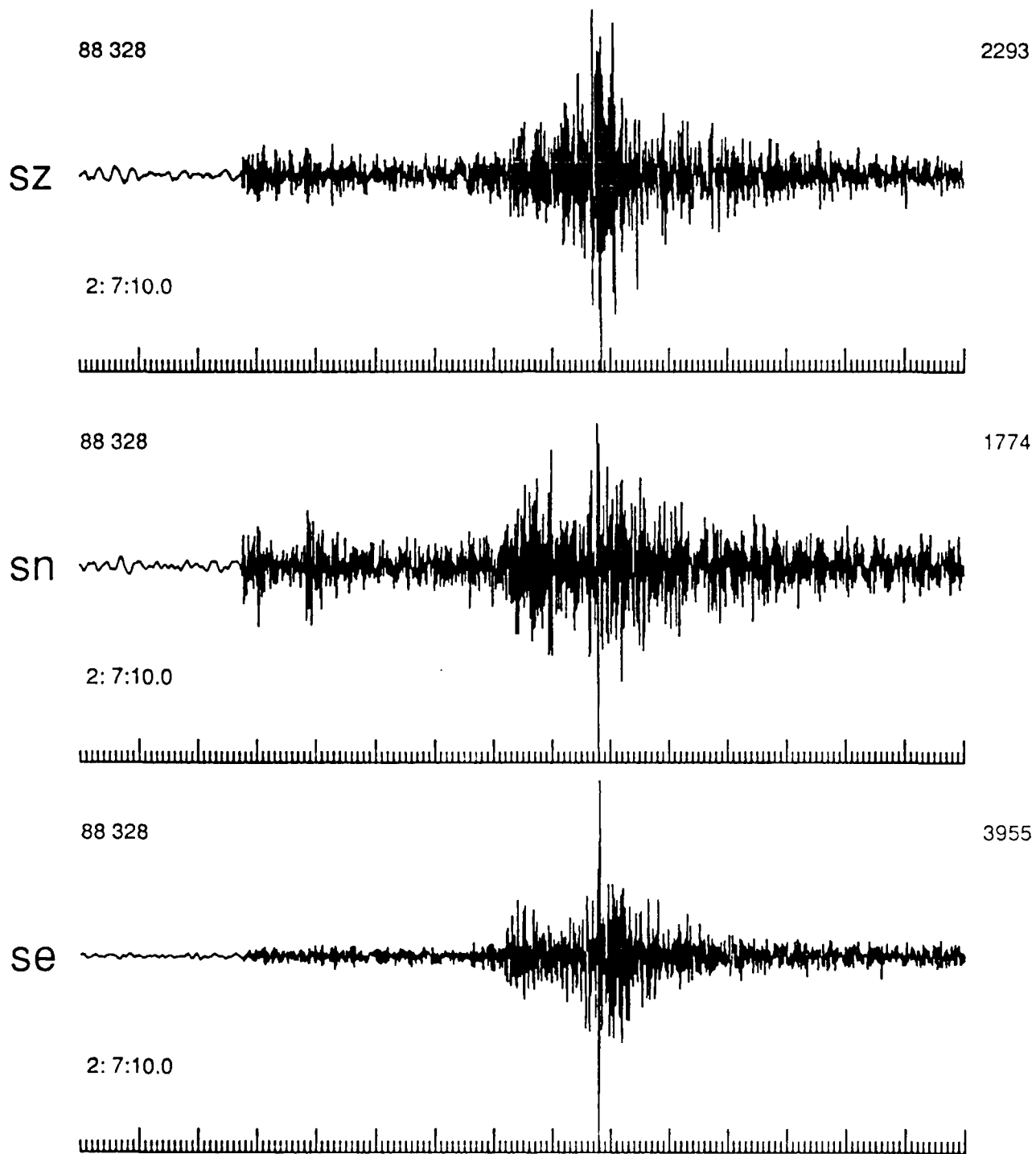


FIGURE 4

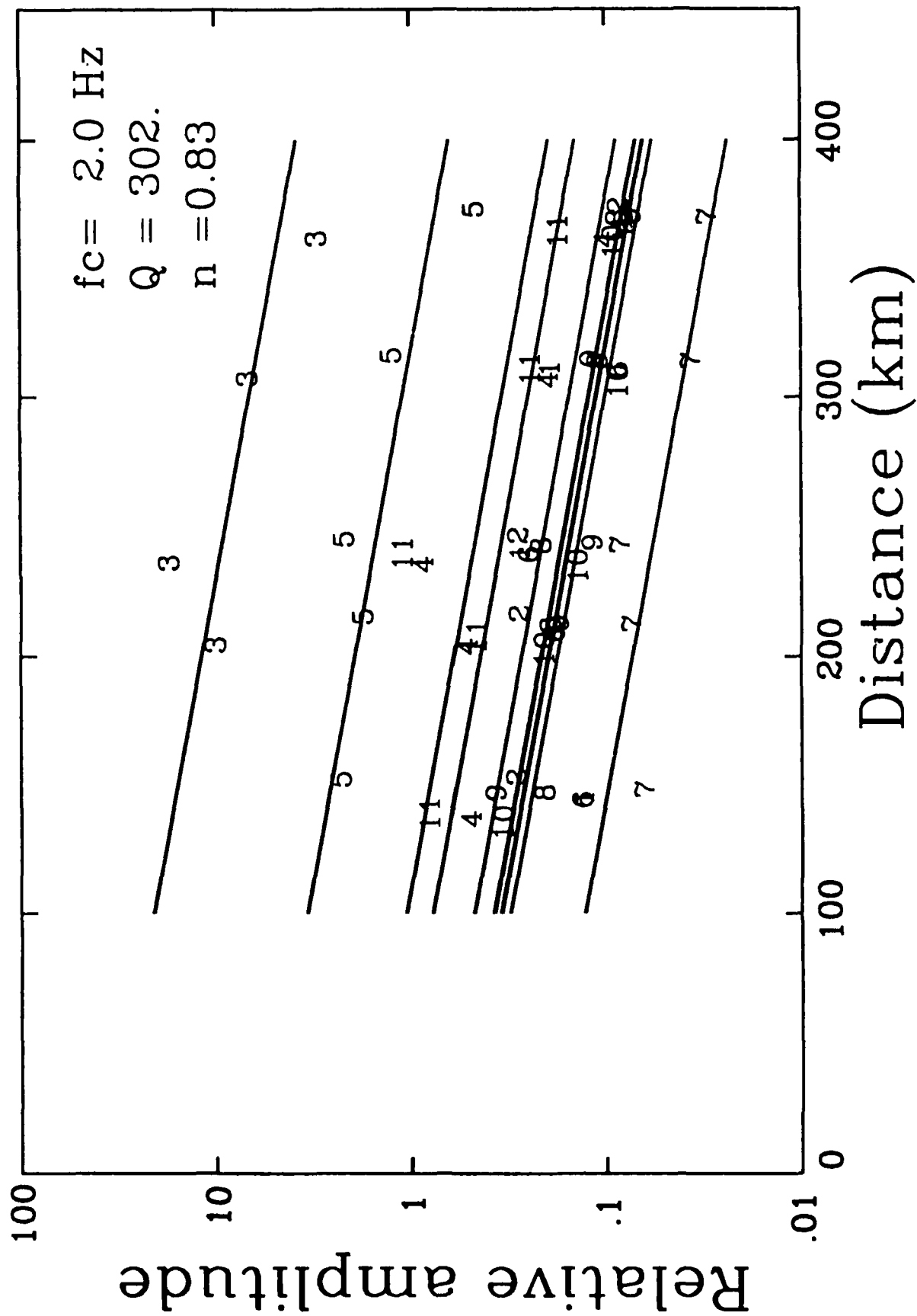


FIGURE 5

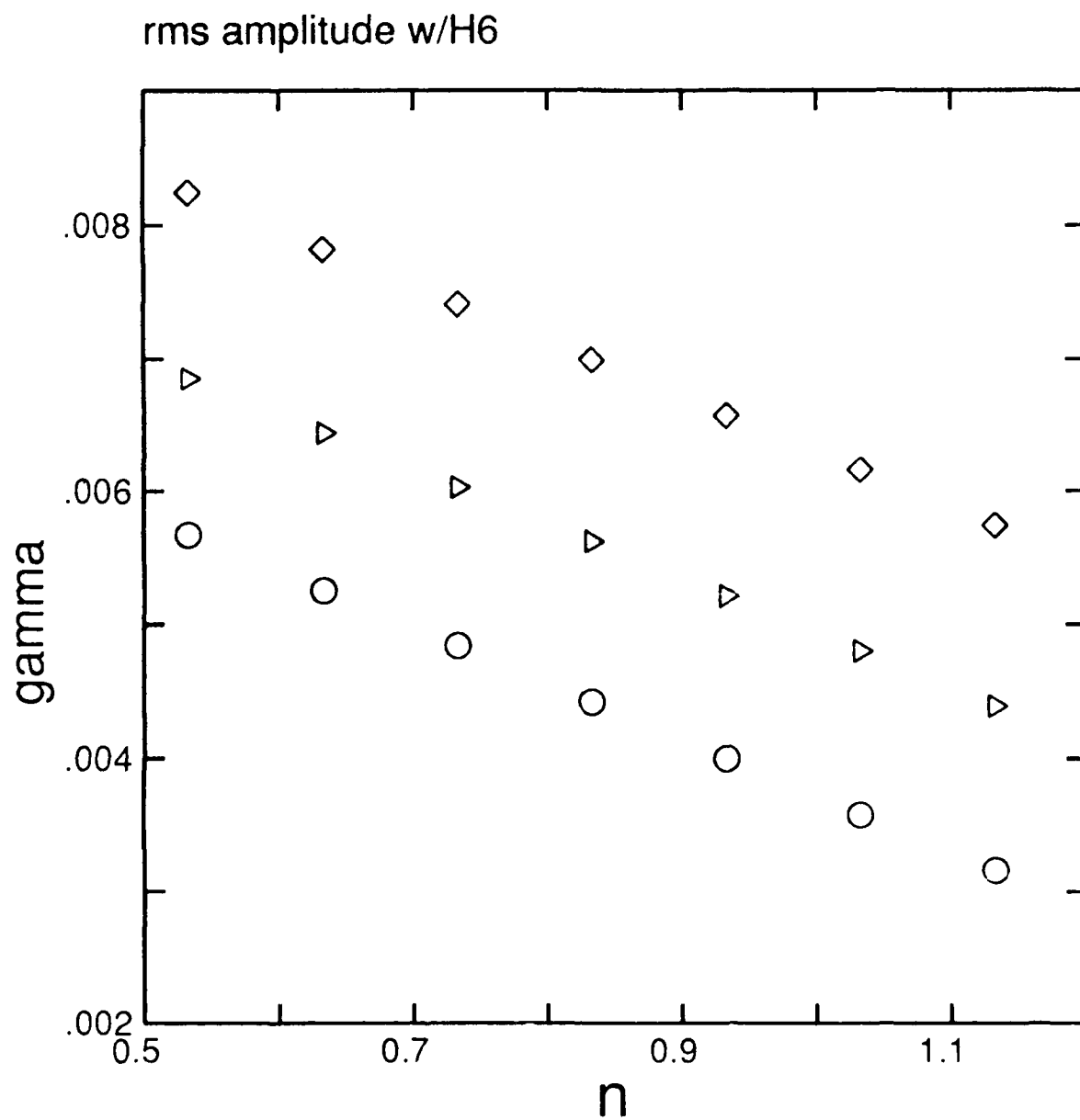


FIGURE 6

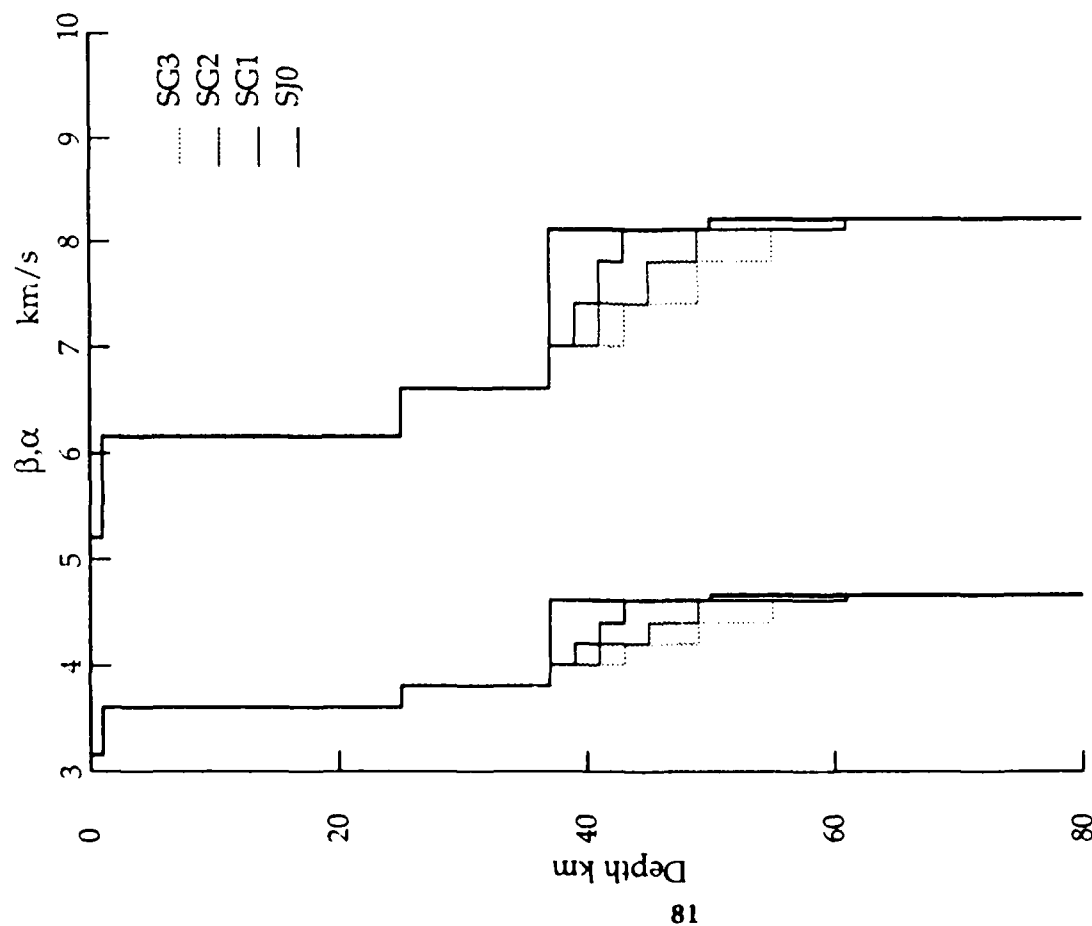
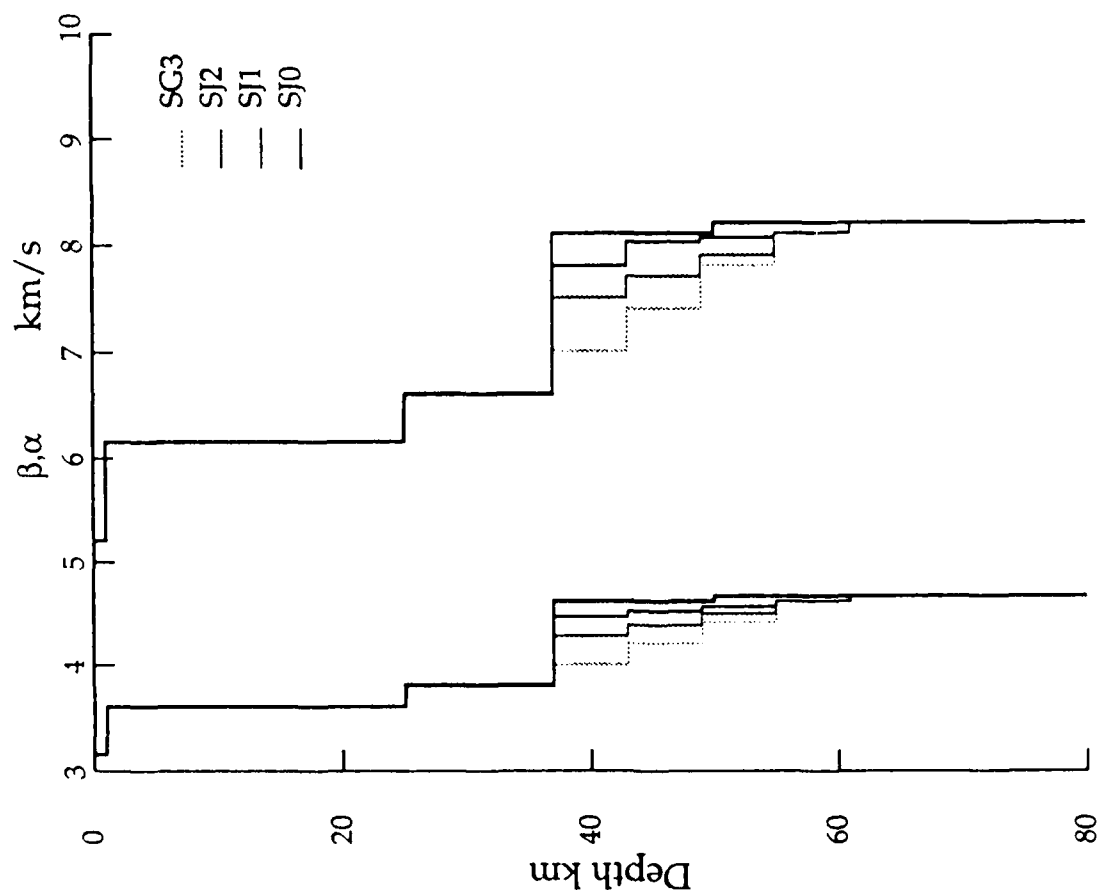


FIGURE 7

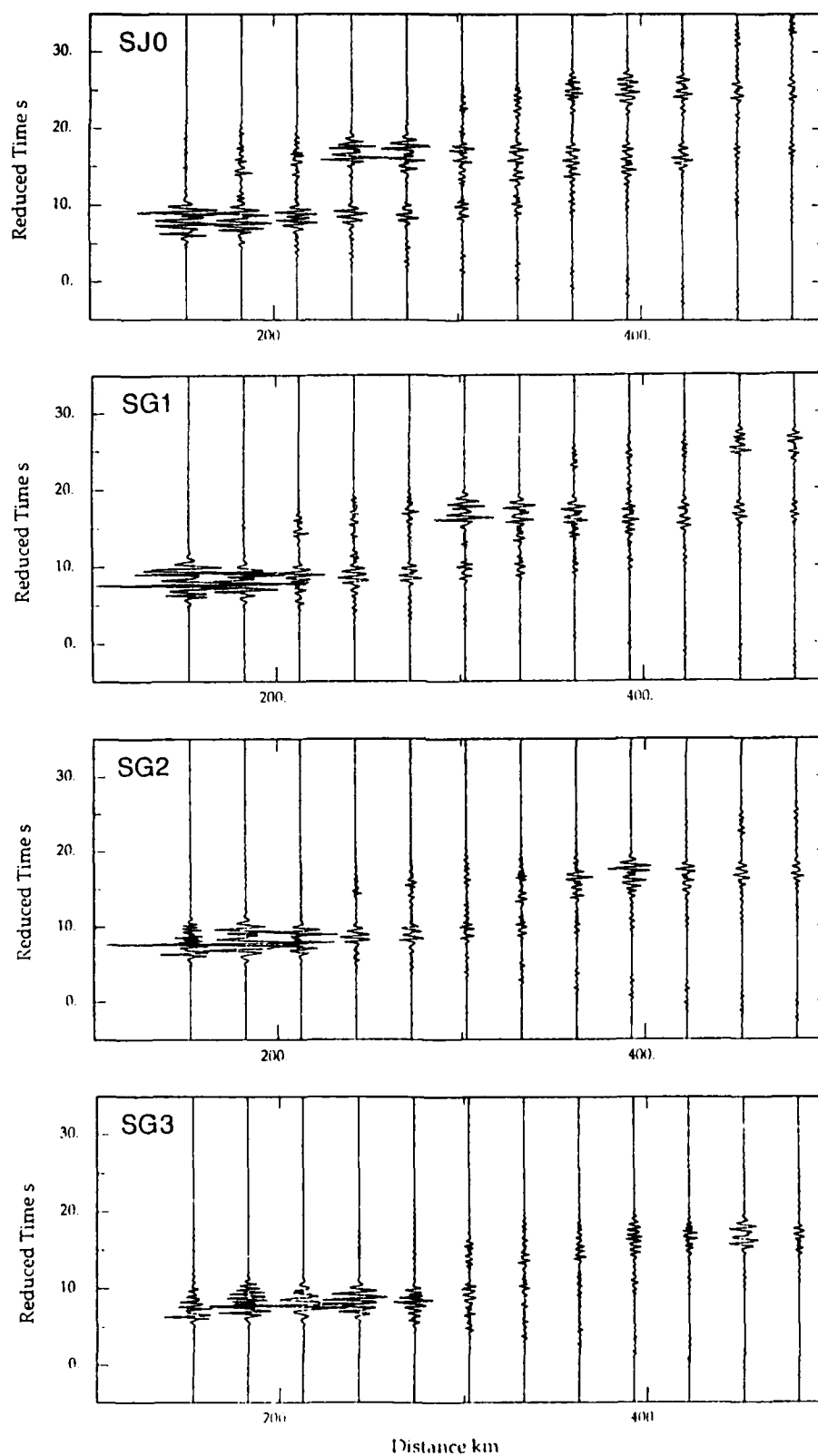


FIGURE 8 (a)

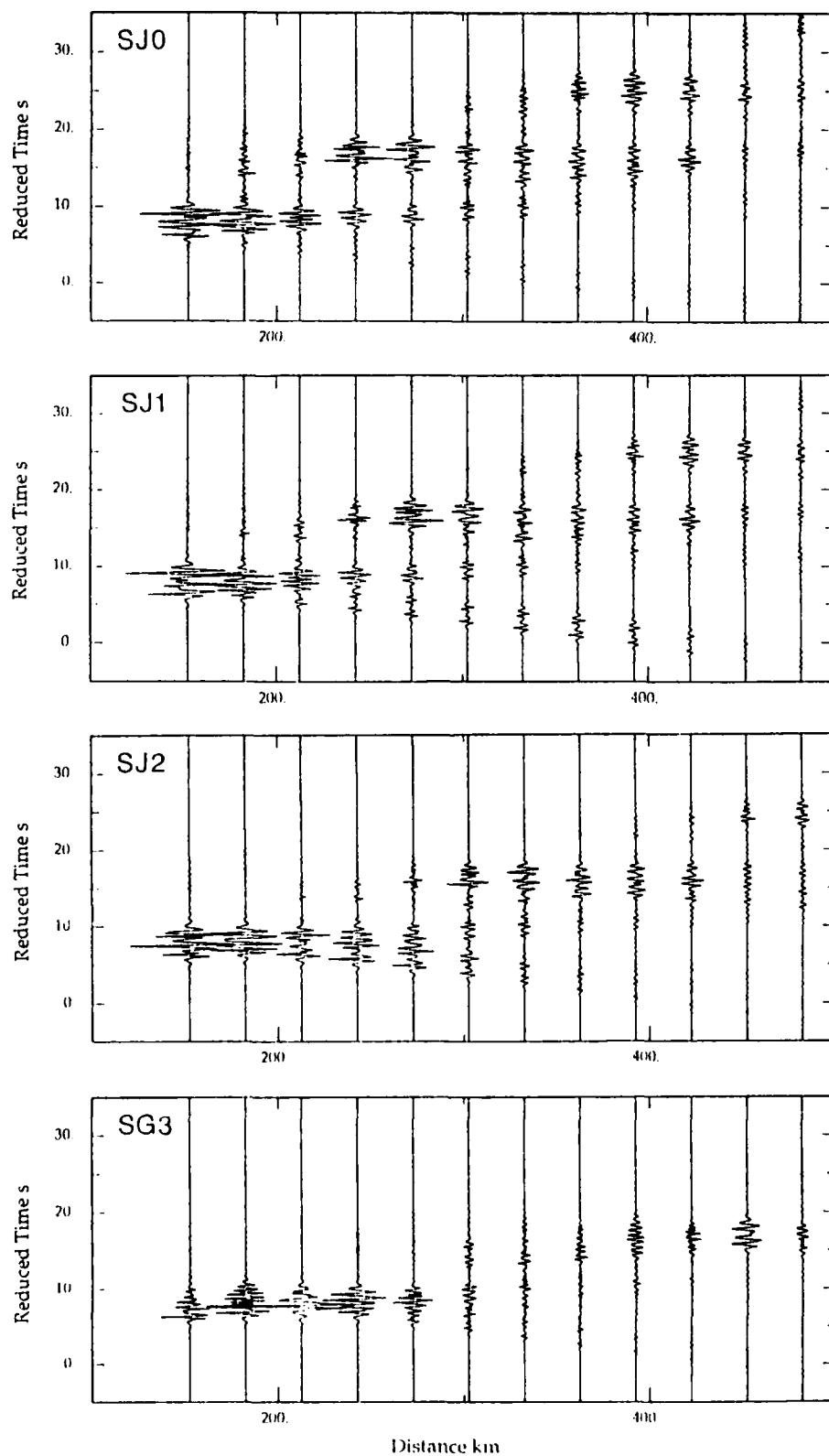


FIGURE 8 (b)

Lg decay - z

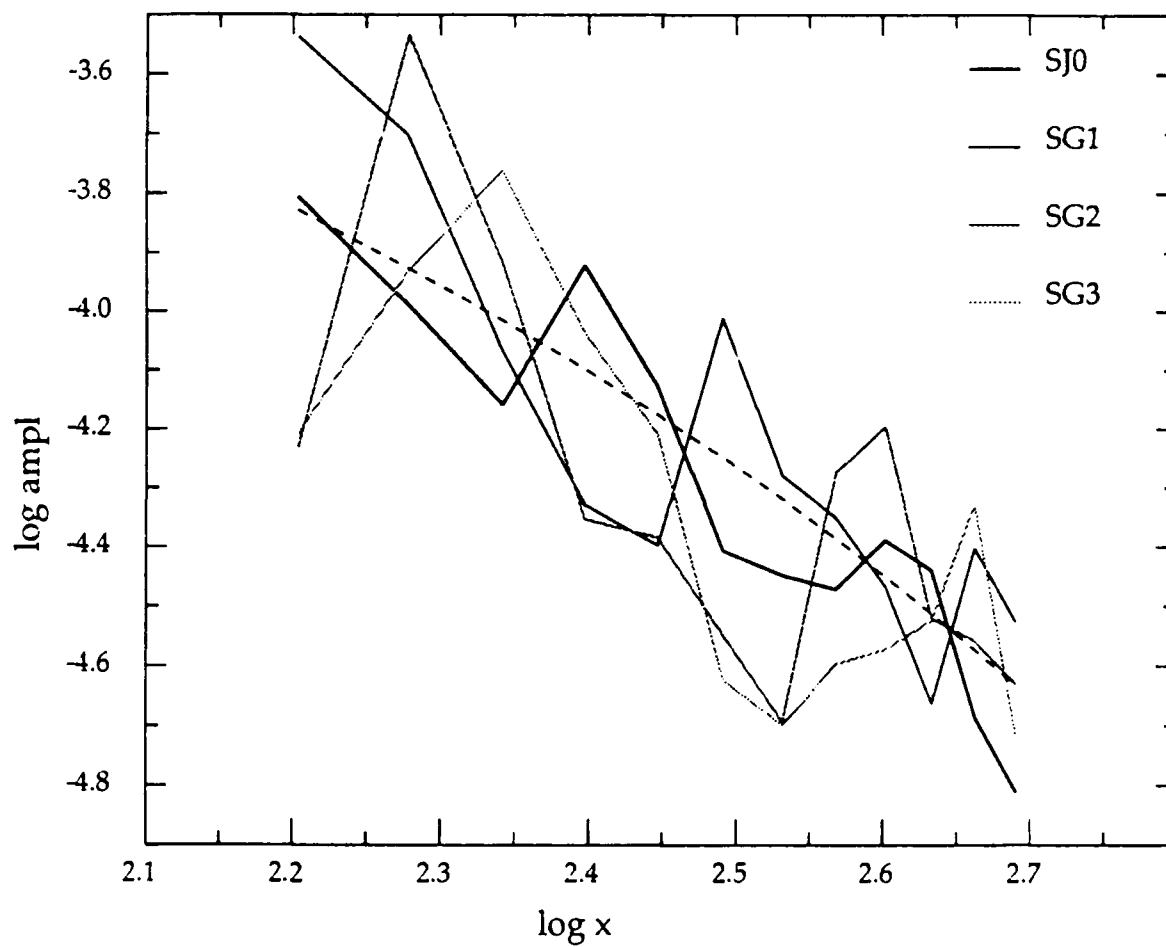


FIGURE 9 (a)

Lg decay - Z

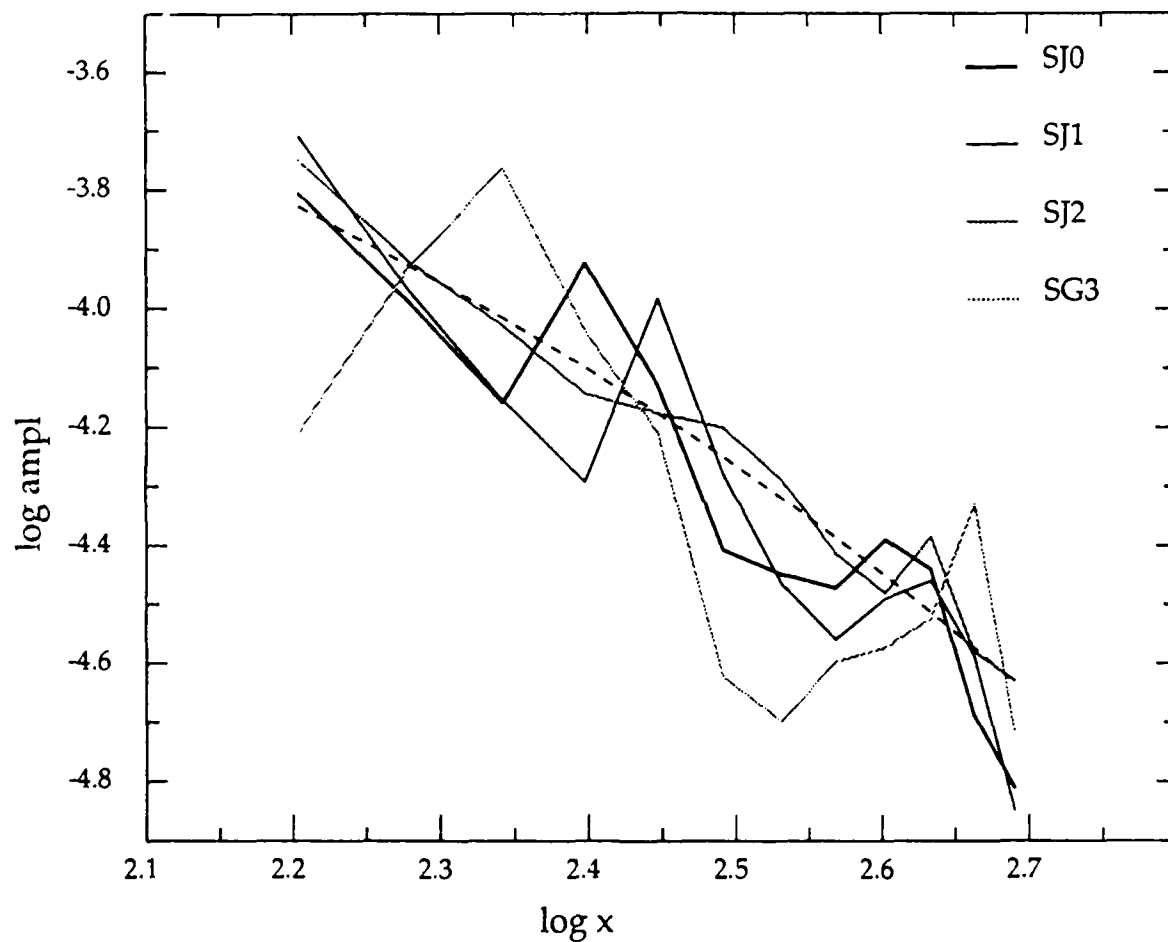


FIGURE 9 (b)

Contractors (United States)

Prof. Thomas Ahrens
Seismological Lab, 252-21
Division of Geological & Planetary Sciences
California Institute of Technology
Pasadena, CA 91125

Dr. Zoltan A. Der
ENSCO, Inc.
5400 Port Royal Road
Springfield, VA 22151-2388

Prof. Charles B. Archambeau
CIRES
University of Colorado
Boulder, CO 80309

Prof. John Ferguson
Center for Lithospheric Studies
The University of Texas at Dallas
P.O. Box 830688
Richardson, TX 75083-0688

Prof. Muawia Barazangi
Institute for the Study of the Continent
Cornell University
Ithaca, NY 14853

Prof. Stanley Flatte
Applied Sciences Building
University of California
Santa Cruz, CA 95064

Dr. Douglas R. Baumgardt
ENSCO, Inc.
5400 Port Royal Road
Springfield, VA 22151-2388

Dr. Alexander Florence
SRI International
333 Ravenswood Avenue
Menlo Park, CA 94025-3493

Prof. Jonathan Berger
IGPP, A-025
Scripps Institution of Oceanography
University of California, San Diego
La Jolla, CA 92093

Prof. Henry L. Gray
Vice Provost and Dean
Department of Statistical Sciences
Southern Methodist University
Dallas, TX 75275

Dr. Lawrence J. Burdick
Woodward-Clyde Consultants
566 El Dorado Street
Pasadena, CA 91109-3245

Dr. Indra Gupta
Teledyne Geotech
314 Montgomery Street
Alexandria, VA 22314

Dr. Karl Coyner
New England Research, Inc.
76 Olcott Drive
White River Junction, VT 05001

Prof. David G. Harkrider
Seismological Laboratory
Division of Geological & Planetary Sciences
California Institute of Technology
Pasadena, CA 91125

Prof. Vernon F. Cormier
Department of Geology & Geophysics
U-45, Room 207
The University of Connecticut
Storrs, CT 06268

Prof. Donald V. Helmberger
Seismological Laboratory
Division of Geological & Planetary Sciences
California Institute of Technology
Pasadena, CA 91125

Professor Anton W. Dainty
Earth Resources Laboratory
Massachusetts Institute of Technology
2 Carleton Street
Cambridge, MA 02142

Prof. Eugene Herrin
Institute for the Study of Earth and Man
Geophysical Laboratory
Southern Methodist University
Dallas, TX 75275

Prof. Steven Day
Department of Geological Sciences
San Diego State University
San Diego, CA 92182

Prof. Robert B. Herrmann
Department of Earth & Atmospheric Sciences
St. Louis University
St. Louis, MO 63156

Prof. Bryan Isacks
Cornell University
Department of Geological Sciences
SNEE Hall
Ithaca, NY 14850

Dr. Rong-Song Jih
Teledyne Geotech
314 Montgomery Street
Alexandria, VA 22314

Prof. Lane R. Johnson
Seismographic Station
University of California
Berkeley, CA 94720

Prof. Alan Kafka
Department of Geology & Geophysics
Boston College
Chestnut Hill, MA 02167

Dr. Richard LaCoss
MIT-Lincoln Laboratory
M-200B
P. O. Box 73
Lexington, MA 02173-0073 (3 copies)

Prof. Fred K. Lamb
University of Illinois at Urbana-Champaign
Department of Physics
1110 West Green Street
Urbana, IL 61801

Prof. Charles A. Langston
Geosciences Department
403 Deike Building
The Pennsylvania State University
University Park, PA 16802

Prof. Thorne Lay
Institute of Tectonics
Earth Science Board
University of California, Santa Cruz
Santa Cruz, CA 95064

Prof. Arthur Lerner-Lam
Lamont-Doherty Geological Observatory
of Columbia University
Palisades, NY 10964

Dr. Christopher Lynnes
Teledyne Geotech
314 Montgomery Street
Alexandria, VA 22314

Prof. Peter Malin
University of California at Santa Barbara
Institute for Crustal Studies
Santa Barbara, CA 93106

Dr. Randolph Martin, III
New England Research, Inc.
76 Olcott Drive
White River Junction, VT 05001

Dr. Gary McCartor
Mission Research Corporation
735 State Street
P.O. Drawer 719
Santa Barbara, CA 93102 (2 copies)

Prof. Thomas V. McEvilly
Seismographic Station
University of California
Berkeley, CA 94720

Dr. Keith L. McLaughlin
S-CUBED
A Division of Maxwell Laboratory
P.O. Box 1620
La Jolla, CA 92038-1620

Prof. William Menke
Lamont-Doherty Geological Observatory
of Columbia University
Palisades, NY 10964

Stephen Miller
SRI International
333 Ravenswood Avenue
Box AF 116
Menlo Park, CA 94025-3493

Prof. Bernard Minster
IGPP, A-025
Scripps Institute of Oceanography
University of California, San Diego
La Jolla, CA 92093

Prof. Brian J. Mitchell
Department of Earth & Atmospheric Sciences
St. Louis University
St. Louis, MO 63156

Mr. Jack Murphy
S-CUBED, A Division of Maxwell Laboratory
11800 Sunrise Valley Drive
Suite 1212
Reston, VA 22091 (2 copies)

Dr. Bao Nguyen
GL/LWH
Hanscom AFB, MA 01731-5000

Prof. Jeremiah Sullivan
University of Illinois at Urbana-Champaign
Department of Physics
1110 West Green Street
Urbana, IL 61801

Prof. John A. Orcutt
IGPP, A-025
Scripps Institute of Oceanography
University of California, San Diego
La Jolla, CA 92093

Prof. Clifford Thurber
University of Wisconsin-Madison
Department of Geology & Geophysics
1215 West Dayton Street
Madison, WI 53706

Prof. Keith Priestley
University of Cambridge
Bullard Labs, Dept. of Earth Sciences
Madingley Rise, Madingley Rd.
Cambridge CB3 0EZ, ENGLAND

Prof. M. Nafi Toksoz
Earth Resources Lab
Massachusetts Institute of Technology
42 Carleton Street
Cambridge, MA 02142

Prof. Paul G. Richards
L-210
Lawrence Livermore National Laboratory
Livermore, CA 94550

Prof. John E. Vidale
University of California at Santa Cruz
Seismological Laboratory
Santa Cruz, CA 95064

Dr. Wilmer Rivers
Teledyne Geotech
314 Montgomery Street
Alexandria, VA 22314

Prof. Terry C. Wallace
Department of Geosciences
Building #77
University of Arizona
Tucson, AZ 85721

Prof. Charles G. Sammis
Center for Earth Sciences
University of Southern California
University Park
Los Angeles, CA 90089-0741

Dr. Raymond Willeman
GL/LWH
Hanscom AFB, MA 01731-5000

Prof. Christopher H. Scholz
Lamont-Doherty Geological Observatory
of Columbia University
Palisades, NY 10964

Dr. Lorraine Wolf
GL/LWH
Hanscom AFB, MA 01731-5000

Prof. David G. Simpson
Lamont-Doherty Geological Observatory
of Columbia University
Palisades, NY 10964

Prof. Francis T. Wu
Department of Geological Sciences
State University of New York
at Binghamton
Vestal, NY 13901

Dr. Jeffrey Stevens
S-CUBED
A Division of Maxwell Laboratory
P.O. Box 1620
La Jolla, CA 92038-1620

Prof. Brian Stump
Institute for the Study of Earth & Man
Geophysical Laboratory
Southern Methodist University
Dallas, TX 75275

OTHERS (United States)

Dr. Monem Abdel-Gawad
Rockwell International Science Center
1049 Camino Dos Rios
Thousand Oaks, CA 91360

Prof. Keiiti Aki
Center for Earth Sciences
University of Southern California
University Park
Los Angeles, CA 90089-0741

Prof. Shelton S. Alexander
Geosciences Department
403 Deike Building
The Pennsylvania State University
University Park, PA 16802

Dr. Kenneth Anderson
BBNSTC
Mail Stop 14/1B
Cambridge, MA 02238

Dr. Ralph Archuleta
Department of Geological Sciences
University of California at Santa Barbara
Santa Barbara, CA 93102

Dr. Thomas C. Bache, Jr.
Science Applications Int'l Corp.
10210 Campus Point Drive
San Diego, CA 92121 (2 copies)

J. Barker
Department of Geological Sciences
State University of New York
at Binghamton
Vestal, NY 13901

Dr. T.J. Bennett
S-CUBED
A Division of Maxwell Laboratory
11800 Sunrise Valley Drive, Suite 1212
Reston, VA 22091

Mr. William J. Best
907 Westwood Drive
Vienna, VA 22180

Dr. N. Biswas
Geophysical Institute
University of Alaska
Fairbanks, AK 99701

Dr. G.A. Bollinger
Department of Geological Sciences
Virginia Polytechnical Institute
21044 Derring Hall
Blacksburg, VA 24061

Dr. Steven R. Bratt
Center for Seismic Studies
1300 North 17th St., Suite 1450
Arlington, VA 22209

Michael Browne
Teledyne Geotech
3401 Shiloh Road
Garland, TX 75041

Mr. Roy Burger
1221 Serry Road
Schenectady, NY 12309

Dr. Robert Burridge
Schlumberger-Doll Research Center
Old Quarry Road
Ridgefield, CT 06877

Dr. Jerry Carter
Rondout Associates
P.O. Box 224
Stone Ridge, NY 12484

Dr. W. Winston Chan
Teledyne Geotech
314 Montgomery Street
Alexandria, VA 22314-1581

Dr. Theodore Cherry
Science Horizons, Inc.
710 Encinitas Blvd., Suite 200
Encinitas, CA 92024 (2 copies)

Prof. Jon F. Claerbout
Department of Geophysics
Stanford University
Stanford, CA 94305

Prof. Robert W. Clayton
Seismological Laboratory
Division of Geological & Planetary Sciences
California Institute of Technology
Pasadena, CA 91125

Prof. F. A. Dahlen
Geological and Geophysical Sciences
Princeton University
Princeton, NJ 08544-0636

Dr. Jeffrey W. Given
Sierra Geophysics
11255 Kirkland Way
Kirkland, WA 98033

Prof. Adam Dziewonski
Hoffman Laboratory
Harvard University
20 Oxford St
Cambridge, MA 02138

Prof. Stephen Grand
University of Texas at Austin
Department of Geological Sciences
Austin, TX 78713-7909

Prof. John Ebel
Department of Geology & Geophysics
Boston College
Chestnut Hill, MA 02167

Prof. Roy Greenfield
Geosciences Department
403 Deike Building
The Pennsylvania State University
University Park, PA 16802

Eric Fielding
SNEE Hall
INSTOC
Cornell University
Ithaca, NY 14853

Dan N. Hagedorn
Battelle
Pacific Northwest Laboratories
Battelle Boulevard
Richland, WA 99352

Prof. Donald Forsyth
Department of Geological Sciences
Brown University
Providence, RI 02912

Kevin Hutchenson
Department of Earth Sciences
St. Louis University
3507 Laclede
St. Louis, MO 63103

Dr. Cliff Frolich
Institute of Geophysics
8701 North Mopac
Austin, TX 78759

Prof. Thomas H. Jordan
Department of Earth, Atmospheric
and Planetary Sciences
Massachusetts Institute of Technology
Cambridge, MA 02139

Prof. Art Frankel
Mail Stop 922
Geological Survey
790 National Center
Reston, VA 22092

Robert C. Kemerait
ENSCO, Inc.
445 Pineda Court
Melbourne, FL 32940

Dr. Anthony Gangi
Texas A&M University
Department of Geophysics
College Station, TX 77843

William Kikendall
Teledyne Geotech
3401 Shiloh Road
Garland, TX 75041

Dr. Freeman Gilbert
Inst. of Geophysics & Planetary Physics
University of California, San Diego
P.O. Box 109
La Jolla, CA 92037

Prof. Leon Knopoff
University of California
Institute of Geophysics & Planetary Physics
Los Angeles, CA 90024

Mr. Edward Giller
Pacific Sierra Research Corp.
1401 Wilson Boulevard
Arlington, VA 22209

Prof. L. Timothy Long
School of Geophysical Sciences
Georgia Institute of Technology
Atlanta, GA 30332

Prof. Art McGarr
Mail Stop 977
Geological Survey
345 Middlefield Rd.
Menlo Park, CA 94025

Dr. George Mellman
Sierra Geophysics
11255 Kirkland Way
Kirkland, WA 98033

Prof. John Nabelek
College of Oceanography
Oregon State University
Corvallis, OR 97331

Prof. Geza Nagy
University of California, San Diego
Department of Ames, M.S. B-010
La Jolla, CA 92093

Prof. Amos Nur
Department of Geophysics
Stanford University
Stanford, CA 94305

Prof. Jack Oliver
Department of Geology
Cornell University
Ithaca, NY 14850

Prof. Robert Phinney
Geological & Geophysical Sciences
Princeton University
Princeton, NJ 08544-0636

Dr. Paul Pomeroy
Rondout Associates
P.O. Box 224
Stone Ridge, NY 12484

Dr. Jay Pulli
RADIX System, Inc.
2 Taft Court, Suite 203
Rockville, MD 20850

Dr. Norton Rimer
S-CUBED
A Division of Maxwell Laboratory
P.O. Box 1620
La Jolla, CA 92038-1620

Prof. Larry J. Ruff
Department of Geological Sciences
1006 C.C. Little Building
University of Michigan
Ann Arbor, MI 48109-1063

Dr. Richard Sailor
TASC Inc.
55 Walkers Brook Drive
Reading, MA 01867

Thomas J. Sereno, Jr.
Science Application Int'l Corp.
10210 Campus Point Drive
San Diego, CA 92121

John Sherwin
Teledyne Geotech
3401 Shiloh Road
Garland, TX 75041

Prof. Robert Smith
Department of Geophysics
University of Utah
1400 East 2nd South
Salt Lake City, UT 84112

Prof. S. W. Smith
Geophysics Program
University of Washington
Seattle, WA 98195

Dr. Stewart Smith
IRIS Inc.
1616 North Fort Myer Drive
Suite 1440
Arlington, VA 22209

Dr. George Sutton
Rondout Associates
P.O. Box 224
Stone Ridge, NY 12484

Prof. L. Sykes
Lamont-Doherty Geological Observatory
of Columbia University
Palisades, NY 10964

Prof. Pradeep Talwani
Department of Geological Sciences
University of South Carolina
Columbia, SC 29208

Prof. Ta-liang Teng
Center for Earth Sciences
University of Southern California
University Park
Los Angeles, CA 90089-0741

Dr. R.B. Tittmann
Rockwell International Science Center
1049 Camino Dos Rios
P.O. Box 1085
Thousand Oaks, CA 91360

Dr. Gregory van der Vink
IRIS, Inc.
1616 North Fort Myer Drive
Suite 1440
Arlington, VA 22209

Professor Daniel Walker
University of Hawaii
Institute of Geophysics
Honolulu, HI 96822

William R. Walter
Seismological Laboratory
University of Nevada
Reno, NV 89557

Dr. Gregory Wojcik
Weidlinger Associates
4410 El Camino Real
Suite 110
Los Altos, CA 94022

Prof. John H. Woodhouse
Hoffman Laboratory
Harvard University
20 Oxford St.
Cambridge, MA 02138

Dr. Gregory B. Young
ENSCO, Inc.
5400 Port Royal Road
Springfield, VA 22151-2388

GOVERNMENT

Dr. Ralph Alewine III
DARPA/NMRO
1400 Wilson Boulevard
Arlington, VA 22209-2308

Paul Johnson
ESS-4, Mail Stop J979
Los Alamos National Laboratory
Los Alamos, NM 87545

Mr. James C. Battis
GL/LWH
Hanscom AFB, MA 01731-5000

Janet Johnston
GL/LWH
Hanscom AFB, MA 01731-5000

Dr. Robert Blandford
DARPA/NMRO
1400 Wilson Boulevard
Arlington, VA 22209-2308

Dr. Katharine Kadinsky-Cade
GL/LWH
Hanscom AFB, MA 01731-5000

Eric Chael
Division 9241
Sandia Laboratory
Albuquerque, NM 87185

Ms. Ann Kerr
IGPP, A-025
Scripps Institute of Oceanography
University of California, San Diego
La Jolla, CA 92093

Dr. John J. Cipar
GL/LWH
Hanscom AFB, MA 01731-5000

Dr. Max Koontz
US Dept of Energy/DP 5
Forrestal Building
1000 Independence Avenue
Washington, DC 20585

Mr. Jeff Duncan
Office of Congressman Markey
2133 Rayburn House Bldg.
Washington, DC 20515

Dr. W.H.K. Lee
Office of Earthquakes, Volcanoes,
& Engineering
345 Middlefield Road
Menlo Park, CA 94025

Dr. Jack Evernden
USGS - Earthquake Studies
345 Middlefield Road
Menlo Park, CA 94025

Dr. William Leith
U.S. Geological Survey
Mail Stop 928
Reston, VA 22092

Art Frankel
USGS
922 National Center
Reston, VA 22092

Dr. Richard Lewis
Director, Earthquake Engineering & Geophysics
U.S. Army Corps of Engineers
Box 631
Vicksburg, MS 39180

Dr. T. Hanks
USGS
Nat'l Earthquake Research Center
345 Middlefield Road
Menlo Park, CA 94025

James F. Lewkowicz
GL/LWH
Hanscom AFB, MA 01731-5000

Dr. James Hannon
Lawrence Livermore Nat'l Laboratory
P.O. Box 808
Livermore, CA 94550

Mr. Alfred Lieberman
ACDA/VI-OA State Department Bldg
Room 5726
320 - 21st Street, NW
Washington, DC 20451

Stephen Mangino
GI/LWH
Hanscom AFB, MA 01731-5000

Dr. Frank F. Pilotte
HQ AFTAC/TT
Patrick AFB, FL 32925-6001

Dr. Robert Masse
Box 25046, Mail Stop 967
Denver Federal Center
Denver, CO 80225

Katie Poley
CIA-OSWR/NED
Washington, DC 20505

Art McGarr
U.S. Geological Survey, MS-977
345 Middlefield Road
Menlo Park, CA 94025

Mr. Jack Rachlin
U.S. Geological Survey
Geology, Rm 3 C136
Mail Stop 928 National Center
Reston, VA 22092

Richard Morrow
ACDA/VI, Room 5741
320 21st Street N.W.
Washington, DC 20451

Dr. Robert Reinke
WL/NTESG
Kirtland AFB, NM 87117-6008

Dr. Keith K. Nakanishi
Lawrence Livermore National Laboratory
P.O. Box 808, L-205
Livermore, CA 94550

Dr. Byron Ristvet
HQ DNA, Nevada Operations Office
Attn: NVCG
P.O. Box 98539
Las Vegas, NV 89193

Dr. Carl Newton
Los Alamos National Laboratory
P.O. Box 1663
Mail Stop C335, Group ESS-3
Los Alamos, NM 87545

Dr. George Rothe
HQ AFTAC/TGR
Patrick AFB, FL 32925-6001

Dr. Kenneth H. Olsen
Los Alamos Scientific Laboratory
P.O. Box 1663
Mail Stop C335, Group ESS-3
Los Alamos, NM 87545

Dr. Alan S. Ryall, Jr.
DARPA/NMRO
1400 Wilson Boulevard
Arlington, VA 22209-2308

Howard J. Patton
Lawrence Livermore National Laboratory
P.O. Box 808, L-205
Livermore, CA 94550

Dr. Michael Shore
Defense Nuclear Agency/SPSS
6801 Telegraph Road
Alexandria, VA 22310

Mr. Chris Paine
Office of Senator Kennedy
SR 315
United States Senate
Washington, DC 20510

Donald L. Springer
Lawrence Livermore National Laboratory
P.O. Box 808, L-205
Livermore, CA 94550

Colonel Jerry J. Perrizo
AFOSR/NP, Building 410
Bolling AFB
Washington, DC 20332-6448

Mr. Charles L. Taylor
GL/LWG
Hanscom AFB, MA 01731-5000

Dr. Thomas Weaver
Los Alamos National Laboratory
P.O. Box 1663, Mail Stop C335
Los Alamos, NM 87545

DARPA/PM
1400 Wilson Boulevard
Arlington, VA 22209

J.J. Zucca
Lawrence Livermore National Laboratory
Box 808
Livermore, CA 94550

Defense Technical Information Center
Cameron Station
Alexandria, VA 22314 (5 copies)

GL/SULL
Research Library
Hanscom AFB, MA 01731-5000 (2 copies)

Defense Intelligence Agency
Directorate for Scientific &
Technical Intelligence/DT1B
Washington, DC 20340-6158

Secretary of the Air Force
(SAFRD)

Washington, DC 20330

AFTAC/CA
(STINFO)
Patrick AFB, FL 32925-6001

Office of the Secretary Defense
DDR & E
Washington, DC 20330

TACTEC
Battelle Memorial Institute
505 King Avenue
Columbus, OH 43201 (Final Report Only)

HQ DNA
Attn: Technical Library
Washington, DC 20305

DARPA/RMO/RETRIEVAL
1400 Wilson Boulevard
Arlington, VA 22209

DARPA/RMO/Security Office
1400 Wilson Boulevard
Arlington, VA 22209

Geophysics Laboratory
Attn: XO
Hanscom AFB, MA 01731-5000

Geophysics Laboratory
Attn: LW
Hanscom AFB, MA 01731-5000

CONTRACTORS (Foreign)

Dr. Ramon Cabre, S.J.
Observatorio San Calixto
Casilla 5939
La Paz, Bolivia

Prof. Hans-Peter Harjes
Institute for Geophysik
Ruhr University/Bochum
P.O. Box 102148
4630 Bochum 1, FRG

Prof. Eystein Husebye
NTNF/NORSAR
P.O. Box 51
N-2007 Kjeller, NORWAY

Prof. Brian L.N. Kennett
Research School of Earth Sciences
Institute of Advanced Studies
G.P.O. Box 4
Canberra 2601, AUSTRALIA

Dr. Bernard Massinon
Societe Radiomana
27 rue Claude Bernard
75005 Paris, FRANCE (2 Copies)

Dr. Pierre Mecheler
Societe Radiomana
27 rue Claude Bernard
75005 Paris, FRANCE

Dr. Svein Mykkeltveit
NTNF/NORSAR
P.O. Box 51
N-2007 Kjeller, NORWAY

FOREIGN (Others)

Dr. Peter Basham
Earth Physics Branch
Geological Survey of Canada
1 Observatory Crescent
Ottawa, Ontario, CANADA K1A 0Y3

Dr. Eduard Berg
Institute of Geophysics
University of Hawaii
Honolulu, HI 96822

Dr. Michel Bouchon
I.R.I.G.M.-B.P. 68
38402 St. Martin D'Herès
Cedex, FRANCE

Dr. Hilmar Bungum
NTNF/NORSAR
P.O. Box 51
N-2007 Kjeller, NORWAY

Dr. Michel Campillo
Observatoire de Grenoble
I.R.I.G.M.-B.P. 53
38041 Grenoble, FRANCE

Dr. Kin Yip Chun
Geophysics Division
Physics Department
University of Toronto
Ontario, CANADA M5S 1A7

Dr. Alan Douglas
Ministry of Defense
Blacknest, Brimpton
Reading RG7-4RS, UNITED KINGDOM

Dr. Roger Hansen
NTNF/NORSAR
P.O. Box 51
N-2007 Kjeller, NORWAY

Dr. Manfred Henger
Federal Institute for Geosciences & Nat'l Res.
Postfach 510153
D-3000 Hanover 51, FRG

Ms. Eva Johannisson
Senior Research Officer
National Defense Research Inst.
P.O. Box 27322
S-102 54 Stockholm, SWEDEN

Dr. Fekadu Kebede
Seismological Section
Box 12019
S-750 Uppsala, SWEDEN

Dr. Tormod Kvaerna
NTNF/NORSAR
P.O. Box 51
N-2007 Kjeller, NORWAY

Dr. Peter Marshal
Procurement Executive
Ministry of Defense
Blacknest, Brimpton
Reading RG7-4RS, UNITED KINGDOM

Prof. Ari Ben-Menahem
Department of Applied Mathematics
Weizman Institute of Science
Rehovot, ISRAEL 951729

Dr. Robert North
Geophysics Division
Geological Survey of Canada
1 Observatory Crescent
Ottawa, Ontario, CANADA K1A 0Y3

Dr. Frode Ringdal
NTNF/NORSAR
P.O. Box 51
N-2007 Kjeller, NORWAY

Dr. Jorg Schlittenhardt
Federal Institute for Geosciences & Nat'l Res.
Postfach 510153
D-3000 Hannover 51, FEDERAL REPUBLIC OF
GERMANY